11. Status of Higgs Boson Physics

Revised August 2025 by M. Cepeda (CIEMAT), L. Reina (Florida State U.) and P. Savard (Toronto U.; TRIUMF).

11.1	Intro	oduction	1
	11.1.1	Searches for the SM Higgs boson	2
	11.1.2	Discovery of the SM Higgs boson	3
	11.1.3	The SM Higgs boson as a portal to new physics	3
		Synopsis of this review	4
11.2	The	Standard Model and the mechanism of electroweak symmetry breaking	4
	11.2.1	The scalar Lagrangian of the Standard Model	4
	11.2.2	The Yukawa Lagrangian of the Standard Model	6
	11.2.3	The Standard Model custodial symmetry	7
	11.2.4	Stability of the scalar potential of the Standard Model	7
	11.2.5	Production and decay modes of the Standard-Model Higgs boson	8
11.3	Pher	nomenology of the 125 GeV Higgs boson	20
	11.3.1	Higgs-Boson Decay Channels	20
	11.3.2	Higgs-Boson Production Channels	21
	11.3.3	Inclusive Cross Section and Branching Ratio Measurements	22
	11.3.4	Differential and Template Cross Sections	26
	11.3.5	Probing the Couplings of the Higgs Boson: κ framework and EFT approach .	29
	11.3.6	Higgs-boson Self-Couplings	39
	11.3.7	Higgs-Boson Mass Measurements	42
	11.3.8	Higgs-boson Width	43
	11.3.9	Higgs-boson Spin and CP Properties	46
11.4	Beyo	ond the Standard Model (BSM) Higgs boson	51
	11.4.1	Weakly coupled approach to EWSB	53
		EWSB induced by strong dynamics	63
	11.4.3	Exotic Higgs-boson decays	67
	11.4.4	Summary of BSM Higgs boson search results	69
11.5	Sum	mary and Outlook	70

11.1 Introduction

Understanding how the masses of the known elementary particles are generated has been one of the fundamental endeavors in particle physics for several decades. Due to the nature of the $SU(2)_L \times U(1)_Y$ electroweak (EW) gauge symmetry that defines the Standard Model (SM) [1], mass terms for the W and Z weak gauge bosons as well as for all fermions (quarks and leptons) can only appear as emergent quantities after the spontaneous breaking of the EW symmetry. The mechanism of electroweak symmetry breaking (EWSB) [2] provides a general framework to keep untouched the structure of the SM gauge interactions at high energies and still generate all observed particle masses at the scale of EW interactions. The EWSB mechanism posits a self-interacting complex EW doublet scalar field, whose CP-even neutral component acquires a vacuum expectation value (VEV) $v \approx 246 \, \text{GeV}^1$, which sets the scale of the symmetry breaking.

¹As measured in muon decay with high precision, see Sec. 11.2.1.

Three massless Goldstone bosons are generated and are absorbed to give masses to the W and Z gauge bosons. The remaining component of the complex doublet becomes the Higgs boson – a new, and so far unique, fundamental scalar particle. The masses of all fermions are also a consequence of EWSB since the Higgs doublet is postulated to couple to the fermions through Yukawa interactions in a way consistent with all the gauge symmetries of the SM.

The existence of a Higgs boson as predicted by the mechanism of EWSB is crucial to the consistency of the SM at the quantum level such that its mass has been indirectly constrained by SM precision measurements well before its discovery. In fact, without the Higgs boson, SM predictions would show clear indications of new phenomena at the TeV scale. Perturbative unitarity [3] would be lost at high energies since the longitudinal W/Z boson scattering amplitudes would grow with the center-of-mass energy. In addition, the radiative corrections to the gauge boson self-energies would exhibit dangerous logarithmic divergences that would be difficult to reconcile with EW precision data.

The observation of a Higgs boson as predicted by the mechanism of EWSB of the SM has therefore been the holy grail of particle physics for the decades that led up to its discovery in 2012.

11.1.1 Searches for the SM Higgs boson

Prior to the observation of the Higgs boson in July of 2012, searches for the SM Higgs boson were carried out by the LEP and Tevatron experiments. The combined results of the LEP experiments [4] yielded a lower bound of $m_H > 114.4$ GeV at the 95% confidence level (CL). The Tevatron experiments [5] subsequently excluded the mass range between 156 and 177 GeV at the 95% CL. These exclusions are shown in Fig. 11.1 (left) together with those obtained by the CERN Large Hadron Collider (LHC) [6] experiments in the Summer of 2011.

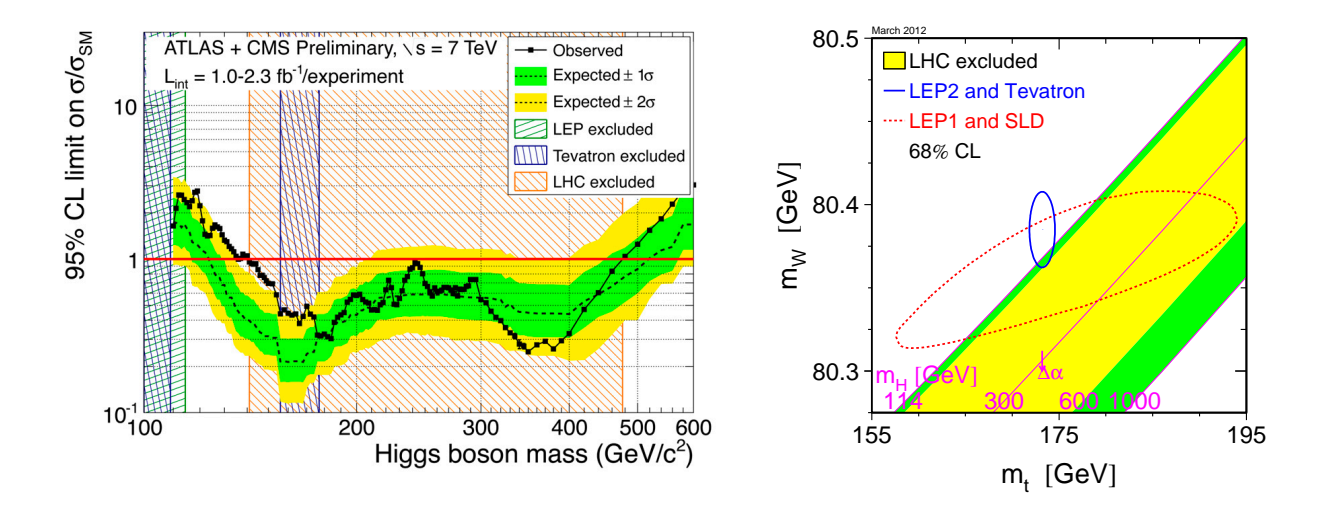


Figure 11.1: Left: Combined 95 % CL upper limits on SM Higgs-boson production prior to the discovery at the LHC in the Summer of 2011. The limits are normalized to the SM expectation, as a function of the Higgs-boson mass. Regions where the observed limit falls below unity are excluded. Right: indirect bounds on m_H from EW precision fits (March 2012).

Right before its discovery, the latest direct searches from the LHC experiments had excluded Higgs-boson mass hypotheses below 600 GeV at the 95% CL, except for a narrow window around $115.5 < m_H < 127$ GeV. This was also the mass range independently favored by indirect constraints from precision measurements of EW-boson masses and couplings in e^+e^- collisions, on and off the

Z-boson mass peak, at SLD, LEP, and LEP2, supplemented by results at the $p\bar{p}$ Tevatron collider that also measured the top-quark mass [7–9]. The right-hand-side plot of Fig. 11.1 illustrates the indirect constraint on m_H from precision fits of the SM as of March 2012 [10], i.e. right before the Higgs-boson discovery. In the SM, m_W and m_t are correlated by their dependence on m_H through radiative corrections. The diagonal green band in Fig. 11.1 represents the region of the (m_t, m_W) plane corresponding to values of m_H between 114 GeV and 1 TeV, a large portion of which (the diagonal yellow band) was already excluded in 2012 by the aforementioned direct LHC limits. On the other hand, the blue ellipse in Fig. 11.1 defines the experimentally allowed region of (m_t, m_W) as of March 2012, greatly improved by LEP2 and Tevatron direct measurements with respect to the case in which LEP1 and SLD data only could be used (red-dashed contour). Consistency with SM measurements, corresponding to the tiny region at the intersection between the blue ellipse and the green diagonal band in Fig. 11.1, yielded a best fit Higgs-boson mass value of $m_H = 94^{+29}_{-24}$ GeV, and a 95% CL upper bound of $m_H < 154$ GeV, in agreement with the LHC exclusion limits and quite on top of where the SM Higgs boson was soon to be found. More details on pre-discovery Higgs-boson direct and indirect bounds can be found in previous PDG reviews [11].

11.1.2 Discovery of the SM Higgs boson

In July 2012, the ATLAS [12] and CMS [13] experiments at CERN's LHC announced the discovery of a new particle with properties consistent with the SM Higgs boson [14,15]. Subsequent analyses of the complete 2011–2012 Run 1 proton–proton dataset provided additional evidence of its compatibility with SM predictions: measurements of its spin, CP properties and width [16–21], and combined fits [22] all agreed well with theoretical expectations.

The characterization of the Higgs boson has continued during the Run 2 (2015-2018) and Run 3 (2022-2026) data-taking periods. The results presented in this Review provide a summary of these measurements.

11.1.3 The SM Higgs boson as a portal to new physics

With the discovery of the Higgs boson, the SM is confirmed to be a spontaneously broken gauge theory and, as such, it could a priori be consistently extrapolated well above the masses of the W and Z bosons. Hence, formally there is no need for new physics at the EW scale. However, as the SM Higgs boson is a scalar particle, it has sensitivity to possible new physics scales. Quite generally, the Higgs-boson mass is affected by the presence of heavy particles and it receives large quantum corrections which destabilize the weak scale barring a large fine-tuning of unrelated parameters. This is known as the Higgs naturalness or hierarchy problem [23], and it has been the prime argument for expecting new physics around and not far above the TeV scale.

To remedy this unsatisfactory feature, theoretically motivated paradigms have been explored for several decades, such as a new fermion-boson symmetry called supersymmetry (SUSY) [24] (for recent reviews, see Refs. [25,26]), or the existence of strong interactions at a scale of the order of a TeV from which the Higgs boson would emerge as a composite state [27] (see Refs. [28,29] for recent reviews). Alternatively, new agents stabilizing the weak scale could also be light but elusive, like in models of neutral naturalness [30,31]. It was also recently appreciated [32,33] that the cosmological evolution of the Universe could drive the Higgs-boson mass to a value much smaller than the cutoff of the theory, alleviating the hierarchy problem without the need for TeV scale new physics, even though there might still be interesting and spectacular signatures [32,34]. This approach spurs a change in perspective invoking our Universe as part of a multiverse that should be treated as a quantum statistical system [35].

Another puzzling aspect of the SM Higgs boson concerns the arbitrariness of its couplings to fermions. This is encoded in the SM through a series of Yukawa couplings, one per massive fermion, proportional to the corresponding fermion mass and therefore displaying a huge and unexplained

scale hierarchy. Furthermore, fermion masses and fermion mass eigenstates are intrinsically related to the origin of flavor mixing and CP-violation in the SM charged gauge currents, where four more arbitrary parameters are embedded in the Cabibbo-Kobayashi-Maskawa (CKM) matrix. Hence, the scalar sector of the SM is responsible for introducing 15 of the 19 input parameters of the theory, 13 of which are related to the Yukawa interaction between the Higgs-boson and massive-fermion (9 masses, excluding neutrinos which are strictly speaking massless in the SM, and 4 CKM parameters) while the remaining two define the scalar potential). These interactions are not of gauge nature and could be messengers of new physics (NP) that will eventually explain the hierarchy of fermion masses and the flavor dynamics of the SM at a deeper level [36].

The Higgs boson offers a special portal to new physics and, in the years since its discovery, it has become a powerful tool to stress test the quantum structure of the SM and to probe the physics landscape beyond it. This has greatly influenced the discussion about future facilities which has emphasized the need for both high-luminosity lower-energy e^+e^- colliders to obtain percent-level measurements of Higgs-boson couplings and higher-energy pp or $\mu^+\mu^-$ colliders to explore NP up to about 10 TeV.

11.1.4 Synopsis of this review

This review is organized as follows. Section 11.2 is a theoretical introduction to the SM Higgs boson, its properties, production mechanisms and decay rates, and a concise updated review of the corresponding theoretical predictions. The state-of-the-art of experimental measurements are described in Section 11.3, including measurements of SM Higgs-boson inclusive cross sections and branching ratios, differential cross sections and simplified template cross sections, couplings to gauge bosons and fermions, self-coupling, mass, width, and spin and CP properties. Section 11.4 reviews how the discovery of the SM Higgs boson has provided a portal to NP exploration and has greatly influenced the direct search for NP at the LHC. Finally, Section 11.5 provides a short summary and a brief outlook.

11.2 The Standard Model and the mechanism of electroweak symmetry breaking 11.2.1 The scalar Lagrangian of the Standard Model

In the SM [1] EWSB [2] is responsible for generating a mass for the W and Z gauge bosons rendering the weak interactions short ranged. The SM $\mathrm{SU}(3)_C \times \mathrm{SU}(2)_L \times \mathrm{U}(1)_Y$ gauge symmetry is spontaneously broken to $\mathrm{SU}(3)_C \times \mathrm{U}(1)_Q$ by introducing a complex scalar field (Φ) , doublet of $\mathrm{SU}(2)_L$ and with hypercharge Y=1, through the gauge-invariant $Higgs\ Lagrangian\ [2]$,

$$\mathcal{L}_{\text{Higgs}} = (D_{\mu}\Phi)^{\dagger}(D^{\mu}\Phi) - V(\Phi), \qquad (11.1)$$

where $D_{\mu}\Phi = (\partial_{\mu} + ig\sigma^{a}W_{\mu}^{a}/2 + ig'YB_{\mu}/2)\Phi$, g and g' are the SU(2)_L and U(1)_Y gauge couplings, respectively, σ^{a} (a = 1, 2, 3) are the Pauli matrices, Y is the hypercharge quantum number, and the potential $V(\Phi)$ reads:

$$V(\Phi) = \mu^2 \Phi^{\dagger} \Phi + \lambda (\Phi^{\dagger} \Phi)^2. \tag{11.2}$$

 $Q = T_{3L} + Y/2$ is the conserved electric charge quantum number, with T_{3L} the eigenvalue of the diagonal generator of $SU(2)_L$ (e.g. $T_{3L} = 1/2$ for up-type quarks, etc.).

The scalar field Φ can be written as

$$\Phi = \frac{1}{\sqrt{2}} \begin{pmatrix} \sqrt{2}\phi^+ \\ \phi^0 + ia^0 \end{pmatrix},\tag{11.3}$$

where ϕ^0 and a^0 denote the doublet's CP-even and CP-odd neutral components, and ϕ^+ its complex charged component, respectively. The covariant-derivative *kinetic* term in Eq. (11.1) contains both

truly kinetic terms and the interaction terms between the gauge fields and the scalar field Φ . Upon spontaneous symmetry breaking it is also responsible for the W and Z gauge-boson mass terms. $V(\Phi)$ is the most general renormalizable scalar potential invariant under $\mathrm{SU}(2)_L \times \mathrm{U}(1)_Y$. If the quadratic term is negative ($\mu^2 < 0$), the global minimum of the $V(\Phi)$ potential occurs for a non-zero vacuum expectation value (VEV) of the field Φ such that $\langle \Phi^\dagger \Phi \rangle = v^2/2 = -\mu^2/2\lambda$. Choosing a particular field configuration that satisfies this condition breaks the $\mathrm{SU}(2)_L \times \mathrm{U}(1)_Y$ gauge symmetry on the vacuum and induces the spontaneous breaking of the electroweak SM gauge symmetry $\mathrm{SU}(2)_L \times \mathrm{U}(1)_Y$ to the residual $\mathrm{U}(1)_Q$ gauge symmetry of quantum electrodynamics (QED). In particular, if one chooses the neutral component of the scalar doublet to acquire a non-zero (real) vacuum expectation value $\langle \phi^0 \rangle \equiv v = \sqrt{-\mu^2/\lambda}$, the global minimum of the theory is realized by

$$\langle \Phi \rangle = \frac{1}{\sqrt{2}} \begin{pmatrix} 0 \\ v \end{pmatrix} \,. \tag{11.4}$$

The global minimum of the theory defines the ground state, and spontaneous symmetry breaking occurs since the (global and/or local) symmetry of the Lagrangian is not respected by the ground state. From the four generators of the $\mathrm{SU}(2)_L \times \mathrm{U}(1)_Y$ SM gauge group, three are spontaneously broken on the vacuum, i.e. they do not leave the ground state invariant. This implies the existence of three massless (would-be) Goldstone bosons identified with three of the four degrees of freedom of the scalar field Φ . Using a gauge choice (unitary gauge) where three components of the scalar field Φ are reabsorbed by an $\mathrm{SU}(2)_L$ gauge transformation into the longitudinal components of the W and Z gauge fields, one can then parametrize the field Φ in terms of a single scalar (CP-even, spin s=0) real component (H), the physical Higgs field, as

$$\Phi = \frac{1}{\sqrt{2}} \begin{pmatrix} 0 \\ H + v \end{pmatrix} . \tag{11.5}$$

This parametrization makes the physical content of the scalar Lagrangian in Eq. (11.1) completely manifest. The scalar field Φ couples to the W_{μ} and B_{μ} gauge fields associated with the $\mathrm{SU}(2)_L \times \mathrm{U}(1)_Y$ local symmetry through the covariant derivative appearing in the kinetic term of the Higgs Lagrangian in Eq. (11.1). The neutral and the two charged massless Goldstone degrees of freedom mix with the gauge fields corresponding to the broken generators of $\mathrm{SU}(2)_L \times \mathrm{U}(1)_Y$ and become, in the unitarity gauge, the longitudinal components of the Z and W physical gauge bosons, respectively. As a result, the Z and W gauge bosons acquire masses,

$$m_W^2 = \frac{g^2 v^2}{4}, \quad m_Z^2 = \frac{(g'^2 + g^2)v^2}{4}.$$
 (11.6)

The fourth generator remains unbroken since it is the one associated with the conserved $\mathrm{U}(1)_Q$ gauge symmetry, and its corresponding gauge field, the photon, remains massless. Similarly, the eight color gauge bosons, the gluons, corresponding to the conserved $\mathrm{SU}(3)_C$ gauge symmetry with eight unbroken generators, also remain massless (though confined inside hadrons and mesons as the result of the asymptotic freedom behavior of Quantum ChromoDynamics (QCD)). Hence, from the initial four degrees of freedom of the Higgs field, two are absorbed by the W^\pm gauge bosons, one by the Z gauge boson, and there is one remaining degree of freedom, H, that is the physical Higgs boson [2].

The Higgs boson couples to the W^{\pm} and Z gauge-boson with strength proportional to their mass square as dictated by the minimal coupling induced by the covariant-derivative terms, namely:

$$\mathcal{L}_{\text{Higgs}}^{V} = \delta_{V} \frac{2m_{V}^{2}}{v} V_{\mu} V^{\mu} H + \delta_{V} \frac{m_{V}^{2}}{v^{2}} V_{\mu} V^{\mu} H^{2}, \qquad (11.7)$$

where $V=W^{\pm}$ or Z and $\delta_W=1, \delta_Z=1/2$. On the other hand, the Higgs boson is neutral under the electromagnetic interactions and transforms as a singlet under $SU(3)_C$. Hence it does not couple at tree level to photons and gluons. The Higgs boson coupling to gluons [37, 38] is induced at the lowest perturbative order by a one-loop process in which H couples to a virtual $t\bar{t}$ pair (with minor contributions from the other lighter quarks). Likewise, the Higgs boson coupling to photons is also generated via loops, although in this case the one-loop graph with a virtual W^+W^- pair provides the dominant contribution [39] and it is interfering destructively with the smaller contribution involving a virtual $t\bar{t}$ pair (as such, the Higgs coupling to photons is sensitive to the relative phase of the interactions between bosons and fermions).

Finally the $V(\Phi)$ potential once expressed in terms of the Higgs-field H through Eq. (11.5) contributes the following terms to the Higgs Lagrangian:

$$\mathcal{L}_{\text{Higgs}}^{H} = -\frac{1}{2}m_{H}^{2}H^{2} - \frac{3m_{H}^{2}}{v}\frac{H^{3}}{3!} - \frac{3m_{H}^{2}}{v^{2}}\frac{H^{4}}{4!},$$
(11.8)

where one can identify the first term as the Higgs-field mass term $(m_H^2 = 2\lambda v^2)$ and the remaining two terms as the H-field cubic and quartic self-interaction terms. We notice that the Higgs Lagrangian depends on two parameters, μ^2 and λ , that can be traded for any other two precisely measured quantities, such as m_H and v, which are normally chosen as input parameters in precision fits of the SM. Indeed, the Higgs-boson mass is not predicted by the SM and its precise measurement (see Sec. 11.3.7) is therefore essential to test the consistency of the SM theory. We remind that $v = (\sqrt{2}G_F)^{-1/2} \simeq 246$ GeV can be determined very precisely in terms of the so-called Fermi constant (G_F) which is measured in muon decay with a precision of 0.6 ppm [40].

11.2.2 The Yukawa Lagrangian of the Standard Model

A separate term in the SM Lagrangian, the so-called Yukawa Lagrangian,

$$\mathcal{L}_{\text{Yukawa}} = -\hat{Y}_{d_{ij}}\bar{q}_{L_{i}}\Phi \ d_{R_{j}} - \hat{Y}_{u_{ij}}\bar{q}_{L_{i}}\tilde{\Phi}u_{R_{j}} - \hat{Y}_{l_{ij}}\bar{l}_{L_{i}}\Phi \ e_{R_{j}} + h.c., \tag{11.9}$$

introduces a renormalizable gauge invariant interaction between the scalar field Φ and all the massive fermions (quarks and leptons) of the SM and, upon spontaneous symmetry breaking, generates their mass terms. In fact, Dirac-type mass terms violates the chiral gauge symmetry of the SM that assigns left-handed and right-handed fermion fields to different $SU(2)_L$ representations. In the Lagrangian above, $\tilde{\Phi} = i\sigma_2 \Phi^*$ and q_L (l_L) and u_R , d_R (e_R) are the quark (lepton) SU(2)_L doublets and singlets, respectively, while in each term $\hat{Y}_{f_{ij}}$ is a 3 × 3 matrix of couplings in family space with indices (i, j = 1, 2, 3) referring to the three families in the up-quark, down-quark or charged lepton sectors (f = u, d, l). The mass term for neutrinos is omitted, but could be added in an analogous manner to the up-type quarks when right-handed neutrinos are supplementing the SM particle content. Neutrinos (having Q=0) can also acquire Majorana masses via nonrenormalizable dimension-5 effective interactions with the Higgs field [41]. Because of the special nature of neutrino masses and their potential origin from the interactions with new physics well above the electroweak scale, the extension of adding right-handed neutrino fields to the SM is considered in the context of models beyond the SM. Once the Higgs field acquires a VEV, and after rotation to the fermion mass-eigenstate basis that also diagonalizes the Higgs-fermion interactions, $\hat{Y}_{f_{ij}} \to y_{f_i} \delta_{ij}$, all fermions acquire a mass given by $m_{f_i} = y_{f_i} v / \sqrt{2}$ (i = 1, 2, 3). Rotating to the fermion mass-eigenstate basis has two major consequences: 1) it simultaneously diagonalizes the fermion mass matrices and their couplings to the Higgs boson therefore forbidding Higgs-mediated flavor changing neutral currents, and 2) since the rotations of the up-type (U_L^u) and down-type (U_L^d) left-handed quarks are independent $(U_L^u \neq U_L^d)$ rotating to the mass eigenstates gives rise to the Cabibbo-Kobayashi-Maskawa (CKM) mixing matrix in the charged gauge currents, where $V_{\text{CKM}} = (U_L^u)^{\dagger} U_L^d$, and can therefore be considered as the origin of flavor dynamics and CP-violation in the EW sector of the SM. The Yukawa Lagrangian therefore connects some of the aspects of the SM that are most likely to offer a natural portal to new physics.

11.2.3 The Standard Model custodial symmetry

The SM Higgs and Yukawa Lagrangians, $\mathcal{L}_{\text{Higgs}} + \mathcal{L}_{\text{Yukawa}}$ of Eq. (11.1) and Eq. (11.9), are, by construction, $\text{SU}(2)_L \times \text{U}(1)_Y$ gauge invariant, but they also have an approximate global symmetry. In the limit $g' \to 0$ and $y_f \to 0$, a global $\text{SU}(2)_R$ symmetry emerges. This symmetry is preserved for non-vanishing Yukawa couplings provided $\hat{Y}_u = \hat{Y}_d$. Once the Higgs field acquires a VEV, both the $\text{SU}(2)_L$ and $\text{SU}(2)_R$ symmetry groups are broken but the diagonal subgroup $\text{SU}(2)_{L+R}$ remains unbroken and it is this subgroup that defines the so-called custodial symmetry of the SM [42].

In the limit $g' \to 0$, the W^{\pm} and Z gauge bosons have equal mass and form a triplet of the $SU(2)_{L+R}$ unbroken global symmetry. Using the expressions for the W and Z gauge boson masses in term of the gauge couplings, one obtains at tree level

$$\frac{m_W^2}{m_Z^2} = \frac{g^2}{g'^2 + g^2} \equiv \cos^2 \theta_W \quad \text{i.e.} \quad \rho \equiv \frac{m_W^2}{m_Z^2 \cos^2 \theta_W} = 1.$$
 (11.10)

The custodial symmetry protects the above relation from large radiative corrections. All corrections to the ρ parameter are therefore proportional to terms that break the custodial symmetry. For instance, radiative corrections involving the Higgs boson are proportional to $\sin^2\theta_W$, $\delta\rho = -11G_F m_Z^2 \sin^2\theta_W \log(m_H^2/m_Z^2)/(24\sqrt{2}\pi^2)$, and vanish in the limit $g' \to 0$. Since $m_t \neq m_b$, there are also relevant radiative corrections generated by massive fermions. They are proportional to $m_t^2 + m_b^2 - 2(m_t^2 m_b^2) \log(m_t^2/m_b^2)/(m_t^2 - m_b^2)$ and would indeed vanish for $m_t = m_b$ [43]. Precision measurements of electroweak observables are powerful in constraining such large radiative corrections.

Given the extreme precision with which the ρ parameter has been measured experimentally, the custodial isospin symmetry is a very powerful probe of physics beyond the SM since it imposes the same strong constraints on any large radiative corrections coming from new-physics degrees of freedom.

11.2.4 Stability of the scalar potential of the Standard Model

Quantum effects determine the evolution of the parameters of the SM and can therefore affect the shape of the scalar potential and the stability of the SM vacuum (for a recent review on the topic see [44]). Proving absolute stability versus metastability depends in a very sensitive way on the values of the Higgs-boson mass, the top-quark mass, and the strong coupling constant, their uncertainties, and correlations [45]. In this respect, the discovery of the Higgs boson with $m_H \approx 125$ GeV has far reaching consequences within the SM framework.

For the value of Higgs-boson mass experimentally measured, the EW vacuum of the Higgs potential is most likely metastable [45], although this is influenced by new physics that may exists below the Planck scale. The high-energy evolution of λ shows that it becomes negative at energies $\Lambda = \mathcal{O}(10^{11})$ GeV (even though λ could remain positive till higher energy, maybe all the way to the Planck scale, if the top quark mass exceeds its current measured value by 3σ). When this occurs, the SM Higgs potential develops an instability and the long term existence of the EW vacuum is challenged. This behavior may call for new physics at an intermediate scale before the instability develops, i.e., below M_{Planck} , even though new physics at M_{Planck} could influence the stability of the EW vacuum and possibly modify this conclusion [46]. The consequences of the instability of the EW vacuum on high-scale inflation have been discussed in Ref. [47]. It was also noticed that Higgs field fluctuations during inflation could seed the formation of primordial black holes, possibly

making up the Dark Matter relic abundance [48] or they could produce a stochastic background of gravitational waves with characteristic structures [49], offering a probe of the EW vacuum near criticality.

The lifetime of the EW metastable vacuum is determined by the rate of quantum tunneling from this vacuum into the true vacuum of the theory (for the most recent computation of the EW vacuum lifetime within the SM, see Ref. [44, 50, 51]).

Within the SM, the running of the Higgs self coupling slows down at high energies with a cancellation of its β -function at energies just one to two orders of magnitude below the Planck scale [52]. This slow evolution of the quartic coupling is responsible for saving the EW vacuum from premature collapse. It might also help the Higgs boson to play the role of an inflaton [53] (see, however, Ref. [54] for potential issues with this Higgs-boson-as-an-inflaton idea).

11.2.5 Production and decay modes of the Standard-Model Higgs boson

Production and decay modes of the SM Higgs boson (H) can be calculated within the Standard Model including quantum corrections. This section briefly reviews the state-of-the-art of SM predictions for Higgs-boson production cross sections at hadron colliders and discusses the main characteristics of Higgs-boson production at lepton colliders. The most updated predictions for the

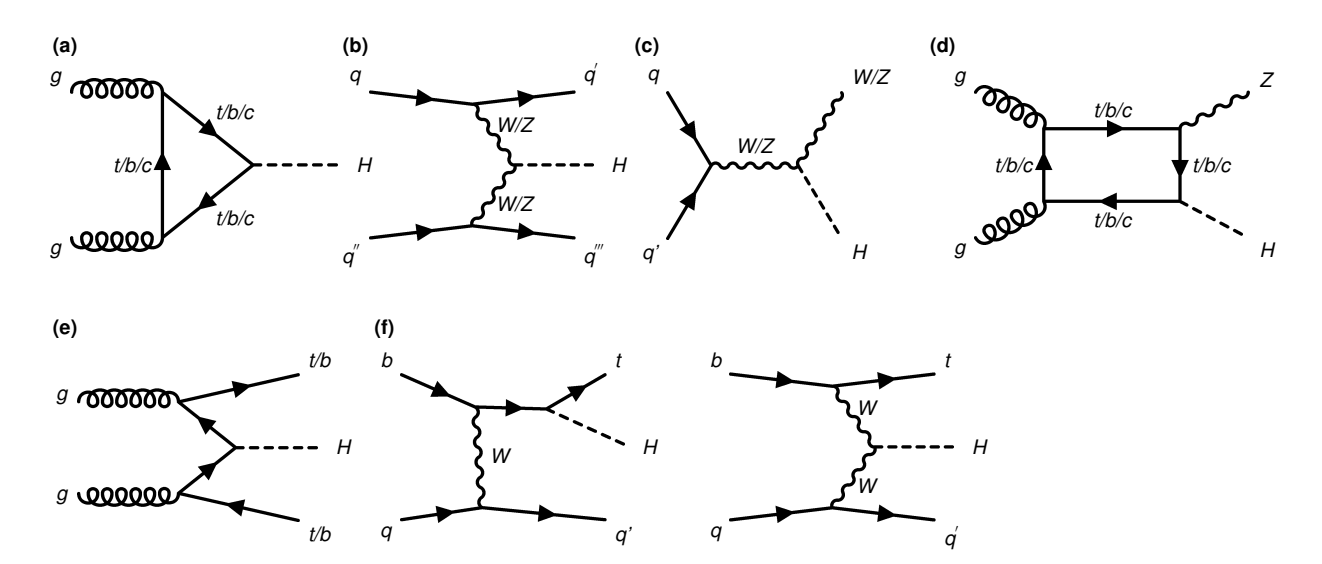


Figure 11.2: Examples of Feynman diagrams for Higgs-boson production via (a) gluon fusion, (b) vector-boson fusion, and associated production with (c)-(d) vector bosons, (e) top- or bottom-quark pairs, or (f) a single top quark.

SM Higgs-boson decay branching ratios and total decay width are also presented. In-depth studies of the corresponding theoretical uncertainties are available in the literature and will be referred to in the following as needed. A summary of all most recent measurements of SM Higgs-boson production and decay rates by the LHC experiments is the subject of Sec. 11.3.

11.2.5.1 Standard-Model Higgs-boson production at hadron colliders

The main production mechanisms of the SM Higgs boson at the Tevatron collider and the LHC are gluon fusion $(gg \to H)$, vector-boson fusion $(qq \to qqH)$, for both quarks and antiquarks), associated production with a gauge boson $(q\bar{q}^{(')} \to ZH/WH)$ and $gg \to ZH$, associated production with a $t\bar{t}$ pair $(q\bar{q}, gg \to t\bar{t}H)$ or $b\bar{b}$ pair $(q\bar{q}, gg \to b\bar{b}H)$, and associated production with a single top

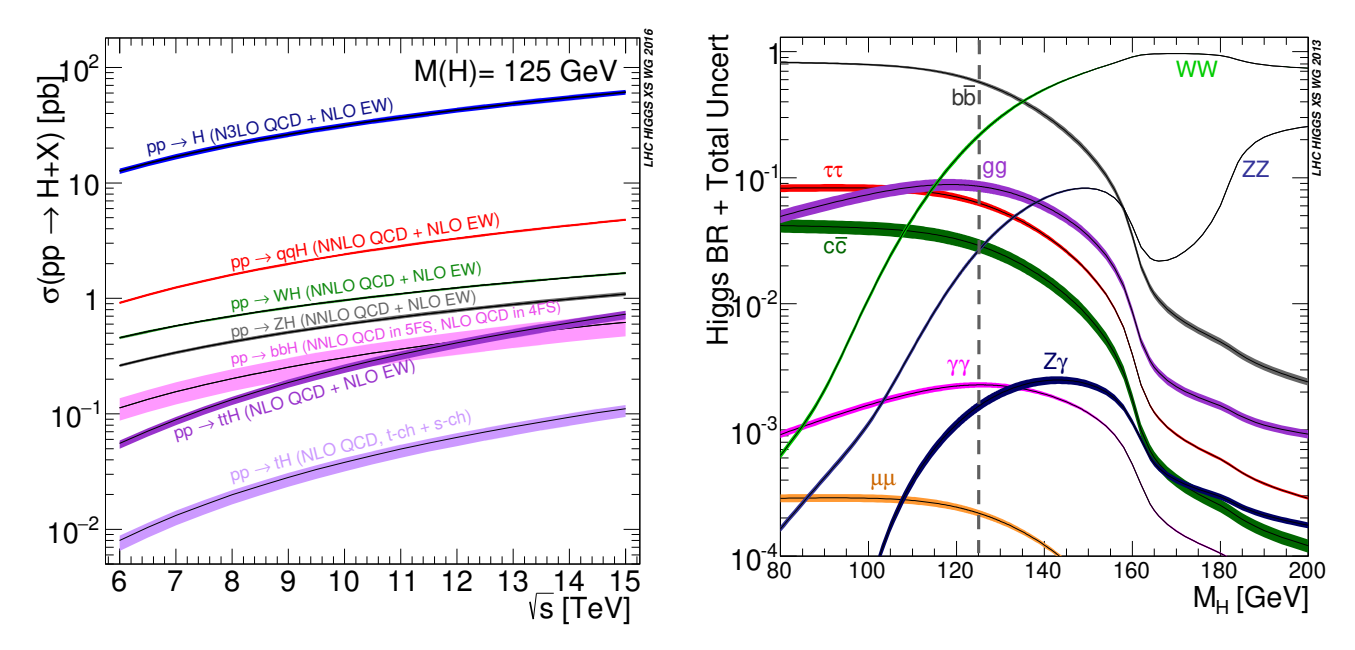


Figure 11.3: (Left) The SM Higgs boson production cross sections as a function of the center-of-mass energy, \sqrt{s} , for pp collisions [55]. The VBF process is indicated here as qqH. (Right) Branching ratios for the main decays of a SM-like Higgs boson in the low mass region, including near $m_H = 125 \,\text{GeV}$ [58, 59]. The theoretical uncertainties are indicated as bands.

quark $(bq \to tH + q')$. ² Examples of Feynman diagrams for each production mode are illustrated in Figures 11.2(a)–(f).

The total cross sections for the main production processes of a SM Higgs boson with $m_H = 125$ GeV in pp collisions (LHC) as a function of \sqrt{s} , the center-of-mass energy, are summarized in Fig. 11.3 (left) [55]. The bands indicate the residual theoretical uncertainties based on the studies presented in Refs. [56–60] and correspond to the perturbative order of QCD and EW corrections indicated on each band. The corresponding results for $\sqrt{s} = 7$, 8, 13, 13.6, and 14 TeV are summarized in Table 11.1 which has been updated with results that will be published in Report 5 of the LHC Higgs Working Group. A detailed discussion, including uncertainties in the theoretical calculations due to missing higher-order effects and experimental uncertainties on the determination of SM parameters involved in the calculations, can be found in Refs. [56–60]. These references also contain state-of-the-art discussions on the impact of PDF uncertainties, QCD scale uncertainties, and uncertainties due to different procedures for including higher-order corrections matched to parton shower simulations, as well as uncertainties due to hadronization and parton-shower effects.

More recent improved calculations and the corresponding accuracy will be highlighted in the following discussion of individual production modes, where the status of the corresponding differential distributions is also illustrated.

i. Gluon fusion production mechanism

At high-energy hadron colliders, the Higgs boson production mechanism with the largest cross section is the gluon-fusion process (ggF), $gg \to H + X$, mediated by the exchange of a virtual heavy quark (see Fig. 11.2-a), where the top quark is dominant due to its large Yukawa coupling [62].

²The order in which the SM Higgs-boson production modes have been listed here reflects their cross-section hierarchy at the LHC for $\sqrt{s}=13$ TeV. The relative importance of various production modes is different between pp and $p\bar{p}$ colliders and depends on the center-of-mass energy.

Table 11.1: The SM Higgs boson production cross sections for $m_H = 125 \,\mathrm{GeV}$: 1) at the Tevatron (*), corresponding to $p\bar{p}$ collisions at center-of-mass energy $\sqrt{s} = 1.96 \,\mathrm{TeV}$, and 2) at the LHC, corresponding to pp collisions at center-of-mass energies $\sqrt{s} = 7.8 \,\mathrm{TeV}$ (Run 1), 13 TeV (Run 2), 13.6 TeV (Run 3), and 14 TeV (Run 4). The predictions for the Tevatron energy are the ones used in Ref. [61], while the ones for the LHC energies are taken from Refs. [55–60] with updates that will be published in the Report 5 of the LHC Higgs Working Group. The uncertainties are estimated assuming no correlation between α_S and PDF uncertainties. Parametric uncertainties are combined linearly with the rest of theoretical uncertainties. A detailed discussion of the estimated uncertainties is given for each case in the references above.

$\frac{\sqrt{s}}{(\text{TeV})}$	Production cross section (in pb) for $m_H = 125 \text{GeV}$							
	ggF	VBF	WH	ZH	$t ar{t} H$	tH	$b ar{b} H$	total
1.96*	$0.95^{+17\%}_{-17\%}$	$0.065^{+8\%}_{-7\%}$	$0.13^{+8\%}_{-8\%}$	$0.079^{+8\%}_{-8\%}$	$0.004^{+10\%}_{-10\%}$	_	_	$1.23^{+13\%}_{-13\%}$
7	$16.7^{+6.3\%}_{-9.4\%}$	$1.25^{+3.4\%}_{-3.4\%}$	$0.582^{+3.1\%}_{-3.3\%}$	$0.342^{+4.8\%}_{-4.5\%}$	$0.09^{+5.6\%}_{-10.2\%}$	$0.013^{+8.2\%}_{-16.6\%}$	$0.171^{+17\%}_{-17\%}$	$19.2^{+5.5\%}_{-8.2\%}$
8	$21.3^{+6.4\%}_{-9.4\%}$	$1.61^{+3.3\%}_{-3.3\%}$	$0.708^{+2.9\%}_{-3.2\%}$	$0.424^{+4.8\%}_{-4.3\%}$	$0.13^{+5.9\%}_{-10.1\%}$	$0.020^{+8.1\%}_{-16.1\%}$	$0.221^{+16\%}_{-16\%}$	$24.4^{+5.6\%}_{-8.2\%}$
13	$48.4^{+6.9\%}_{-9.5\%}$	$3.81^{+3.4\%}_{-3.4\%}$	$1.38^{+2.4\%}_{-2.6\%}$	$0.893^{+5.4\%}_{-4.8\%}$	$0.531^{+5.5\%}_{-6.3\%}$	$0.076^{+8.5\%}_{-18\%}$	$0.528^{+15\%}_{-16\%}$	$55.6^{+6.0\%}_{-8.3\%}$
13.6	$52.1^{+6.9\%}_{-9.5\%}$	$4.11^{+3.3\%}_{-3.3\%}$	$1.47^{+2.4\%}_{-2.6\%}$	$0.954^{+5.6\%}_{-5.0\%}$	$0.592^{+4.3\%}_{-5.0\%}$	$0.085^{+8.5\%}_{-18\%}$	$0.569^{+12\%}_{-12\%}$	$59.9^{+6.0\%}_{-8.3\%}$
14	$54.5^{+7.0\%}_{-9.5\%}$	$4.32^{+3.3\%}_{-3.3\%}$	$1.52^{+2.3\%}_{-2.5\%}$	$0.995^{+5.6\%}_{-4.9\%}$	$0.639^{+4.3\%}_{-5.0\%}$	$0.092^{+8.0}_{-17\%}$	$0.597^{+14\%}_{-15\%}$	$62.7^{+6.1\%}_{-8.3\%}$

Perturbative corrections to the gluon-fusion process are extremely important and have been studied in detail with the goal of reducing the theoretical uncertainty to a few percent, as needed to realize the HL-LHC Higgs-physics program. Including the full dependence on the quark and Higgs boson masses, the cross section has been calculated at the next-to-leading order (NLO) α_s in Refs. [63,64]. To a very good approximation, the leading top-quark contribution can be evaluated in the limit $m_t \to \infty$ by matching the SM to an effective theory [65]. The gluon-fusion amplitude is then evaluated from an effective Lagrangian containing a local $HG^a_{\mu\nu}G^{a\mu\nu}$ operator [37,38]. In this approximation, the cross section has been first calculated at next-to-next-to-leading order (NNLO) [66] and is now known at next-to-next-to-next-to-leading order in the α_s expansion (N3LO QCD) [67,68]. Recently, first building blocks towards the next-to-N3LO calculation (N4LO) have appeared in the literature [69–72]. Public tools such as iHixs [73] and SusHi [74] allow to derive state-of-the-art predictions for ggF inclusive production in the $m_t \to \infty$ approximation³.

The validity of the effective theory with infinite m_t is greatly enhanced by rescaling the result by the exact LO result: $\sigma = (\sigma_{m_t}^{\rm LO}/\sigma_{m_t=\infty}^{\rm LO}) \times \sigma_{m_t=\infty}$ [59]. The large top-quark mass approximation, after this rescaling of the cross section, yields a NNLO QCD result that has been found to approximate the full NNLO total cross section to percent level accuracy [66], as confirmed by the the exact NNLO QCD calculation including full top-quark mass dependence [75]. Contributions from lighter quarks propagating in the loop are suppressed proportionally to m_q^2/m_H^2 . Their leading contribution arise from the interference with top-quark induced gluon fusion, and can be enhanced

³In iHixs, the top-quark mass dependence is exact at NLO, and only the NNLO is calculated in the $m_t \to \infty$ approximation

by logarithms of m_q^2/m_H^2 [76–78]. Finite-mass effects from bottom-top quark interference at NNLO in QCD have been recently calculated [79] including their dependence on the light-quark renormalization and flavor scheme [80]. These studies have reduced the residual 6% theoretical uncertainty of the N3LO results by more than a third.

The LO contribution and NLO QCD corrections [65] amount to about 80% of the total N3LO QCD cross section. The NNLO QCD corrections [81] further enhance the cross section by approximately 30% of the LO plus NLO result (at $\mu_f = \mu_r = m_H/2$). At N3LO QCD, the perturbation series is rather stable with a mere enhancement of 3% with respect to the NNLO QCD total cross section, and a central value quite insensitive to threshold resummation effects with the scale choice $\mu_f = \mu_r = m_H/2$ [59, 67, 68, 82, 83]. EW radiative corrections have been computed at NLO and increase the LO cross section by about 5% for $m_H \simeq 125\,\mathrm{GeV}$ [84]. Mixed QCD-EW corrections have been intensively investigated beyond initial studies obtained in either limit of heavy [85] or massless [86] gauge bosons, and first estimates including most relevant building blocks have been calculated, reducing the residual uncertainties from mixed QCD-EW corrections to less than 1% [87]. The residual PDF uncertainty, estimated to contribute 1-2% to the total theoretical uncertainty. relies on NNLO or approximate N3LO (aN3LO) PDF sets [88–90], and, given the shift observed when using aN3LO versus NNLO PDF, may have been underestimated. Up-to-date values of the N3LO QCD+NLO EW predictions for ggF production of a SM Higgs boson with $m_H = 125$ GeV for different LHC center-of-mass energies are collected in Table 11.1, from an update of the results reported in Ref. [59] to which we refer for a comprehensive discussion of input parameters and residual uncertainties.

Besides considering the inclusive Higgs boson production cross section at the LHC, it is crucial to study differential distributions in order to probe the properties of the Higgs boson in regions that could be particularly sensitive to new physics effects. The Higgs boson rapidity distribution has been computed in the $m_t \to \infty$ limit at the N3LO QCD order in Ref. [91] and fully differential N3LO QCD predictions for Higgs production in gluon fusion have been obtained by combining N3LO QCD predictions for the Higgs rapidity distribution with NNLO QCD predictions for H+jet [92,93]. First results for the prediction of H+jet at N3LO have been presented in Ref. [94]. Finite quark-mass effects in the Higgs-boson p_T distribution significantly alter its shape. At NLO QCD both top-quark mass effects [95–97] and bottom-quark mass [76,77,98] as well as topbottom interference effects [99] are known in an approximation based on expansions in the quark mass. Beyond NLO, the first differential calculation of NNLO QCD corrections with full top-quark mass dependence, consistently matched to parton shower has been presented in Ref. [100]. Experimental analyses often impose cuts on the kinematics of final-state products in order to improve the signal-to-background ratio. To provide a more exclusive account of Higgs-boson production, NNLO fully differential calculations have been interfaced with parton-shower event generators in various frameworks [101–103]. Using soft-collinear effective theory, large fiducial power corrections induced by fiducial cuts have been resummed at N3LO+N3LL' QCD accuracy, i.e. at next-tonext-to-next-leading-log (N3LL), incorporating the complete $\mathcal{O}(\alpha_s^3)$ singular structure for $q_T \to 0$ allowing one to consistently match to N3LO QCD [83]. This allows for the direct comparison with fiducial measurements and explore different fiducial cuts to suppress fiducial effects. At the same time, resummed calculation are often less flexible and less transparent than fixed-order ones. Given the level of precision currently reached in fixed-order calculations, recent studies for $H \to \gamma \gamma$ in gluon fusion [104] motivate revisiting the choice of standard fiducial cuts and design new ones that could at the same time maximize signal significances and minimize experimental and perturbative systematics, to fully retain the power and conceptual simplicity of fixed-order calculations.

In addition progress has been made to improve the calculation of the Higgs-boson production cross section with a jet veto (the "0-jet bin" or in the presence of a veto bounding the transverse

momentum of the hardest accompanying jet) [105], reaching NNLL accuracy matched to N3LO QCD. These accurate predictions for the jet-veto cross section are required, e.g., to suppress the $t\bar{t}$ background in the $H \to WW$ channel [106,107], and to accurately quantify Higgs-boson production in specific regions of phase space.

ii. Vector-boson fusion production mechanism

The SM Higgs boson production mode with the second-largest cross section at the LHC is vector-boson fusion (VBF). At the Tevatron collider, VBF also occurred, but for $m_H=125\,\mathrm{GeV}$ had a smaller cross section than Higgs boson production in association with a W or Z boson. Higgs boson production via VBF, $qq \to qqH$, proceeds by the scattering of two (anti-)quarks, mediated by t- or u-channel exchange of a W or Z boson, with the Higgs boson radiated off the weak-boson propagator (see Fig. 11.2-b). The scattered quarks give rise to two hard jets in the forward and backward regions of the detector with a large rapidity gap [108]. Because of the color-singlet nature of the weak-gauge boson exchange, gluon radiation from the central-rapidity regions is strongly suppressed. These characteristic features of VBF processes can be exploited to distinguish them from overwhelming QCD backgrounds, including gluon-fusion induced Higgs boson + 2 jet production, and from s-channel WH or ZH production with a hadronically decaying weak gauge boson. After the application of specific selection cuts, the VBF channel provides a clean environment, not only for the Higgs boson searches originally performed, but also for the subsequent determination of Higgs boson couplings at the LHC.

The cross-section is known at N3LO QCD at the inclusive level [109] and at NNLO enforcing the VBF cuts [110–112]. Uncertainties have been estimated to be quite small (permille) at the inclusive level but can be larger (percent) at differential and fiducial level. However, this result is obtained in the DIS/factorized approximation [113] where the fusing gauge bosons are emitted from the two quark legs independently. The leading non-factorizable contributions with two forward jets have been estimated [114,115] and the impact of non-factorizable effects have been studied in Ref. [116]. They give some corrections, also of the order of few permille, to inclusive quantities, but they are an order of magnitude larger for differential observables. Overall, the residual uncertainty is of the order of a few percent but is quite sensitive to the tagging jet cuts and jet radius modeling [117]. VBF production followed by $H \to bb$ or $H \to W^+W^-$ with the W bosons decaying leptonically have been studied at NLO QCD in Ref. [118]. Extensive studies on VBF at fixed order and with parton shower matched computations can be found in Ref. [119], and more recently in Ref. [120]. In addition, EW corrections have been calculated and the VBF process is known at NLO QCD+EW order for some time [121, 122]. When EW corrections are considered, a separation of the H+2 jets production process into VBF and HV (V = W, Z) contributions is no longer straightforward and recent studies [123] have implemented the NLO QCD+EW calculation of H+2 jets with partonshower including both VBF and HV topologies. A state-of-the-art review of VBF can be found in Ref. [124].

iii. WH and ZH associated production mechanism

The next most relevant Higgs boson production mechanisms are associated production with W and Z gauge bosons (see Fig. 11.2-c). The cross sections for the associated production processes, $pp \to VH + X$, with $V = W^{\pm}, Z$ receive contributions at NLO from NLO QCD corrections to the Drell-Yan cross section [125,126] and from NLO EW corrections. The latter, unlike the QCD corrections, do not respect the factorization into Drell-Yan production since there are irreducible box contributions already at one loop [121,127]. At NNLO QCD, while Drell-Yan-like contributions

give the bulk of the corrections to WH production, corrections to ZH production consist of both Drell-Yan-like [128] and gluon-gluon induced contributions that do not involve a virtual Z gauge boson but are such that the Z gauge boson and H boson couple to gluons via top-quark loops (see Fig. 11.2-d) [129]. NLO QCD virtual corrections to the partonic cross section for $qq \to ZH$, in the high-energy and large top mass limits were calculated in Ref. [130], while NLO QCD corrections with full top-quark mass dependence have obtained in Ref. [131, 132], and an updated review can be found in Ref. [133]. In addition, WH and ZH production receive non Drell-Yan-like corrections in the $q\bar{q}'$ and $q\bar{q}$ initiated channels, respectively, at the NNLO level in QCD, where the Higgs boson is radiated off top-quark loops [134]. The full QCD corrections up to NNLO order, the NLO EW corrections and the NLO corrections to the gluon-gluon channel are available in VH@NNLO [135]. NNLO QCD corrections to $pp \to WH+$ jet are important for signal modeling. NLO corrections to the cross section inclusive in the number of jets show excellent convergence while NNLO QCD corrections to exclusive single jet cross section are much more significant [136]. More recently, the inclusive cross section for associated Higgs boson production with a massive gauge boson has been determined up to N3LO QCD too [137]. Recently, the inclusive cross section for associated Higgs-boson production with a massive gauge boson has been determined up to N3LO QCD [137].

As neither the Higgs boson nor the weak gauge bosons are stable particles, their decays also have to be taken into account. Providing full kinematical information for the decay products can furthermore help in the suppression of large QCD backgrounds. Differential distributions for the processes $pp \to WH \to \bar{\nu}_\ell \ell H$ and $pp \to ZH \to \ell^+ \ell^- H/\nu_\ell \bar{\nu}_\ell H$, including NLO QCD and EW corrections, have been presented in Ref. [138]. The NNLO QCD corrections to differential observables for WH production at the LHC, including the leptonic decays of the W boson and the decay of the Higgs boson into a $b\bar{b}$ pair, are presented in Ref. [139]. Full NNLO QCD results for both the production and decay are available [140] and show a large impact of radiation from the final-state bottom quarks. Calculations at the same level, including also the ZH process have been performed [141]. The WH production mode has also been matched to a parton shower at NNLO QCD accuracy [142]. The WH and ZH production modes, especially in the boosted regime, provide a relatively clean environment for studying the decay of the Higgs boson into bottom quarks [143]. Bottom mass effects have been computed at NNLO [144, 145] and tend to increase the rates by 6-7%.

iv. Higgs boson production in association with $t\bar{t}$

Higgs boson radiation off top quarks, $pp \to t\bar{t}H$ (see Fig. 11.2-e), provides a direct probe of the top-Higgs Yukawa coupling. The LO cross section for this production process was computed in Ref. [146]. Later, the NLO QCD [147] and NLO EW corrections [148] were evaluated yielding a moderate increase in the total cross section of at most 20%, but significantly reducing the scale dependence of the inclusive cross section. The EW corrections can be enhanced by large electroweak Sudakov logarithms in particular in the boosted regime often used in the phenomenological analyses [149]. The resummation of soft and Coulomb gluon corrections is presented in Ref. [150] while the resummation of soft gluon contributions close to the partonic kinematical threshold are considered in Refs. [151] to reach a result at NLO+NNLL QCD order. Full off-shell calculations with decaying top quarks are computed at NLO QCD [152] and NLO QCD + EW [153] order, respectively. The fixed-order NLO QCD calculation has been interfaced with the standard parton shower Monte-Carlo generators in Refs. [154], allowing an accurate description of the $t\bar{t}H$ signal, from the energy scale of the hard scattering to the hadronization energy scale. These programs provide the most flexible tools to date for the computation of differential distributions, including experimental selection cuts and vetoes on the final-state particles and their decay products.

The total theoretical uncertainty has been further reduced from 10-15% to about 4% at 13 TeV center-of-mass energy by the first approximate NNLO QCD calculation [155, 156] combined with NLO EW corrections in a fully differential comprehensive study of this production mode [157]. These results do not yet include the two-loop virtual corrections, but they evaluate them using two different methods that yield consistent results within their respective uncertainties. The first method relies on a soft Higgs-boson factorization formula, while the second is based on a high-energy expansion in the small top-quark mass limit. The missing two-loop virtual contributions, which are essential to have a consistent NNLO calculation of $pp \to t\bar{t}H$, are quite challenging and at the cutting edge of current technologies due to the presence of several mass scales (m_H , m_t , plus five kinematic invariants of the 2 \to 3 process). Partial results for well-defined gauge-invariant classes of leading-color two-loop QCD virtual amplitudes have been calculated [158–160] and progress is ongoing to complete the remaining building blocks. For a recent review of the state-of-the-art of theoretical predictions for $pp \to t\bar{t}H$ production see Ref. [161].

Also recently, the fragmentation and splitting functions for the production of a Higgs boson have been computed at order $y_t^2\alpha_s$ and they can be used in the fragmentation region to compute differential cross sections with arbitrary top-quark and Higgs-boson masses directly from the results in the massless limit [162].

Apart from the case in which $H \to \gamma \gamma$, the exploitation of the ttH channel requires a proper description of the background, in particular $t\bar{t}b\bar{b}$, which exhibits an enhancement from shower effects, see Ref. [59] for a detailed discussion. Off-shell effects in $t\bar{t}b\bar{b}$ have been studied in Ref. [163]. Besides the $H \to b\bar{b}$ decay mode, the focus has been broadened and other modes have been studied, in particular the multilepton channel (which combines $H \to \tau^+\tau^-$, $H \to WW^*$, and $H \to ZZ^*$ with subsequent decay to leptons). Other backgrounds such as $t\bar{t}W$ and $t\bar{t}Z$ have also become relevant and intensively analyzed.

v. Other single Higgs-boson production mechanisms at the LHC

The Higgs boson production in association with a single top quark, though subdominant, can bring valuable information on the sign of the top Yukawa coupling. This is due to an almost totally destructive interference between two large contributions, one where the Higgs boson couples to a space-like W boson and the other where it couples to the top quark (see Fig, 11.2-f). This process has been computed at NLO QCD in a five-flavor scheme [164] and amounts to about 90 fb at $\sqrt{s} = 14 \,\text{TeV}$ (with the opposite sign of the top Yukawa coupling, the cross section increases by one order of magnitude while the cross section for associated production with a pair of top quarks is unaffected). Recently, the tHj (and tZj) process has been computed at NLO QCD+EW accuracy [165]. The NLO EW correction is found to be within the NLO QCD theory uncertainties if the 4 vs 5 flavor scheme uncertainty is taken into account. The EW corrections reduce the total cross section by 3-4%.

The inclusive Higgs boson production in association with a pair of bottom quarks $(b\bar{b}H)$ has been computed at the N3LO QCD order in the 5-flavor scheme [166]⁴, while the production with one/two b-jets, defined by specific kinematic cuts, is known respectively at NLO QCD in the 4-flavor scheme and at NNLO QCD in the 5-flavor scheme [167, 168]. Recently, full-color two-loop amplitudes for the $pp \to b\bar{b}H$ have been computed [169], extending previous leading-color results [170]. They contribute at NNLO QCD to the production of a Higgs boson with 2 tagged b jets, and at N3LO QCD to the production with 1 tagged b jet. The first NNLO calculation of $b\bar{b}H$ production in the 4FS interfaced with parton-shower has been recently presented in Ref. [171].

⁴The Higgs boson production in association with charm quarks at N3LO QCD can also be obtained from the same calculation modulus a change of parton densities. NNLO QCD results for the cross section as a function of m_H can be found in [59].

The coupling of the Higgs boson to a bottom quark is suppressed in the SM by the bottom-quark mass over the Higgs VEV, m_b/v , implying that associated production of a SM Higgs boson with bottom quarks is small at the LHC. Yet, at high energy, large logarithms are present and need to be resummed, leading to an enhancement of the inclusive cross section. At $\sqrt{s} = 14 \,\text{TeV}$, the $b\bar{b}H$ cross section can be as large as 550 fb, still two orders of magnitude below the ggF production cross section. Furthermore, the overwhelming ZH and VBF backgrounds (at the inclusive but also differential levels) make it challenging to extract a genuine bottom-quark Yukawa signal in a traditional cut-based analysis [172]. Innovative machine-learning techniques are a promising avenue to obtain information complementary to the ones extracted from $gg \to h \to b\bar{b}$, in particular for what concerns the phase of the bottom-quark Yukawa coupling [173]. In a two Higgs doublet model or a SUSY model, which will be discussed in Section 11.4, this coupling is proportional to the ratio of neutral Higgs boson vacuum expectation values, $\tan \beta$, and can be significantly enhanced for large values of this ratio. Consequently, the $b\bar{b}H$ mode can even become the dominant production process for the Higgs boson, unlike in the SM.

The Higgs boson production in association with charm quarks is also known at NNLO QCD and its cross section is approximately 85 fb at $\sqrt{s} = 13 \text{ TeV}$ [59].

vi. Double Higgs boson production at the LHC

The main interest in the double Higgs-boson production is that it can provide invaluable information on the Higgs potential. In particular, it gives access to the Higgs-boson trilinear self coupling. The dominant production is via ggF $gg \to HH$ (slightly more than 33 fb at 13 TeV) which accounts for more than 90% of the total inclusive cross-section. The sub-leading production mechanisms are VBF HHjj (around 1.7 fb at 13 TeV), HHW^+ (0.33 fb), HHW^- (0.17 fb), HHZ (0.36 fb), and $t\bar{t}HH$ (0.8 fb).⁵ Examples of ggF and VBF double-Higgs production are illustrated in Fig. 11.4, where the possibility of anomalous couplings parametrized by κ_X rescaling factors have also been indicated for future reference (see Sec. 11.3.5.1).

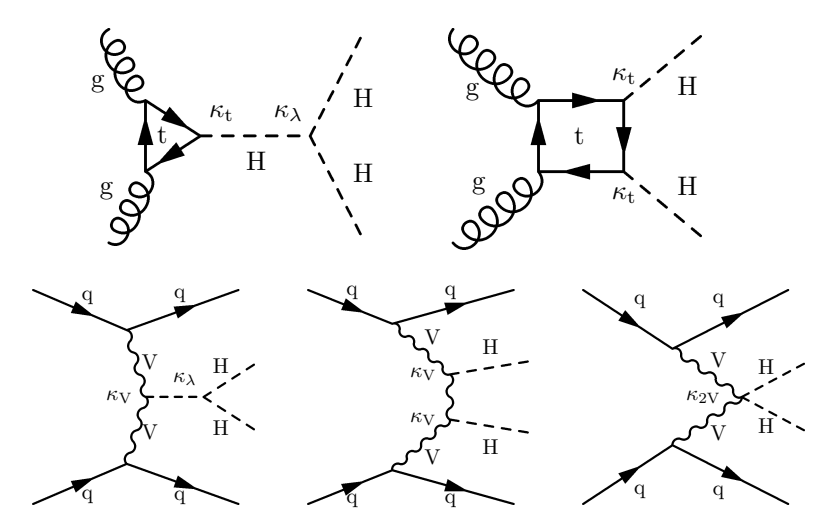


Figure 11.4: Feynman Diagrams for double-Higgs production in proton-proton collisions for ggF (top) and VBF (bottom) production. κ_X factors denote ratios of measured to SM couplings that will be introduced in the discussion of Higgs-boson couplings in Sec. 11.3.5.1.

The fixed order QCD corrections to ggF double-Higgs production, computed in the infinite top

⁵Results for the subleading modes are from the wiki-page of WG4 of the LHC Higgs Working Group (https://twiki.cern.ch/twiki/bin/view/LHCPhysics/LHCHWGHH.

mass limit, are large, typically doubling the cross section from LO to NLO QCD [174], further enhancing it by 20% and reducing the scale uncertainty by a factor 2-3 from NLO to NNLO QCD [175], with a milder increase of order 3% at N3LO [176]. The complete NLO corrections with all top-quark mass effects has also become available numerically [177], revealing a differential K-factor much less flat than predicted in the large top-quark mass approximation. The non-trivial dependence of the results on the renormalization scheme and scale for the top-quark mass has been recognized as one of the main sources of uncertainty and progress has been made in identifying the logarithmic terms responsible for such dependence [178]. In terms of accounting for the top-quark mass dependence, the most complete results so far have been obtained in Ref. [179]. These results include the full top-quark mass dependence at NLO and in the NNLO QCD real radiation matrix elements, and and form the basis of the current recommendation of the LHC Higgs Working Group. A definite assessment of the scale uncertainty would warrant a proper NNLO computation that remains out of reach for the moment, although considerable progress towards it has been recently made [180–182]. The current state-of-the-art for Higgs-pair production via ggF is N3LO+N3LL QCD including full top-quark mass dependence at NLO QCD, with a predicted cross section at 13 TeV of

$$\sigma(gg \to HH)_{\text{ggF}}^{\text{N3LO}+N3LL} = 33.47_{-0.85\%}^{+0.88\%} \text{ fb.}$$
 (11.11)

Among the subleading production modes, double-Higgs production in VBF can be used to derive bounds on both the triple Higgs-boson coupling and the quartic HHVV coupling. Although the rate is quite small, the experiments have been performing searches including the VBF channel [183,184]. The process is known at N3LO QCD [185] and NLO EW [186]. While the NNLO QCD [111,187, 188] and NLO-EW corrections are quite sizable in some kinematic regions, the N3LO QCD are small. NNLO-QCD non-factorizable corrections have been calculated and shown to be small [116]. VBF di-Higgs production has also been interfaced with parton-shower at NLO QCD in multiple frameworks [189, 190].

With a small inclusive cross section and a difficult signal vs background discrimination, the double-Higgs boson production remains a challenging channel to probe and will greatly benefit from the high-luminosity run of the LHC. Nevertheless, as discussed in Section 11.3.6, by combining various decay modes, and using full Run 2 and partial Run 3 data, both ATLAS and CMS have already been able to constrain the trilinear Higgs-boson coupling via double-Higgs production beyond expectations. Continuous theoretical progress will therefore be necessary and timely.

11.2.5.2 Standard-Model Higgs-boson production at lepton colliders

Recently Higgs-boson production at lepton colliders has been a major component of the discussion for future colliders [191, 192]. For a more detailed discussion of Higgs boson production properties at lepton colliders see for example Refs. [193–198].

Lepton colliders, both e^+e^- and $\mu^+\mu^-$, provide alternative mechanisms of Higgs-boson production compared to hadron colliders. The leading production modes depend on the center-of-mass energy and the type of collider.

The dominant Higgs-boson production cross sections at an e^+e^- collider are from the Higgs-strahlung process [37,199], $e^+e^- \to ZH$, and the WW fusion process [200], $e^+e^- \to \bar{\nu}_e\nu_eW^*W^* \to \bar{\nu}_e\nu_eH$. The cross-section for the Higgs-strahlung process scales as the inverse of the collision center-of-mass squared energy, s, and is predominant at lower energies, while the cross-section for the WW-fusion process scales as $\ln(s/m_H^2)$ and dominates at higher energies [201]. The ZZ-fusion mechanism, $e^+e^- \to e^+e^-Z^*Z^* \to e^+e^-H$, also contributes to the Higgs boson production, with a cross-section suppressed by an order of magnitude with respect to that of WW-fusion. The process $e^+e^- \to t\bar{t}H$ [202] becomes important for $\sqrt{s} \geq 500\,\text{GeV}$. e^+e^- lepton colliders with energies between 350 and 500 GeV can provide an absolute measurement of the $e^+e^- \to ZH$ cross section

independent of the Higgs-boson detailed properties by counting events with an identified Z boson and a recoiling mass against the Z that clusters around the Higgs-boson mass. This allows for a model-independent measurement of the HZZ coupling. Combined with the measurement of the $H \to ZZ$ branching ratio, this allows for an indirect measurement of the Higgs-boson width.

All e^+e^- Higgs-production modes are known at NLO of SM interactions (QCD+EW). First results for two-loop EW corrections to $e^+e^- \to ZH$ have been calculated in Refs. [203, 204]. In order to match the experimental precision expected at potential future e^+e^- colliders all processes will have to be known at NNLO, SM input parameters will have to be known with higher precision, and matching schemes between EW corrections and QED parton shower event generators will have to be fully developed [205,206]. In this respect, interesting progress has been made recently [207] to accurately account for beamstrahlung and initial state radiation using the factorization approach primarily developed for hadron colliders and this method is being implemented in Monte Carlo event generators.

Muon colliders running at low-energy can scan the Higgs-boson threshold around $m_H=125~{\rm GeV}$ and measure the Higgs-boson line shape through $\mu^+\mu^-\to H$ s-channel Higgs-boson production. This could give direct access to a precision absolute measurement of the Higgs-boson width and of the muon Yukawa coupling, as well as other couplings entering in the decay of the resonant Higgs boson. Most recently, the focus has shifted to multi-TeV muon collider scenarios with center-of-mass energies between 3 and 10 TeV. In this regime, the virtual electroweak gauge boson content of the muon beam becomes relevant and vector-boson, as W-boson fusion $\mu^+\mu^-\to H\nu_\mu\bar{\nu}_\mu$ and Z-boson fusion $\mu^+\mu^-\to H\mu^+\mu^-$, dominates by several orders of magnitude over off-shell production and associated production $(\mu^+\mu^-\to ZH~{\rm or}~\mu^+\mu^-\to t\bar{t}H)$.

11.2.5.3 Standard-Model Higgs-boson decays: branching ratios and total width

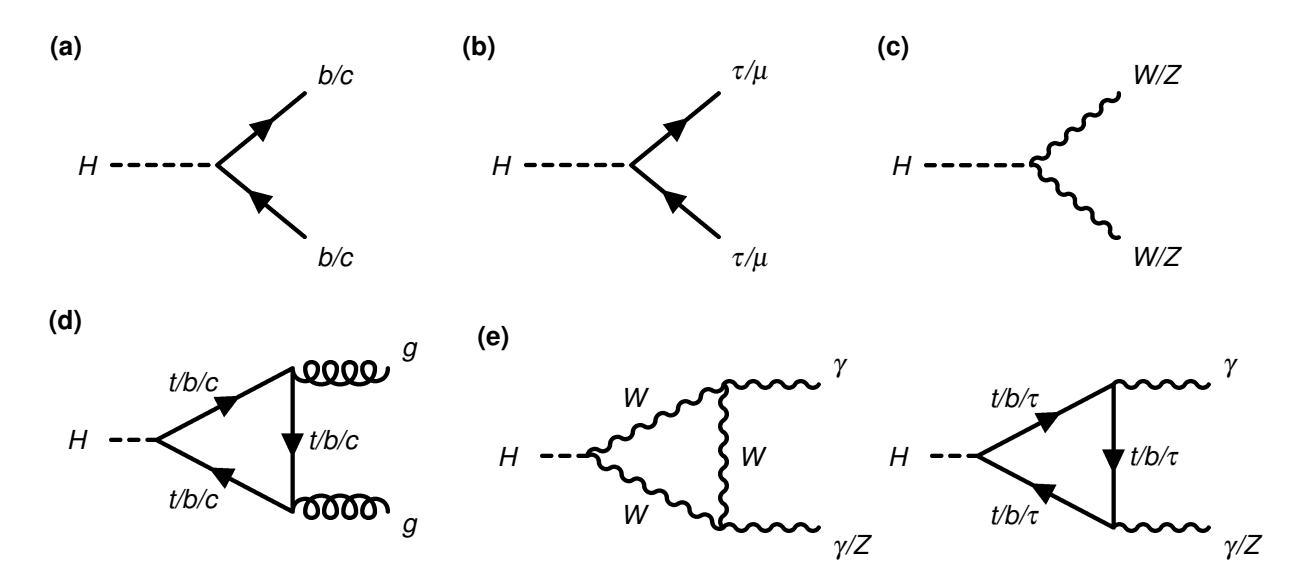


Figure 11.5: Feynman diagrams for the Higgs-boson decays into (a) a pair of quarks, (b) a pair of charged leptons, (c) a pair of vector bosons, (d) a pair of gluons, (e) a pair of photons or a Z boson and a photon.

For the understanding and interpretation of the experimental results, the computation of all relevant Higgs boson decay widths is essential, including an estimate of their uncertainties and, when appropriate, the effects of Higgs boson decays into off-shell particles with successive decays

into lighter SM ones.

The most relevant decay modes of a SM Higgs boson are illustrated in Fig. 11.5(a)-(e) and the corresponding branching ratios as a function of m_H , for m_H up to 200 GeV, are shown in Fig. 11.3 (right), including the most recent theoretical uncertainties. It is interesting to notice how a Higgs boson in the low-mass region allows for the exploration of its couplings to many SM particles through a variety of available decay channels. For the SM Higgs boson with a mass of about 125 GeV the dominant decay modes are $H \to b\bar{b}$ and $H \to WW^*$, followed by $H \to gg$, $H \to \tau^+\tau^-$, $H \to c\bar{c}$ and $H \to ZZ^*$. With much smaller rates follow the Higgs boson decays into $H \to \gamma\gamma$, $H \to Z\gamma$ and $H \to \mu^+\mu^-$. Since the decays into pairs of gluons or photons, and $Z\gamma$ are loop induced, they provide indirect information on the Higgs-boson couplings to WW, ZZ and $t\bar{t}$ in different combinations. They are also sensitive to possible NP contributions running in the loop.

Theoretical results for the branching ratios of the most relevant decay modes of the SM Higgs boson with $m_H = 125\,\text{GeV}$ are listed in Table 11.2. The uncertainties in the branching ratios include the missing higher-order corrections in the theoretical calculations as well as the errors in the SM input parameters, in particular fermion masses and the QCD gauge coupling, involved in the decay. In the following the state-of-the-art of the theoretical calculations compiled by the LHC Higgs Working Group [55] will be discussed and the reader is referred to Refs. [56–59,208] for more details.

The evaluation of the radiative corrections to the fermionic decays of the SM Higgs boson are implemented in HDECAY [209] at different levels of accuracy. The computations of the $H \to b\bar{b}$ and $H \to c\bar{c}$ decays include the NLO QCD corrections with full mass effects and up to N4LO QCD corrections with leading mass corrections, resulting in a corresponding scale dependence of about 0.1% [210,211]. The top-induced QCD corrections, which are related to interference effects between $H \to gg$ and $H \to q\bar{q}$, are known at NNLO in the limit of heavy top quarks and light bottom quarks [211–213] and more recently including the full mass dependence [214–217] with first results at N3LO [218]. Both the electroweak corrections to $H \to b\bar{b}$, $c\bar{c}$ as well as $H \to \tau^+\tau^-$ are known at NLO [219] providing predictions with an overall accuracy of about 1–2% for $m_H \simeq 125\,\text{GeV}$.

The loop induced decays of the SM Higgs boson are known fully at NLO and partially beyond that approximation. For $H \to gg$, the N4LO QCD corrections calculated in the limit of heavy top quarks [220] have reduced the uncertainty from scale dependence to about 0.6% from the 3% uncertainty of the N3LO prediction [64, 221]. For $H \to \gamma\gamma$, the full NLO QCD corrections are available [64, 222] and the three-loop QCD corrections have also been evaluated [223]. The NLO electroweak corrections to $H \to gg$ and $H \to \gamma\gamma$ have been computed in Ref. [224]. All these corrections are implemented in HDECAY [209]. For $m_H \simeq 125\,\text{GeV}$, the overall impact of known QCD and EW radiative effects turns out to be well below 1%. In addition, the contribution of the $H \to \gamma e^+ e^-$ decay via virtual photon conversion has been computed in Ref. [225]. The partial decay width $H \to Z\gamma$ is only implemented at LO in HDECAY, including the virtual W, top-, bottom-, and τ -loop contributions. The NLO QCD corrections have been calculated in Refs. [226–228] leaving a residual estimated uncertainty of about 1.7%. The theoretical uncertainty due to unknown electroweak corrections is estimated to be less than 5%, an accuracy that will be hard to achieve in the measurement of this process at the LHC.

The decays $H \to WW/ZZ \to 4f$ can be simulated with the Prophecy4f Monte-Carlo generator [229] that includes complete NLO QCD and EW corrections for Higgs decays into any possible four-fermion final state. All calculations are consistently performed with off-shell gauge bosons, without any on-shell approximation. For the SM Higgs boson, the missing higher-order corrections are estimated to be roughly 0.5%. Such uncertainties will have to be combined with the parametric uncertainties, in particular those associated to the bottom-quark mass and the strong gauge cou-

Table 11.2: The branching ratios and the relative uncertainty for a SM Higgs boson with $m_H = 125 \,\text{GeV}$. The uncertainties in the branching ratios include the missing higher-order corrections in the theoretical calculations as well as the errors in the SM input parameters, in particular fermion masses and the QCD gauge coupling, involved in the decay [55, 58, 59].

Decay channel	Branching ratio	Rel. uncertainty
$H o b ar{b}$	5.82×10^{-1}	$\pm 1.7\%$
$H \to W^+W^-$	2.14×10^{-1}	$\pm 2.2\%$
$H \to gg$	8.18×10^{-2}	$\pm 7.2\%$
$H \to \tau^+ \tau^-$	6.27×10^{-2}	$\pm 2.3\%$
$H \to c\bar{c}$	2.89×10^{-2}	$^{+6.6\%}_{-2.8\%}$
$H \to ZZ$	2.62×10^{-2}	$\pm 2.2\%$
$H \to \gamma \gamma$	2.27×10^{-3}	2.8%
$H \to Z \gamma$	1.53×10^{-3}	$\pm 6.9\%$
$H \to \mu^+ \mu^-$	2.18×10^{-4}	$\pm 2.4\%$

pling, to arrive at the full theory uncertainty. A detailed treatment of the differential distributions for a Higgs boson decay into four charged leptons in the final state is discussed in Refs. [58, 230].

The total width of a 125 GeV SM Higgs boson is $\Gamma_H = 4.1$ MeV, with a relative uncertainty of $\pm 1.37\%$. As discussed in Section 11.3.8, the width of the SM Higgs-boson is too narrow to allow for a direct mass line-shape measurement at the LHC. Even the channels with the best mass resolution, namely $H \to \gamma \gamma$ and $H \to ZZ^{(*)} \to 4\ell$ ($\ell = \text{leptons}$), can only place an upper bound on Γ_H around 50 MeV at 68% CL (330 MeV at 95% CL) [231]. On the other hand, much stricter indirect constraints on the Higgs-boson widths can be obtained using simultaneously on-shell and off-shell measurements in the $pp \to VV \to 4\ell$ (V = Z, W) channels [232, 233]. For a given Higgs-boson production channel i (i = ggF, VBF, etc.) followed by the decay of the Higgs boson to four leptons ($pp \to H \to VV \to 4\ell$), the on-shell and off-shell cross sections are proportional to

$$\sigma_i^{\text{on-shell}} \propto \frac{g_p^2 g_d^2}{\Gamma_H} \propto \mu_i^{\text{on-shell}} \quad \text{and} \quad \sigma_i^{\text{off-shell}} \propto g_p^2 g_d^2 \propto \mu_i^{\text{off-shell}},$$
 (11.12)

where g_p and g_d are the couplings associated with the Higgs boson production and decay, respectively, and $\mu_i^{\text{on/off-shell}} = \sigma_i^{\text{on/off-shell}}/\sigma_{i,\text{SM}}^{\text{on/off-shell}}$ are the on/off-shell signal strengths. Measuring only on-shell production cannot constrain the Higgs-boson width since, in the presence of new physics, the rescaling of the couplings and of the total width can conspire to compensate each other. On the other hand, a bound on the Higgs boson width can then be obtained at hadron colliders from the simultaneous measurements of the on-shell and off-shell signal strengths. This assumes that no new physics alters the Higgs boson couplings in the on-shell and off-shell regime differently [234, 235].

While $pp \to 4\ell$ production on the Higgs-boson peak is dominated by the Higgs-boson exchange (signal), off-peak other $pp \to VV \to 4\ell$ background processes dominate ($gg \to VV \to 4\ell$ for ggF and $qq/q\bar{q} \to VV \to 4\ell$ for EW Higgs-boson production). Nevertheless, the Higgs-mediated signal

is still sizable due to the enhanced couplings of the Higgs boson to the longitudinal polarization of the massive vector bosons at high energy. Furthermore, the interference between signal and background processes is quite large and negative, leaving as a characteristic feature a deficit of expected events from background only. Based on the most recent theoretical prediction for both on-shell and off-shell $pp \to VV \to 4\ell$ production [232, 233, 236–238] the LHC experiments have obtained the quite constraining bounds on Γ_H presented in Section 11.3.8.

11.3 Phenomenology of the 125 GeV Higgs boson

The properties of the SM Higgs boson, discovered at CERN in 2012 with a mass near 125 GeV, have been measured with increasing precision by both the ATLAS and CMS experiments. At the LHC, Higgs-boson measurements typically focus on a specific production mechanism and decay mode, taking advantage of the fact that each production—decay combination exhibits distinctive kinematic and topological features. Analysis selections are designed to exploit these features to enhance the separation of the Higgs-boson signal from background processes, and to distinguish among different production and decay modes. To improve the analysis sensitivity, events are typically categorized into exclusive regions based on kinematic properties, such as jet multiplicity, transverse momentum, or invariant mass, as well as lepton flavor. In addition, multivariate algorithms, including boosted decision trees (BDTs) and deep neural networks (DNNs), are used to exploit correlations among observables and to improve the separation between signal and background. The combined use of categorization and multivariate techniques has led to significant improvements in the overall sensitivity of Higgs boson production and decay measurements.

The discussion in this section begins with the experimental features and challenges associated with each decay channel, followed by a treatment of the main production channels. It then reviews the latest measurements of inclusive cross sections, branching ratios, differential cross sections, and simplified template cross sections, and concludes with measurements of the Higgs-boson couplings, mass, width, spin, and CP properties.

11.3.1 Higgs-Boson Decay Channels

As discussed in Section 11.2.5.3, a Higgs boson with a mass of 125 GeV is predicted to decay within 10^{-21} seconds to a wide variety of final states. The identification of each decay mode relies on the distinctive experimental signatures summarized below.

- $H \to bb$: This decay mode has by far the largest branching ratio but its measurement is particularly challenging due to a very large multi-jet background, which can be suppressed by identifying the presence of two b hadrons and also requiring the presence of additional particles associated with the WH or ZH, VBF and $t\bar{t}H$ production processes. Despite these challenges, this channel is particularly useful for Higgs boson transverse momentum measurements in the high- $p_{\rm T}$ regime, where the signal-to-background ratio is enhanced.
- $H \to W^+W^-$: the fully leptonic final state is targeted for this decay mode as it presents two important advantages. The first is the reduction of the multi-jet background that would dominate if one or both W bosons decayed hadronically. The second is related to the particular kinematics resulting from the decay of a scalar and the subsequent decay of the W bosons via the (V-A) interaction. This leads to the charged leptons having a smaller opening angle and a smaller invariant mass compared to the inclusive WW background. The disadvantage of this final state is the presence of neutrinos, which, because they are not detected, leads to a loss of information and prevents a full reconstruction of the final state.
- H → gg: This final state has not been searched for directly since the multi-jet background would overwhelm the signal. It can be inferred indirectly as an "unobserved" decay in combinations of measurements.

- $H \to \tau \bar{\tau}$: The final states targeted for this decay process involve all the decay modes of the tau leptons. Typically, the most sensitive final state involves a combination of one tau lepton that decayed hadronically, and one that decayed leptonically. This decay mode provides sensitive measurements particularly when paired with the VBF production process and in the Higgs boson high- p_t regime when using the ggF production process.
- $H \to c\bar{c}$: Like the $b\bar{b}$ decay mode above, $c\bar{c}$ suffers from a large multi-jet background, from a smaller branching ratio than $b\bar{b}$, and from the $H \to b\bar{b}$ background. In addition, the efficiency for identifying c quarks is less than for b quarks. All of these factors make this final state very challenging to observe at a hadron collider.
- H → ZZ: the decay of the Z bosons to charged leptons is targeted for most measurements, except for off-shell measurements where the decay of one Z boson to neutrinos is also considered. The four charged lepton final state has the advantage of having small backgrounds and allows for a full and precise reconstruction of the Higgs boson's kinematics, including its mass. Its main drawback is the limited event yield, which results in large statistical uncertainties.
- $H \to \gamma \gamma$: Although this final state suffers from a small branching ratio and a very large continuum $\gamma \gamma$ background, a clear resonance in the $\gamma \gamma$ spectrum can be observed thanks to the excellent electromagnetic calorimeter resolution of both experiments. Like the ZZ decay mode, this channel allows for a full reconstruction of the Higgs boson kinematics and provides a high-resolution mass peak used in mass measurements.
- $H \to Z\gamma$: The final state targeted for this decay mode involves the decay of the Z boson to charged leptons. As was the case for $\gamma\gamma$, this decay mode suffers from a very large continuum background and an even smaller branching ratio.
- $H \to \mu \bar{\mu}$: This decay mode is particularly challenging because of the very small branching ratio predicted in the SM and the comparatively much larger Drell-Yan background. However, this Higgs boson final state can be fully reconstructed and features a narrow dimuon mass peak.

There are other SM Higgs boson decays often referred to as 'rare'. Examples of these are the decays to lighter quarks, to meson plus photon final states, or to an electron–positron pair. While many of these modes are searched for at the LHC, either directly or indirectly, the current experimental sensitivity is far from the SM expectation.

11.3.2 Higgs-Boson Production Channels

The main production processes of a SM Higgs boson were discussed in Section 11.2.5. The experimental signatures used to identify these various production modes in measurements at the LHC are summarized below:

- ggH: ggH is the process that contributes the most to Higgs production at the LHC. Unlike other production processes, it does not result in extra particles in the final states (at leading order), which turns out to be its distinguishing feature.
- VBF: This process is characterized by the presence of two forward jets that result from the emission of the two fusing W or Z bosons from the quarks that originate from the incoming protons. The final state consists of two jets that tend to be emitted in the forward and backward directions, respectively, resulting in a large rapidity difference between the jets and a large invariant mass. These kinematic features are also used to reduce the multi-jet background.
- ZH: This production process takes advantage of the leptonic decay of the Z boson, either to two charged leptons or to two neutrinos, to reduce the background.

- WH: The final state targeted by this process also involves the leptonic decay of the W boson. The final state signature of a charged lepton and missing momentum from the undetected neutrino allows for a clear identification of the production process and a reduction of the backgrounds.
- ttH: This production process results in the most complex of the final states considered in this list. The two top quarks decay to a b quark and a W boson, which in turn can decay leptonically or hadronically. The presence of two b hadrons that can be identified and the possible presence of leptons from the W decays allow for what is generally a clear identification of the production process.
- bbH: this production process corresponds to about 1% of the Higgs production cross section and no attempt has yet been made to distinguish it from ggH. It has therefore been added to the ggH process in the categorization of production modes.
- tH: The experimental considerations for this process are similar to ttH, but the production rate is smaller, and the final state has only one top quark which reduces the identification efficiency compared to ttH. Finally, ttH itself can contribute as a background.

11.3.3 Inclusive Cross Section and Branching Ratio Measurements

The most basic experimental results in Higgs boson physics are measurements of the product of the production cross section and the decay branching fraction, $\sigma \times BR$, for a given combination of production and decay modes. These quantities correspond to the number of Higgs bosons produced through a particular process and observed in a specific decay channel, normalized to the integrated luminosity and corrected for acceptance and efficiency.

As mentioned previously, analyses are typically divided into event categories defined by final-state or kinematic properties in order to maximize the precision of these $\sigma \times BR$ measurements. For example, in measurements targeting $H \to \tau^+\tau^-$ decays, separate categories may be defined according to the τ -lepton decay mode (leptonic or hadronic) and the presence of additional jets, which can indicate a specific production process such as vector boson fusion. The sensitivity in each category depends on factors such as the production cross section for the chosen mode, its decay branching fraction, the reconstructed mass resolution, the selection efficiency, and the background level in the final state. These categories form the input granularity for more advanced combinations that will be discussed later, including those aimed at measuring production cross sections, extracting branching fractions, or determining Higgs boson couplings.

The extraction of the coupling strengths of the Higgs boson with various SM particles proceeds through the simultaneous fit of many such measurements. The contributions of those input measurements in the combination depend on the relative sensitivity of each analysis, which is determined by their associated statistical or systematic uncertainties. Both ATLAS and CMS have performed comprehensive combinations of measurements that use the full Run 2 dataset collected at a center-of-mass energy of 13 TeV. The input measurements presented below were mostly performed with this dataset.

The agreement between the measurement of the signal yields and the SM predictions can be expressed in terms of the signal-strength modifiers μ : the ratio of the observed yield to that of the SM prediction. The specific definition of μ will depend on the analysis. For given initial (i) and final (f) state, the signal-strength modifiers for individual production channels, μ_i , and decay modes, μ^f , are defined as the ratio of the measured event rate to its SM prediction:

$$\mu_i = \sigma_i/(\sigma_i)_{\rm SM}, \quad \mu^f = B^f/(B^f)_{\rm SM}, \quad \text{and}$$

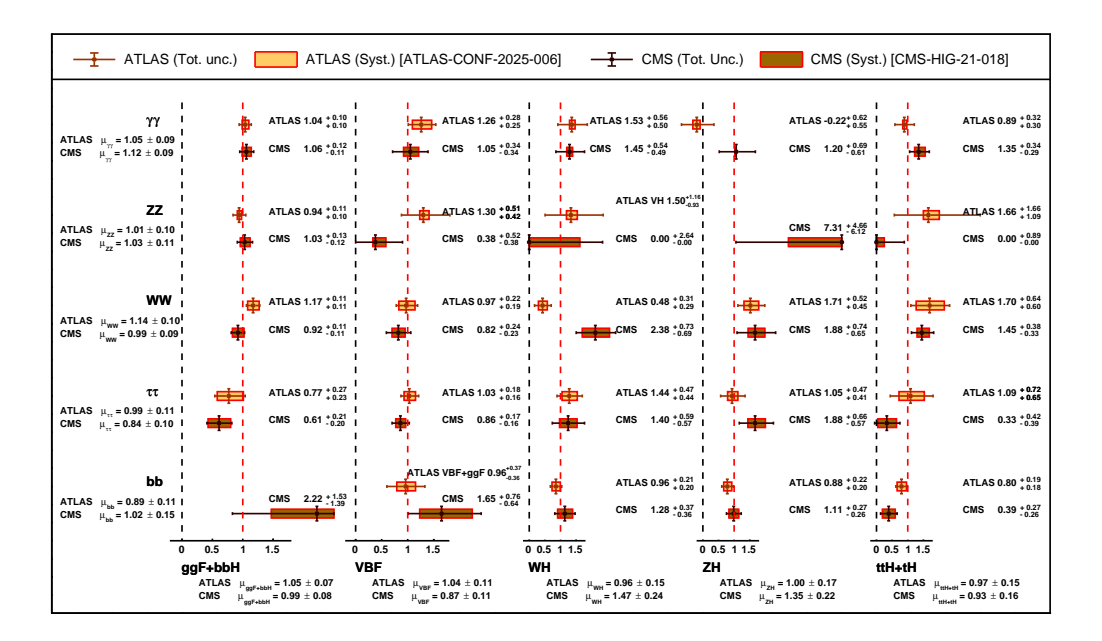


Figure 11.6: Ratio of observed rate to predicted SM event rate (μ_{if}) for different combinations of Higgs boson production and decay processes. The theoretical predictions are based on a Higgs boson mass of 125.09 GeV in the ATLAS fit [240] and 125.38 in the CMS one [239]. The original references consider similar but not identical set of measurements in the combined fit. As a result, in some cases a particular measurement is only available for one of the experiments. This is clarified in the labels with the numerical value. Both experiments also include the $\mu\mu$ and $Z\gamma$ decay modes in their fits, and, in the case of ATLAS, the VH $c\bar{c}$ process as well.

$$\mu_{if} = \frac{\sigma_i \times B_f}{\left(\sigma_i^{\text{SM}} \times B_f^{\text{SM}}\right)}.$$

This way of presenting the experimental results gives a global indication of their compatibility with the Standard Model. A more generic treatment of potential BSM effects will be given in Section 11.4.

The input measurements of the CMS [239] and ATLAS [240] experiments that enter some of the combinations presented below are shown in Figure 11.6. It is important to note that the theoretical uncertainty on the SM prediction is included in μ measurements through the denominator in the formula above. The p-value for the compatibility of the measurements and the SM predictions is 3% for CMS and 84% for ATLAS. Taking into account the results of both experiments, the overall agreement between the data and the SM prediction is good.

The combination of Higgs boson analysis channels, both within each experiment and across the two experiments, is performed by fitting a combined signal–plus–background model to the data. The principle underlying this combination is captured by the combination formula 11.13. As mentioned previously, the input granularity for the fits is the "category", where the category can represent, for example, particular kinematic selections or lepton flavours. Then, for each category "c" within a given channel, the measured number of signal events, n_s^c , is expressed in terms of a

small set of parameters as follows:

$$n_s^c = \left(\sum_{i,f} \mu_i \ \sigma_i^{\text{SM}} \times A_{if}^c \times \varepsilon_{if}^c \times \mu_f \ \text{BR}_f^{\text{SM}}\right) \times \mathcal{L}^c. \tag{11.13}$$

The production index is defined as $i \in \{\text{ggF}, \text{VBF}, ZH, WH, t\bar{t}H, tH, \ldots\}$ (including specific modes and regions of phase space) and the decay index is defined as $f \in \{\gamma\gamma, WW, ZZ, bb, \tau\tau, \mu\mu, Z\gamma\}$, while σ_i^{SM} and BR_fSM are the corresponding production cross sections and decay branching fractions, estimated as described in Section 11.2.5, assuming that the observed Higgs boson is described by the SM. A_{if}^c and ε_{if}^c are the signal acceptance and the reconstruction efficiency for the given production and decay modes in the category c. Bins are defined such that the acceptance A_i and efficiency ε_i are approximately uniform within each bin and stable under plausible BSM-induced shape variations. As a result, A_i and ε_i can be computed from SM simulation. \mathcal{L}^c is the integrated luminosity used for that specific category.

In the combination formula, the parameters of interest are the signal strengths for production (μ_i) and decay (μ_f) . The expression assumes factorization of the production cross section and decay branching fraction, which are valid under the narrow-width approximation. The observation of a narrow resonance in high-mass-resolution channels is sufficient for the precision required here. The equation also makes it clear that μ_i and μ_f cannot be extracted independently, which implies that the total cross sections or branching fractions cannot be determined without additional assumptions.

The combination formula also highlights an important limitation in the interpretation of the signal strength parameters. If these are treated as scale factors for the production cross sections or branching fractions, then all other inputs, such as the acceptances and efficiencies, A_{if}^c and ε_{if}^c , must be assumed independent of the couplings and fixed to their Standard Model estimates. Another caveat is that, in the combined fits, only the overall normalization is varied, and the shapes of the discriminating variables for the signal are kept fixed. These assumptions are particularly relevant when using the combination to extract the Higgs boson coupling properties, as discussed in Section 11.3.5. For small deviations of the couplings from their Standard Model values, these approximations remain valid.

In an individual measurement, the quantity directly determined is the product of the production cross section and the decay branching fraction, $\sigma \cdot BR$, which corresponds to $\mu_i \times \mu_f$ in the signal strength framework. These products can be treated as free parameters and, provided there is sufficient sensitivity from the chosen categories, can be measured without additional assumptions. The separate values of μ_i and μ_f can then be inferred only through a global combination of multiple measurements.

The most constrained fit in the combination allows for only one single parameter to vary, i.e., $\forall (i, f), \mu_i = \mu_f = \mu$. This global signal strength model provides the simplest probe of the compatibility of the signal with the SM Higgs boson. Indeed, it is sensitive to any deviation from the SM Higgs boson couplings provided that these deviations do not cancel overall. The ATLAS measurement of this inclusive μ yields [240]:

$$\mu = 1.023^{+0.056}_{-0.053} = 1.023 \pm 0.028 \text{ (stat.)} ^{+0.026}_{-0.025} \text{ (exp.)} ^{+0.039}_{-0.036} \text{ (sig. theo.)} \pm 0.012 \text{ (bkg. theo.)}$$

where (stat.) refers to the statistical uncertainties, (exp.) to the experimental systematic uncertainties, (sig. theo.) to theory uncertainties on the Higgs boson signal, and (bkg. theo.) to theory uncertainties on the background processes.

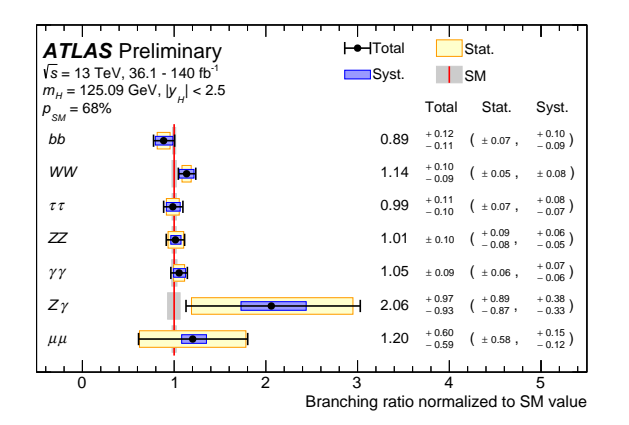
The equivalent result for CMS yields [239]:

$$\mu = 1.014^{+0.055}_{-0.053} = 1.014 \pm 0.028\,(\mathrm{stat})^{+0.025}_{-0.024}\,(\mathrm{exp})^{+0.040}_{-0.039}\,(\mathrm{theory})$$

The results from the two experiments are in excellent agreement with each other and with the Standard Model prediction. It is worth emphasizing that the overall theoretical uncertainty is larger than both the experimental systematic component and the statistical component, making it the dominant contribution to the total uncertainty. Reducing this theoretical component is therefore essential for fully exploiting the increasing precision of current and future measurements.

In one variant of the Higgs boson combination, the focus is placed on determining the branching fractions for various decay modes. For each mode included in the combinations performed by ATLAS and CMS, a specific production process is identified via event classification, based on the properties of particles produced in association with the Higgs boson, as described above. The branching fractions are then extracted by fixing the cross sections for all Higgs boson production processes to their Standard Model values. The resulting measurements [240] for the ATLAS experiment are shown in Figure 11.7 (left), and equivalent results from CMS can be found in [239].

In another variant of the Higgs boson combination, the emphasis is placed on the determination of the production process. Where several production processes are combined, the combination assumes the relative fractions to be those from the SM within their corresponding theory uncertainties. Here, Higgs boson branching fractions are then set to their SM values, within the uncertainties specified in Ref. [59]. The results [240] are shown for the ATLAS experiment in Figure 11.7 (right). The corresponding production cross section results expressed in picobarns are provided in Table 11.3, and the equivalent results for CMS, adapted from [239] are presented in Table 11.4. It is important to note that the SM theory predictions from ATLAS and CMS differ from those presented in 11.1 because of the addition of a fiducial cut on rapidity, different mass assumptions, and different decay mode selections for associated particles (e.g. for the W and Z bosons in WH and ZH production).



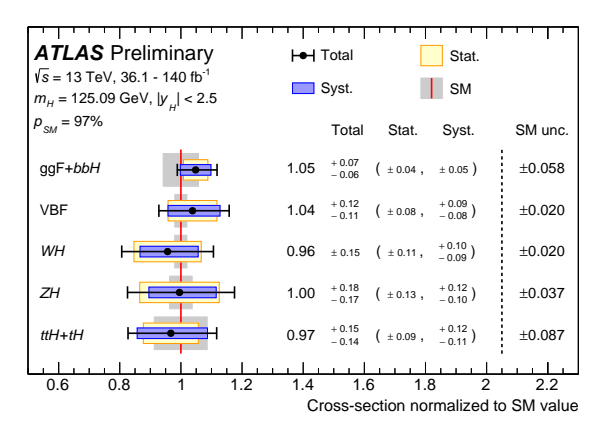


Figure 11.7: (Left) Observed and predicted branching fractions for different Higgs boson decay modes assuming SM values for the production cross sections. (Right) Observed and predicted cross sections for different Higgs boson production processes, assuming SM values for the decay branching fractions. Equivalent results from CMS can be found in Ref. [239]

The branching fractions of the $\gamma\gamma$, ZZ, $W^{\pm}W^{\mp}$, bb, and $\tau^{+}\tau^{-}$ decays, are measured with a precision of 10%. The observed signal significance for the rare $H \to \mu^{+}\mu^{-}$ decay was found to be above 3σ by CMS [241] using the Run 2 dataset, and above 3σ by ATLAS [242] using a combination of Run 2 and Run 3 datasets. The significance for the rare $H \to Z\gamma$ decay mode was found to be above 3σ when ATLAS and CMS combined their Run 2 search results [243]. All production modes are in agreement with the SM prediction. The gluon fusion process yields the most precise

Table 11.3: Measured values of Higgs boson production cross-sections by ATLAS [240] at a center-of-mass energy of 13 TeV, assuming branching ratios to match their expectations in the SM. The second column provides SM predictions with theory uncertainties based on a Higgs boson mass of 125.09 GeV, and the third column gives the ratio of the measured values to the SM predictions.

Cross-section	Measurement (pb)	SM prediction (pb)	Ratio to SM
ggF + bbH	$47.0^{+3.1}_{-2.7}$	44.8 ± 2.6	$1.05^{+0.07}_{-0.06}$
VBF	3.6 ± 0.4	3.50 ± 0.07	$1.04_{-0.11}^{+0.12}$
WH	1.17 ± 0.18	1.216 ± 0.024	0.96 ± 0.15
ZH	0.80 ± 0.14	0.796 ± 0.029	$1.00^{+0.18}_{-0.17}$
ttH + tH	$0.57^{+0.09}_{-0.08}$	0.58 ± 0.05	$0.97^{+0.15}_{-0.14}$

Table 11.4: Measured values of Higgs boson production cross-sections by CMS [239] at a center-of-mass energy of 13 TeV, assuming branching ratios to match their expectations in the SM. The second column provides SM predictions with theory uncertainties based on a Higgs boson mass of 125.38 GeV, and the third column gives the ratio of the measured values to the SM predictions.

Cross-section	n Measurement (pb) SM prediction (pb	Ratio to SM
ggF+bbH	$44.9^{+2.7}_{-2.7}$	$44.9^{+3.4}_{-3.3}$	$1.00^{+0.06}_{-0.06}$
VBF	$2.96_{-0.39}^{+0.39}$	$3.52_{-0.08}^{+0.08}$	$0.84^{+0.11}_{-0.11}$
V(qq)H	$0.77^{+0.86}_{-0.94}$	$1.27^{+0.02}_{-0.02}$	$0.61^{+0.68}_{-0.74}$
WH	$0.58^{+0.10}_{-0.09}$	$0.39_{-0.01}^{+0.01}$	$1.49^{+0.26}_{-0.24}$
ZH	$0.33^{+0.06}_{-0.05}$	$0.24^{+0.02}_{-0.02}$	$1.38^{+0.\overline{26}}_{-0.22}$
ttH	$0.38^{+0.07}_{-0.07}$	$0.50^{+0.03}_{-0.05}$	$0.76_{-0.15}^{+0.\overline{15}}$
tH	$0.55^{+0.21}_{-0.20}$	$0.088^{+0.013}_{-0.007}$	$6.25^{+2.36}_{-2.22}$

cross-section measurement, with a 6% uncertainty, which is of comparable size to the theoretical uncertainty on the SM prediction. In general, for both the production and decay processes, the statistical uncertainties are comparable to the systematic uncertainties.

Measuring the Higgs boson production cross section as a function of the center-of-mass energy also provides an important test of Standard Model predictions. This is illustrated in Figure 11.8, which shows the combined results from the diphoton and four-lepton decay channels at four different collision energies collected from Run 1 to Run 3 [244]. The predicted cross sections increase steadily with center-of-mass energy, more than doubling from Run 1 to Run 3. The measurements follow this trend and are, overall, consistent with Standard Model predictions.

In summary, Higgs boson measurements from both ATLAS and CMS exhibit good overall agreement with SM expectations, reinforcing the interpretation of the observed particle as a very "SM-like" Higgs boson. In some cases, the experimental uncertainties have reached a level comparable to that of theoretical uncertainties on cross sections. This highlights the critical importance of reducing theoretical uncertainties to fully exploit the precision of current and future Higgs measurements, especially in the high-luminosity LHC era.

11.3.4 Differential and Template Cross Sections

The characterization of Higgs boson production at the LHC goes beyond inclusive cross section measurements. The large datasets collected enable the experiments to perform detailed studies of kinematic observables that can be essential for probing the structure of the Higgs sector and

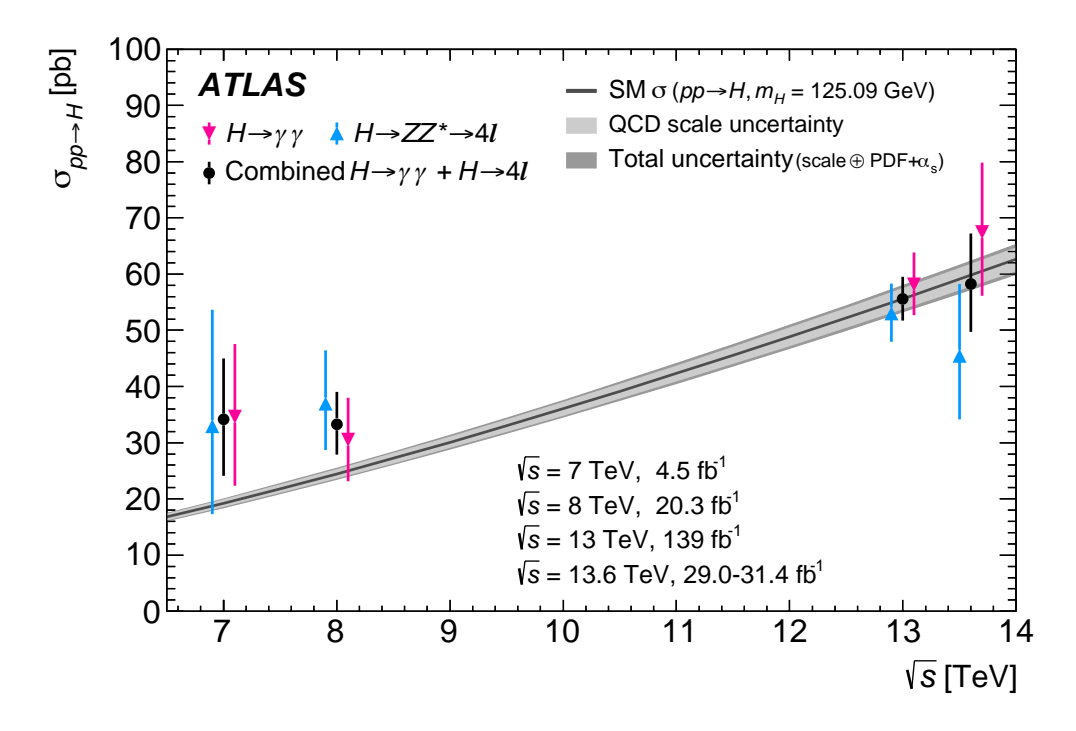


Figure 11.8: ATLAS measurements of the Higgs boson production cross section in the four-lepton and diphoton channels as a function of the proton-proton center-of-mass energy.

identifying potential deviations from SM expectations. Differential cross section measurements as a function of key variables offer a sensitive test of higher-order corrections in perturbative theory and allow for indirect constraints on new physics. These measurements are also key for improving the modeling accuracy of Higgs boson production in Monte Carlo simulations, providing essential input for both theoretical predictions and experimental analyses. Two primary approaches are employed by the LHC experiments to characterize this information: traditional differential cross-section measurements and simplified template cross sections (STXS).

Differential distributions have been measured in the decay modes of the Higgs boson ($H \to ZZ$, $H \to \gamma\gamma$, $H \to WW$, $H \to \tau^+\tau^-$, and $H \to b\bar{b}$), mapping the kinematics of Higgs production. The size of the Run 2 dataset allows for the measurement of single- and in some cases double-differential cross sections for key observables such as the transverse momentum of the Higgs boson (p_T^H). These measurements are unfolded to particle or parton level to enable direct comparison with theoretical predictions (see the PDG review on Statistics [245] for a general discussion of unfolding techniques).

The decay channels $H \to ZZ^* \to 4\ell$ and $H \to \gamma\gamma$ provide the cleanest experimental signatures due to their fully reconstructed final states and excellent invariant mass resolution. Despite their relatively small branching ratios, these modes allow for the most precise measurements of differential cross sections, including a broad array of observables related to the Higgs boson and its decay products, the accompanying jets, and global event topology. Double-differential cross sections have also been extracted for key observables, offering a deeper view into the event structure.

Complementing these channels are the higher-branching-ratio decay modes $H \to bb$, $H \to WW$, and $H \to \tau^+\tau^-$, which enable differential studies in regions of phase space with lower production cross sections such as events with high jet multiplicities or large Lorentz boosts of the Higgs boson. These channels are especially valuable for probing the high- p_T regime, where the sensitivity to BSM physics is enhanced. Advances in the identification of large-radius jets originating from

highly boosted decays to $b\bar{b}$ or $\tau^+\tau^-$ pairs have been fundamental to enabling these measurements in the highest p_T ranges. See for instance Refs. [246–248].

While most of these measurements currently focus on the gluon-gluon fusion (ggF) production mode, subleading modes such as VBF and ttH are also now being mapped differentially with increasing precision. Individual final state measurements of the cross section have been combined in ATLAS [249] and CMS [250,251]. Figure 11.9 shows an example of two observables.

These measurements of Higgs kinematics can be exploited to constrain Higgs boson couplings and other parameters of the theory. For instance, the shape of the Higgs p_T distribution is sensitive to loop-level effects and can be used to place bounds on the charm Yukawa coupling modifier κ_c . See 11.3.5 for further discussion on coupling constraints.

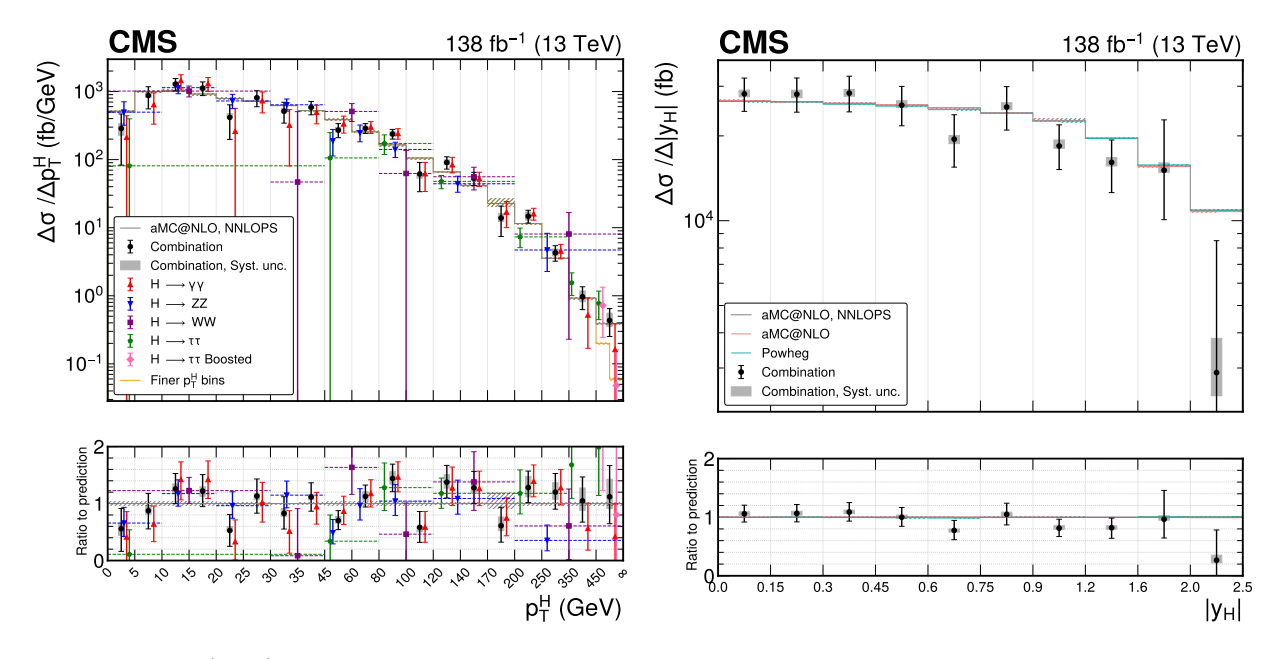


Figure 11.9: (Left) Combination of the fiducial differential cross sections in Higgs boson transverse momentum in the $H \to \gamma \gamma$, $H \to ZZ$, $H \to WW$, $H \to \tau \tau$ decay modes. (Right) Differential cross section as a function of the Higgs boson rapidity, combining the $H \to \gamma \gamma$ and $H \to ZZ$ modes, comparing to different Monte Carlo generators [251].

An alternative approach to characterizing Higgs boson production is the Simplified Template Cross Sections (STXS) framework [252]. In this method, fiducial cross sections are measured for each production mode in a set of predefined kinematic regions (bins) of phase space. These regions are defined using observables such as the transverse momentum of the Higgs boson (p_T^H) , the dijet invariant mass (m_{jj}) , the transverse momentum of the Higgs plus leading jets (p_T^{Hj}) , and the transverse momentum of the associated vector boson (p_T^V) . The STXS bins are carefully chosen through consensus between the theoretical and experimental community to optimize sensitivity to new physics while minimizing minimal theoretical uncertainties. These regions isolate contributions from different production mechanisms and improve the stability of theoretical predictions. They are designed with the combination of measurements across decay channels and experiments in mind. The goal is to reduce the dependence on extrapolations beyond the experimentally accessible phase space, improving the fidelity of comparisons between data and theory. STXS measurements serve as well-defined benchmarks that test both Standard Model (SM) predictions and potential BSM deviations in differential distributions.

The LHC Higgs Working Group proposed this framework [59,252] to address the challenges of combining measurements across a large number of decay channels, each affected by its own set of systematic uncertainties. To facilitate this, fiducial phase space definitions are standardized across analyses, focusing on Higgs boson production characteristics rather than specific decay signatures. The observables used correspond to the production modes $gg \to H$ (gluon fusion and $gg \to Z(\to qq)H$), EW qqH (vector boson fusion and $qq \to V(\to qq)H$), VH (associated production with vector bosons in leptonic channels, $qq + gg \to V(\to \text{leptons})H$), and top-associated production $(t\bar{t}H)$, constrained to well-defined and mutually exclusive kinematic regions.

ATLAS and CMS experiment has produced STXS measurements in all the main production modes and decay channels with the Run-2 dataset. A combination of STXS across decay channels has also been carried out by ATLAS [253–255] and CMS [239], also with the full Run-2 dataset. Figure 11.10 illustrates the results obtained by ATLAS in each of the kinematic regions. These combined STXS measurements provide a powerful probe of Higgs production mechanisms and constitute an important input for interpretations in the κ formalism, in global EFT fits, or in dedicated BSM analyses.

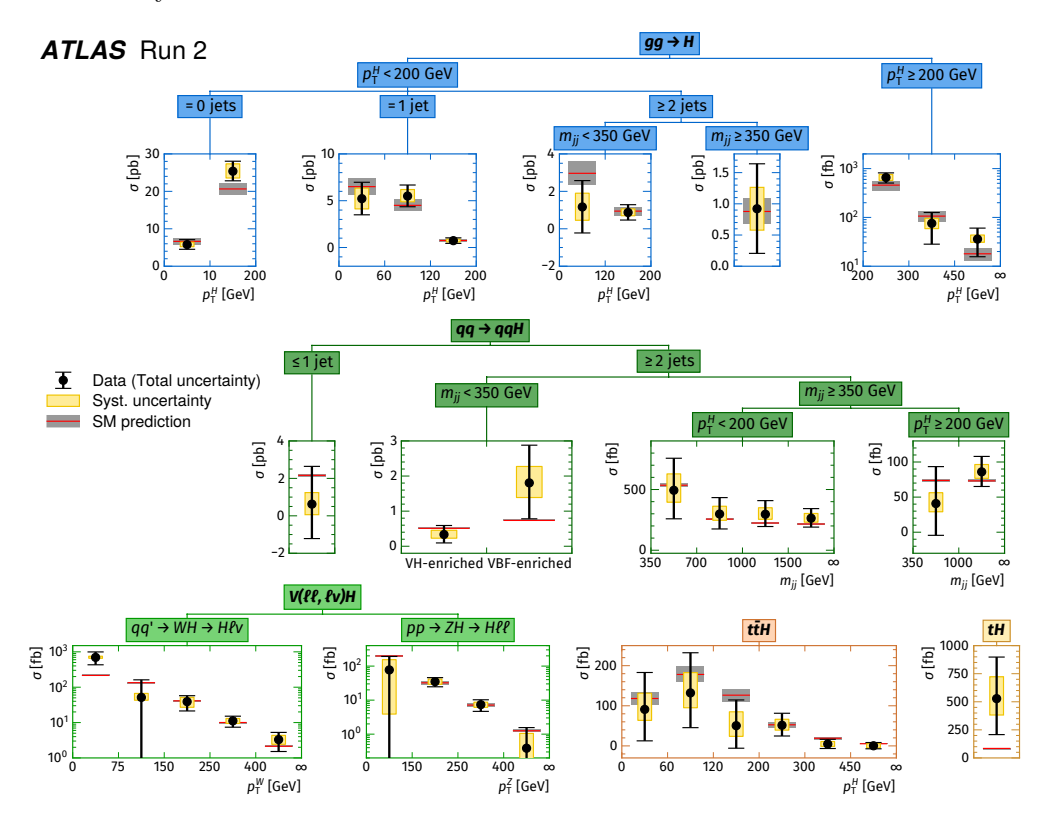


Figure 11.10: Simultaneous combined measurement of simplified template cross sections assuming SM branching fractions of the Higgs boson [255].

11.3.5 Probing the Couplings of the Higgs Boson: κ framework and EFT approach

As discussed in Section 11.2.1 and Section 11.2.2, all the SM Higgs-boson couplings are proportional to the mass of the particle it couples to. More precisely, the SM Higgs-boson couplings to fundamental fermions are linearly proportional to the fermion masses, whereas the couplings to bosons are proportional to the square of the boson masses. The Higgs terms in the SM Lagrangian were presented in Eqns. 11.8 and 11.9. Reformulating these expressions to highlight the SM Higgs-boson couplings to gauge bosons and fermions, as well as the Higgs-boson self coupling, we find the

following Lagrangian:

$$\mathcal{L} = -g_{Hf\bar{f}}\bar{f}fH - \frac{g_{3H}}{6}H^3 - \frac{g_{4H}}{24}H^4 + \delta_V V_\mu V^\mu \left(g_{HVV}H + \frac{g_{HHVV}}{2}H^2\right), \qquad (11.14)$$

with

$$g_{Hf\bar{f}} = \frac{m_f}{v}, \ g_{HVV} = \frac{2m_V^2}{v}, \ g_{HHVV} = \frac{2m_V^2}{v^2}, \ g_{3H} = \frac{3m_H^2}{v}, \ g_{4H} = \frac{3m_H^2}{v^2},$$
 (11.15)

where $V = W^{\pm}$ or Z and $\delta_W = 1, \delta_Z = 1/2$. The Higgs-boson couplings are therefore unambiguously determined once the particle masses are known. Any deviation from such pattern in the measurement of the couplings of the Higgs boson would therefore provide a clear indication of the existence of BSM physics. Later in this section (see Figure 11.11), we will present the recent results of the ATLAS and CMS constraints of these potential deviations.

Measuring the Higgs-boson couplings without relying on the SM assumption requires a general framework treating deviations from the SM coherently at the quantum level in order to provide theoretical predictions for relevant observables to be confronted with experimental data. Out of the different approaches to this problem, two approaches have been mainly followed by the LHC experimental collaborations in interpreting their measurements. The first is the so-called kappa (κ) formalism [256], in which Higgs-boson couplings are rescaled by arbitrary multiplicative factors (κ parameters), while preserving the Lorentz structure of the SM interactions. This approach has been extensively used by the LHC experimental collaborations due to its close connection to the measurement of the signal strengths described in Section 11.3.3. It allows for well-defined scenarios with various degrees of flexibility for incorporating BSM effects, and provides a global picture of the behavior in the Higgs sector. However, this κ formalism is limited in scope, as it does not fully account for modifications to the tensor structure of the interactions that influence both the kinematic distributions and the total rates. Also, arbitrary rescalings can destroy gauge invariance.

An alternative approach is the use of Effective Field Theories (EFTs) to parameterize BSM effects through higher-dimensional effective operators originating from the EW-scale projection of generic extensions of the SM living at a much higher ultraviolet (UV) scale. Indeed, while light new physics cannot be fully excluded, stringent direct limits on many well-motivated models makes the assumption of heavy new physics a very well-justified starting point. The EFT approach reaches beyond a purely phenomenological approach, and, as a coherent quantum-field-theory, also allows for the correlation of different effects and a systematic estimate of the residual uncertainties of its predictions. Depending on the assumptions made on the scalar field introduced in the SM to generate EWSB, two main EFT options have been considered in exploring potential deviations from SM-like Higgs-boson couplings: the so-called Standard Model Effective Field Theory (SMEFT), where the scalar field is assumed to be a doublet of $SU(2)_L$ as in the SM, and the Higgs Effective Field theory (HEFT) where such assumption is not made. The SMEFT approach has received particular attention in recent phenomenological explorations of BSM physics. This approach includes both targeted analyses in specific final states (e.g., $H \to ZZ$, $H \to \tau^+\tau^-$), which directly probe operators through the use of dedicated discriminators that are sensitive to specific BSM-induced deformations of the Higgs-boson kinematics, and also global analyses that typically exploit cross section measurements including differential distributions, and target a full spectra of observables. The latter normally require combination with other precision measurements, such as electroweak precision observables (EWPO), top-quark, Drell-Yan, as well as flavor-physics and low-energy observables, for a complete coverage. On the other hand, the HEFT approach has been recently considered in analyses aimed at constraining the Higgs-boson self-coupling since, at the lowest order, the EFT couplings involved in this case have a straightforward relation to the κ formalism.

In the following, the κ and SMEFT approaches are discussed in more detail given their broad applications to the interpretation of experimental data.

11.3.5.1 Kappa Framework

The κ -formalism [256] was developed within the LHC Higgs Working Group [55]. It introduces arbitrary factors called κ parameters that rescale the SM Higgs boson couplings (e.g. $\kappa_j = g_{Hjj}/g_{Hjj}^{SM}$ for j=f,V and similarly for other couplings), keeping the same Lorentz structure of the SM interactions. It followed earlier attempts [257] and initial phenomenological studies of the first hints of the existence of the Higgs boson [258]. It has been utilized to test various physics scenarios, like the existence of additional new particles contributing to the radiative Higgs-boson production and decays, or to probe various symmetries of the SM itself, as for example the custodial symmetry (see Sec. 11.2.3). It only compares the experimental measurements to their best SM predictions and does not require any new BSM computations per se. From a more theoretical perspective, its relevance arises from the fact that it fully captures the leading effects in Higgs processes of well-motivated scenarios.

The κ framework, described in detail in Refs. [58,256], facilitates the characterization of Higgs coupling properties in terms of a series of Higgs coupling strength modifier parameters κ_i , which are defined as the ratios of the couplings of the Higgs boson to particles i and their corresponding SM values. It is the simplest parametrization directly related to experimental measurements of the Higgs boson production and decay modes, and, in some cases, it coincides with the lowest-order of the consistent EFT framework of the HEFT. The κ framework has been widely used by the community, exploiting the framework described in Section 11.3.3 to combine the very large number of exclusive categories aimed at reconstructing the main production and decay modes of the Higgs boson. The μ_i and μ_f signal strength parameters defined there can be further interpreted in terms of modifiers of the SM couplings κ_j . The list of couplings g_j included in the experimental fits has been expanded progressively since the first results. In the latest experimental combinations, $j \in \{HZZ, HWW, H\tau\tau, Hbb, Htt, H\mu\mu, Hcc, Hgg, H\gamma\gamma, HZ\gamma\}$.

The κ framework assumes a single narrow resonance so that the narrow-width approximation can be used to decompose the cross section as a product of two factors characterizing the production and the decay of the Higgs boson. The κ parameters are introduced by expressing each of the these factors as their SM expectation multiplied by the square of a coupling strength modifier for the corresponding process at leading order:

$$(\sigma \cdot BR)(i \to H \to f) = \frac{\sigma_i^{SM} \kappa_i^2 \cdot \Gamma_f^{SM} \kappa_f^2}{\Gamma_H^{SM} \kappa_H^2} \to \mu_i^f \equiv \frac{\sigma \cdot BR}{\sigma_{SM} \cdot BR_{SM}} = \frac{\kappa_i^2 \cdot \kappa_f^2}{\kappa_H^2}, \quad (11.16)$$

where μ_i^f is the rate relative to the SM expectation, Γ_H is the total Higgs width, and κ_H^2 is an expression that adjusts the SM Higgs width to take into account the modifications induced by the deformed Higgs boson couplings. κ_H is a priori an independent parameter. However, when it is assumed that the Higgs boson cannot decay to new particles beyond those of the SM, κ_H can also be treated as an effective parameter and expressed in terms of the coupling modifiers to the SM field content. The κ_j modifiers scale either production cross sections or decay partial widths:

$$\kappa_i^2 = \frac{\sigma_i}{\sigma_i^{\text{SM}}} \quad \text{or} \quad \kappa_j^2 = \frac{\Gamma_j}{\Gamma_i^{\text{SM}}},$$
(11.17)

depending on the process. Here, σ_i is the measured cross section in production mode i and Γ_j the partial Higgs width in decay mode j. $\sigma_i^{\rm SM}$ and $\Gamma_j^{\rm SM}$ are their respective theoretical predictions in the SM. When all κ_j are set to 1, the SM is reproduced.

In the simplest configuration of the kappa framework, all loops in Higgs boson production and decay diagrams are resolved, coupling modifiers are introduced for each tree-level Higgs boson coupling to another SM particle, and no BSM decay of the Higgs is considered. The parameters include therefore κ_W , κ_Z , κ_t , κ_b , κ_τ , and κ_μ . This configuration can be extended to account for loop induced processes and to better incorporate possible new physics effects. For loop-induced processes, $gg \to H$, $H \to \gamma \gamma$ and $H \to Z \gamma$, there is a choice of either resolving the coupling strength modification in its SM expectation, e.g. $\kappa_{\gamma}(\kappa_t, \kappa_W)$, or keeping them as an effective coupling strength parameter, determined in the fit [259].

In the absence of a measurement of the Higgs-boson width the LHC requires some hypotheses in order to extract the Higgs couplings from the measured Higgs signal strengths. In particular, one can assume either (i) that there are no BSM particles in the decay, (ii) that any BSM particles in the decay would only give rise to invisible signatures and therefore be detectable through invisible Higgs boson channels (or in other terms that there is no BSM undetected contribution), or (iii) that BSM physics would modify the κ_j according to specific patterns favored by several new physics models. An external constraint is needed when BSM decays are allowed. For instance, the requirement that $|\kappa_V| \leq 1$ (V = W, Z) (see for instance the ATLAS+CMS Run 1 combination [260] for a discussion of this constraint) or constraints on Γ_H from indirect measurements (eg offshell/onshell cross sections (see Section 11.3.8). The general expression of the total width of the Higgs boson can be written as follows:

$$\Gamma_H = \frac{\kappa_H^2 \Gamma_H^{\text{SM}}}{1 - \text{BR}_{\text{BSM}}} = \frac{\kappa_H^2 \Gamma_H^{\text{SM}}}{1 - (\text{BR}_{\text{inv}} + BR_{\text{undet}})}$$
(11.18)

where $\Gamma_H^{\rm SM}$ is the total width of the SM Higgs boson and BR_{BSM} is the branching fraction of the Higgs boson to new particles beyond the SM. This BSM fraction can be broken down into two contributions. The first one, BR_{inv}, corresponds to an "invisible" branching ratio of the Higgs boson that can be directly constrained through H \rightarrow (invisible) searches (see Section 11.4.3) and included as an input in the coupling fits. The second, BR_{undet}, corresponds to the *undetected* or *unprobed* Higgs-boson branching ratio. This contribution is not directly measured by any search, and therefore not included as an input to the fits.

Negative values of Higgs couplings, i.e. negative κ_j , are not excluded a priori although they are not favored by the most recent measurements (see Table 11.5). With increased sensitivity to interference effects between vector $(\kappa_V, V = W, Z)$ and fermion couplings $(\kappa_F, F = t, ...)$, their relative sign could be established. The relative sign of κ_W and κ_Z has also been explored through associated production of Higgs and W bosons via vector-boson fusion (VBF) in Refs. [261, 262], which exclude opposite-sign scenarios for κ_W and κ_Z with a significance of more than 5 standard deviations. Among the five main Higgs-boson decay channels, only the $\gamma\gamma$ channel is sensitive to the sign of κ_F (or κ_V) through the interference of the W and t loops (see Ref. [259] for the parametrization). Access to the sign of the κ_F coupling can be obtained through the inclusion of analyses targeting single top-quark production, proposed in Ref. [263, 264], and currently part of the standard LHC combinations.

Taking into account the above discussion of the different possible scenarios that can be implemented, the ATLAS and CMS collaborations followed a common interpretation approach that yielded the first LHC combination of Higgs-boson couplings results already at the end of the first Run of the LHC [260]. A very similar configuration is used in the subsequent Run-2 results [239, 240, 255, 265].

Figure 11.11 and Table 11.5 summarize the measurements of the kappa parameters by AT-LAS [240] and CMS [239], using the full LHC Run-2 dataset, with an integrated luminosity of up to 140 fb⁻¹ of pp collisions at $\sqrt{s} = 13$ TeV. For the statistically dominated modes, $H \to Z\gamma$ and

 $H \to \mu\mu$, ATLAS has also included partial Run-3 statistics, 165 fb⁻¹ of 13.6 TeV collisions. These correspond to the cross section measurements presented in Section 11.3.3. Figure 11.11 (left) shows one of the interpretations discussed above: the measured coupling modifiers in the approach where the Higgs-boson loop couplings are resolved, as a function of the mass of the probed particles. Remarkable agreement with the SM is observed over several orders of magnitude. See the original references [239, 240] for further details.

Table 11.5: Coupling modifier combined measurements assuming no new physics in the decay of the Higgs boson. No assumption is made for the loop level couplings of the Higgs boson to gluons and photons which are considered as effective. The last column gives the expected precision at the HL-LHC.

	LHC Run 1 [260]	ATLAS Run 2 [240]	CMS Run 2 [239]	HL-LHC [266]
		+ Run 3 ($\mu\mu$, Z γ)		(expected)
κ_W	$0.87^{+0.13}_{-0.09}$	1.00 ± 0.05	1.03 ± 0.06	1.6%
κ_Z	-0.98 ± 0.10	0.96 ± 0.05	1.07 ± 0.06	1.6%
κ_{γ}	$0.87^{+0.14}_{-0.09}$	0.97 ± 0.06	1.10 ± 0.07	1.8%
κ_g	$0.91^{+0.07}_{-0.06}$	$0.99^{+0.07}_{-0.06}$	$0.91^{+0.07}_{-0.06}$	2.4%
κ_t	$1.40^{+0.24}_{-0.21}$	0.99 ± 0.09	$0.92^{+0.09}_{-0.08}$	3.4%
κ_b	$0.49^{+0.27}_{-0.15}$	$0.89^{+0.10}_{-0.09}$	$0.98^{+0.13}_{-0.12}$	3.6%
$\kappa_{ au}$	$0.84^{+0.15}_{-0.11}$	0.94 ± 0.06	0.91 ± 0.07	1.9%
κ_{μ}	_	$1.04^{+0.23}_{-0.30}$	$1.09_{-0.22}^{+0.20}$	3.0%
$\kappa_{Z\gamma}$	_	$1.36^{+0.30}_{-0.36}$	$1.61^{+0.32}_{-0.35}$	6.8%

Table 11.5 presents the coupling measurements for the scenario that includes effective couplings. The Run-2 results (13 TeV, $\approx 140\,\mathrm{fb^{-1}}$) are compared to the Run-1 ATLAS+CMS combination (7 and 8 TeV, 5+20 fb⁻¹) and the latest HL-LHC projection for the measurements, based on a combination of ATLAS and CMS for an integrated luminosity of 3000 fb⁻¹ per experiment. The interpretation included in the table assumes no BSM physics in the decay of the Higgs boson.

The combinations and projections can incorporate in the fit the searches for invisible decays of the Higgs boson. These searches directly constrain $BR_{\rm inv}$ and enable the distinction between invisible (directly constrained) versus undetermined or unprobed (not accesses experimentally in any measurement or search) decays mentioned earlier through a modification of the combination fit. Starting from the no BSM scenario, one may relax the assumptions on the Higgs boson decay by introducing BR_{inv} and BR_{undet} as parameters, allowing for a modification of the decays but introducing an external constraint to alleviate a complete degeneracy in the Higgs boson total decay width, where each coupling modifier can be scaled up equally to account for a non-zero BR_{undet} . An example of constraint is $\kappa_V \leq 1$, commonly used since Run-1, as shown for example in Ref. [260]. An alternative constraint uses the Higgs boson width derived from the off-shell Higgs boson production measurements. In this interpretation, the off-shell Higgs measurement constrains the visible, invisible and undetected branching fractions. The visible branching fractions corresponds to the measured Higgs decays to SM particles. The invisible branching fraction is constrained from the direct, invisible Higgs searches. The undetected branching fraction will be then constrained by the off-shell Higgs boson measurements. Figure 11.11 (right) shows a comparison of the kappa measurements in the three models: no BSM allowed, BSM constrained by $\kappa_V \leq 1$,

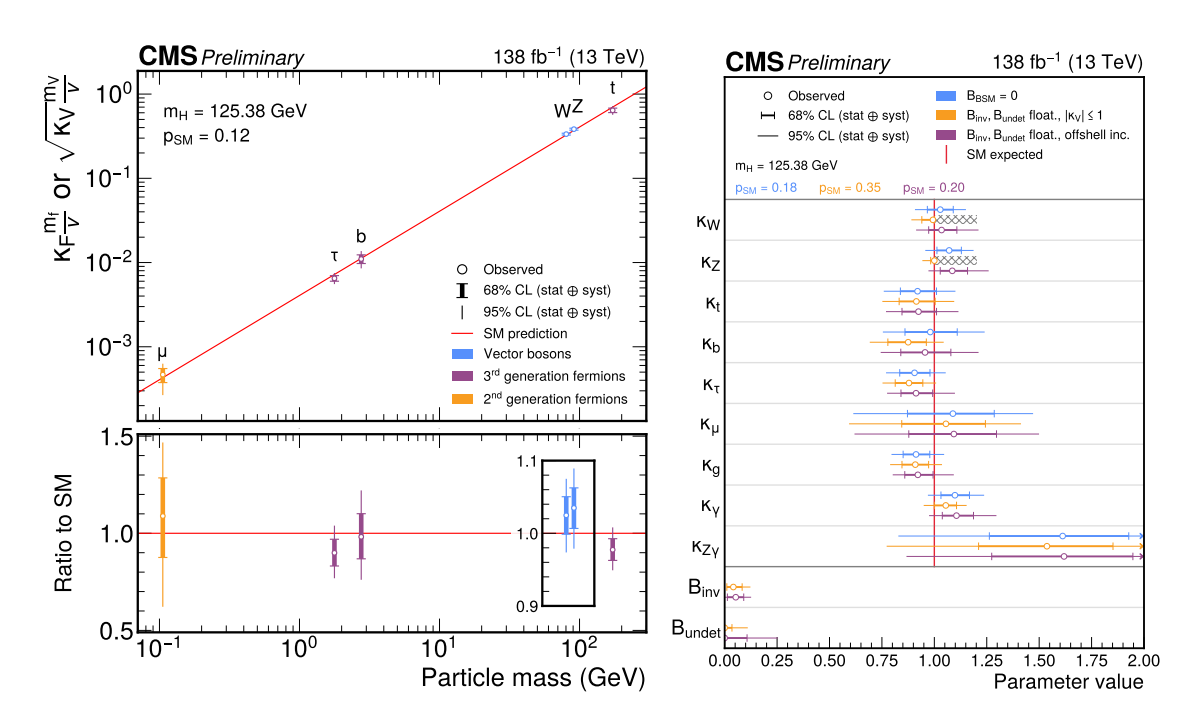


Figure 11.11: Reduced Higgs boson coupling strength modifiers and their uncertainties, CMS [239] (left). Combined measurements of coupling modifiers with various assumptions, CMS [239] (right). Equivalent plots for ATLAS can be found in Ref. [240].

and BSM constrained by the inclusion of off-shell production $(H \to 4\ell)$. More details on this comparison can be found in the CMS paper [239], and a discussion of off-shell production and the measurement of the total width in Section 11.3.8.

The limits obtained at the 95%CL on the invisible and undetected branching fractions with the Higgs combination and the corresponding HL-LHC constraints are:

$$\begin{split} BR_{inv} &< 13\% \;,\; BR_{undet} < 12\% \; (ATLAS \; [255], \; Run2) \;, \\ BR_{inv} &< 12\% \;,\; BR_{undet} < 11\% \; (CMS \; [239], \; Run2) \;, \\ BR_{inv} &< 1.9\% \;,\; BR_{undet} < 4\% \; (HL\text{-LHC} \; [194]) \;. \end{split} \label{eq:Rundet} \tag{11.19}$$

A longer discussion of the different Higgs invisible searches can be found in Section 11.4.3, including updated BR_{inv} constraints not yet included in some of these combinations.

Interpretations which are less sensitive to modeling systematic uncertainties and require no constraints on the natural width of the Higgs bosons have been considered, either through the ratio of cross section and branching ratios (see Ref. [263]) or through a more generic approach to avoid the degeneracy in the measurement of the coupling modifiers, probing the coupling properties of the Higgs boson through ratios of couplings ($\lambda_{ij} = \kappa_i/\kappa_j$). In the latter model, all combination signals can be parametrized with the ratios of coupling modifiers. For example, (i) the $\lambda_{Zg} = \kappa_Z/\kappa_g$ ratio which is mainly probed by the measurements of the VBF and ZH production; (ii) the $\lambda_{tg} = \kappa_t/\kappa_g$ ratio constrained by the $t\bar{t}H$ production process; (iii) the $\lambda_{WZ} = \kappa_W/\kappa_Z$ ratio mainly probed by the WW and ZZ decay modes; (iv) the $\lambda_{\tau Z} = \kappa_{\tau}/\kappa_Z$ ratio constrained by the $\tau^+\tau^-$ channel; (v) the $\lambda_{bZ} = \kappa_b/\kappa_Z$ ratio probed mainly by the $VH(b\bar{b})$ channels; and (vi) the $\lambda_{\gamma Z} = \kappa_{\gamma}/\kappa_Z$ ratio constrained by the diphoton channel. In this parametrization, the ZZ channel plays an important normalization role, and a reference combined coupling modifier, κ_{qZ} , is introduced to represent

the high-precision measurement of the $gg \to H \to ZZ$ production rate $\kappa_{gZ} = \kappa_g \times \frac{\kappa_Z}{\kappa_H}$. Current uncertainties on the ratios vary from 5 to 20% [239]. They are expected to be reduced to a few percent level at the HL-LHC [266].

It is important to note that the global fit described above does not include all possible Higgs couplings, but only those related to measurements included as inputs in the fit. A particularly important example is the coupling to charm quarks, κ_c . The significant experimental challenges in isolating Higgs decays to charm at the LHC limit the LHC sensitivity. Generally speaking, this coupling is considered a target for future Higgs factories, that will be able to measure it precisely [194]. Nevertheless, the progress in recent years has been impressive and it deserves a special mention. Dedicated analyses have been developed in ATLAS and CMS to probe this coupling both directly and indirectly. Direct searches target the decay mode $H \to c\bar{c}$, relying heavily on associated production and advanced charm-tagging algorithms. The most stringent current constraint comes from CMS using the full Run-2 dataset, which combines VH and ttH production and yields a constraint at 95% CL of $|\kappa_c| < 3.5$ (expected 2.7) [267]. ATLAS set a limit of $|\kappa_c| < 4.2$ at 95% CL [268] using the VH channel alone. These limits are significantly looser than those for third-generation fermions, illustrating the difficulty of separating charm from background in hadronic environments. Indirect constraints on κ_c have also been derived from differential distributions sensitive to loop contributions involving charm quarks [249,251]. Searches for rare Higgs boson decays to a meson and a photon [269] as well as searches for Higgs boson production in association with a charm quark (cH) [270, 271] or a photon (γ H) [272] have also been used to set constraints on $|\kappa_c|$. At present, these searches allow values of κ_c several times larger than the SM expectation. Looking ahead, the HL-LHC is expected to improve sensitivity significantly, potentially reaching observation of the decay and its first measurement. The available projections [266] propose a sensitivity to the charm Yukawa coupling of $\kappa_c < 1.5$ by the end of HL-LHC at 95%. This projection is likely conservative considering the newest results and the rate of improvement in recent years. Measuring κ_c remains one of the key challenges in precision Higgs-boson physics and a critical test of the Yukawa-type interaction assumed in the SM.

Beyond the charm quark, probing the Yukawa couplings of the first- and second-generation fermions remains an even greater challenge. Current LHC studies can only set very loose indirect constraints on the light quark Yukawa couplings. As an example, in Ref. [272] CMS excludes scenarios where first- or second-generation quarks have Yukawa couplings comparable to those of the third generation, probing $H\gamma$ production. The Yukawa coupling to the electron has also been constrained via direct searches for $H \to ee$ by ATLAS [273] and CMS [274], with limits several orders of magnitude above the SM prediction. Future lepton colliders and dedicated Higgs factories are expected to significantly improve these constraints.

A more in-depth discussion of the kappa framework formalism can be found in the LHC Higgs Working Group Reports [58, 256].

11.3.5.2 SMEFT Formalism and Results

The SMEFT Lagrangian has the same field content and it respects the same linearly-realized $SU(3)_C \times SU(2)_L \times U(1)_Y$ local symmetry as the SM. The difference is the presence of operators with canonical mass-dimension d larger than 4, built of SM fields, and representing the projection at the EW scale of generic extensions of the SM living at a UV mass scale Λ well above the EW scale. At the EW scale the heavy particles of the UV-complete theory cannot be produced as physical states and only leave their imprint as quantum effects induced by d>4 effective operators that can affect SM couplings and masses but also introduce new interactions not present in the SM Lagrangian. While a modification of the SM Higgs-boson couplings as introduced by the κ -formalism discussed in Sec. 11.3.5.1 can only describe BSM effects that amount to a rescaling of

production rates and branching ratios, the SMEFT formalism (similarly to the HEFT formalism) can be used to also explain anomalies arising in differential distributions since it introduces Lorentz structures not existing in the SM Lagrangian. Furthermore, the same SMEFT operators contribute not only to Higgs-boson processes but to a much larger number of observables and can therefore be constrained by a broad spectrum of measurements that could reveal underneath correlations among EFT couplings and point to classes of preferred BSM models.⁶ Last but not least, the SMEFT is a full fledged quantum field theory and as such can systematically include effects induced by SM quantum corrections below the scale Λ and can also seamlessly be matched to low-energy EFT below the EW scale, e.g. the 4-fermion operator Lagrangian commonly used to describe the dynamics of flavor physics⁷.

The SMEFT Lagrangian consists of the SM Lagrangian (\mathcal{L}_{SM}) and a series of operators organized in a systematic expansion in d, where each consecutive term is suppressed by an increasingly larger power of a the high mass scale Λ such that the SMEFT Lagrangian can be written as:

$$\mathcal{L}_{\text{SMEFT}} = \mathcal{L}_{\text{SM}} + \sum_{d} \sum_{i} \frac{C_i^{(d)}}{\Lambda^{(d-4)}} \mathcal{O}_i^{(d)}. \qquad (11.20)$$

The contribution of the SMEFT operators of dimension d > 4 to physical amplitudes is therefore suppressed by $(E/\Lambda)^{d-4}$, where E is the relevant energy scale of the process. The applicability of the SMEFT approach requires that $\Lambda \gg E$, under which assumption the expansion in d can be truncated and only a finite number of new interactions is considered. The Wilson coefficients $C_i^{(d)}$ encode the virtual effects of the heavy new physics in low-energy observables. For a given UV completion of the SM, their dependence on masses and couplings of the new particles can be obtained via matching with the UV theory at the scale Λ . More generally, and in the absence of a specific assumption on the UV theory, they can be inferred using specific power-counting rules [278, 279], or constrained by fitting to specific sets of observables. All parameters of the SMEFT Lagrangian, namely SM parameters and Wilson coefficients, are scale dependent and their scale dependence is determined by the renormalization group equations of the full SMEFT.

The SMEFT approach is clearly very general, and can be made more specific and predictive by further assumptions on the UV physics of which it is a low-energy projection. For instance, assuming baryon and lepton number conservation, the most general SMEFT Lagrangian only contains even-dimension operators. This is commonly assumed in studies of Higgs-boson and more generally collider observables which therefore start by including d = 6 operators, while the inclusion of d = 8 or higher-dimension operators is considered in assessing the validity of truncating the SMEFT expansion at d = 6 or for those observables that are more sensitive to d = 8 operators, such as e.g. certain Drell-Yan angular distributions [280–282].

The list of d = 6 operators was first classified in a systematic way in Ref. [283] after the works of Ref. [284]. Subsequent analyses pointed out the presence of redundant operators, and a minimal and complete list of operators was finally provided in Ref. [285]⁸. For a single family of fermions, i.e. not considering flavor indices, the SMEFT Lagrangian can be expressed in terms of 59 independent operators. Considering the 3 families of fermions of the SM, flavor indices can be added to these 59 operators, and furthermore, new operator structures, that have been dismissed by means of Fierz

⁶It should be pointed out that some of the processes considered in global fits of the SMEFT are backgrounds to Higgs-boson analyses and their SMEFT interpretation should be consistently considered along with the signal one in such analyses. This is true in general for all background processes, and, together with other improvements, is part of the ongoing effort to improve SMEFT global fits.

⁷For comprehensive reviews of the SMEFT see Ref. [275–277].

⁸Complete enumerations of d=8 operators have been obtained [286] and some preliminary constraints on particular subsets of these operators have been derived from experimental measurements [287]. Still, in this review, the SMEFT Lagrangian will be truncated at the level of dimension-6 operators.

transformations in the single family case, have to be considered, for a total of 2499 independent operators that do not violate baryon and lepton number [288].

The numbers of operators can be reduced by requiring additional symmetry properties of the UV-complete theory. For instance, requiring no additional CP-violation besides the one already introduced in the SM via the CKM matrix restricts the number of d=6 operators for a single family to 53 (out of 59) and requires the Wilson coefficients to be real. At the same time, assumptions on the level of flavor-violation introduced by NP at the UV scale can drastically limit the number of flavor-structures allowed in the SMEFT operators. Requiring the UV theory to have maximal flavor symmetry, namely $U(3)^5$, and therefore assuming that the SM Yukawa couplings are the only sources of $U(3)^5$ breaking (a.k.a. Minimal Flavor Violation), reduces the number of allowed SMEFT operators to 41. If NP breaks flavor by distinguishing the first two generations from the third one, the SMEFT operators only respect a $U(2)^5$ flavor symmetry, and a total of 124 SMEFT operators needs to be considered [289]. Further generalization are possible although most of the existing studies have so far considered the $U(3)^5$ and $U(2)^5$ benchmarks, or a hybrid $U(2)^3$ for quarks and $U(3)^2$ for leptons.

Given a set of d=6 SMEFT operators generated at the UV scale Λ , their mixing under renormalization and the scale evolution of the corresponding Wilson coefficients is completely known at leading-order of SM interactions (QCD and EW). The tree-level matching conditions at the UV scale have been systematically calculated [290–293] and their evolution from Λ to the EW scale can be obtained via the LO anomalous dimensions of SMEFT operators [288, 294, 295]. A variety of tools exist that allow to automatically perform both the matching at the UV scale [292, 293, 296] and the LO scale evolution [297–299]. Observables at the EW scale are either computed with independent codes or obtained with automated tools such as MadGraph5_aMC@NLO [300] interfaced with SMEFT Feynman-rules generators such as SMEFTsim [301,302] or SMEFT@NLO [303]. They can be calculated including d=6 effects at linear or quadratic order, although these last ones are technically of $O(1/\Lambda^4)$ and therefore of the same order in Λ as the effects generated by the d=8 operators. Several studies have included them to quantitatively estimate their impact and test the validity of the EFT expansion.

Once the EFT formalism is in place, it can be used either top-down with a specific UV-completion in mind and a specific decoupling scale Λ or bottom-up when no or little assumptions are made on the BSM physics above a generic scale Λ . In the first case the matching to the SMEFT at the given scale Λ can be calculated at the desired perturbative order, singling out only a limited number of operators that are generated by such theory and testing how they can successfully reproduce the EW and low-energy phenomenology. Vice versa, if the UV theory is not known, the Wilson coefficients at the scale Λ are fitted, together with the SM parameters, to existing data and information on the UV theory is obtained. In this last case, the fit will identify preferred $c_i(\Lambda)/\Lambda^2$ ratios, such that from perturbativity arguments a lower bound on the scale of new physics Λ can be placed.

The Higgs-boson mass, width, branching ratios, as well as total and differential cross sections can be calculated in the SMEFT in terms of Wilson coefficients at the EW scale and the role of different SMEFT operators can be constrained by comparing to LHC experimental measurements. Individual Higgs-boson couplings can be expressed in terms of SMEFT Wilson coefficients such that their deformation can be related to effects in non-Higgs related observables. In fact, through the EFT formalism individual operators both mix by the effect of SM radiative corrections and at the same time contribute to multiple processes, not only Higgs-boson related, such that considering their broad impact can stress-test the SMEFT framework and isolate the regions of SMEFT parameters that are phenomenologically allowed. An exhaustive review of the SMEFT and its phenomenological studies, including studies limited to specific Higgs-boson observables and assuming different orders

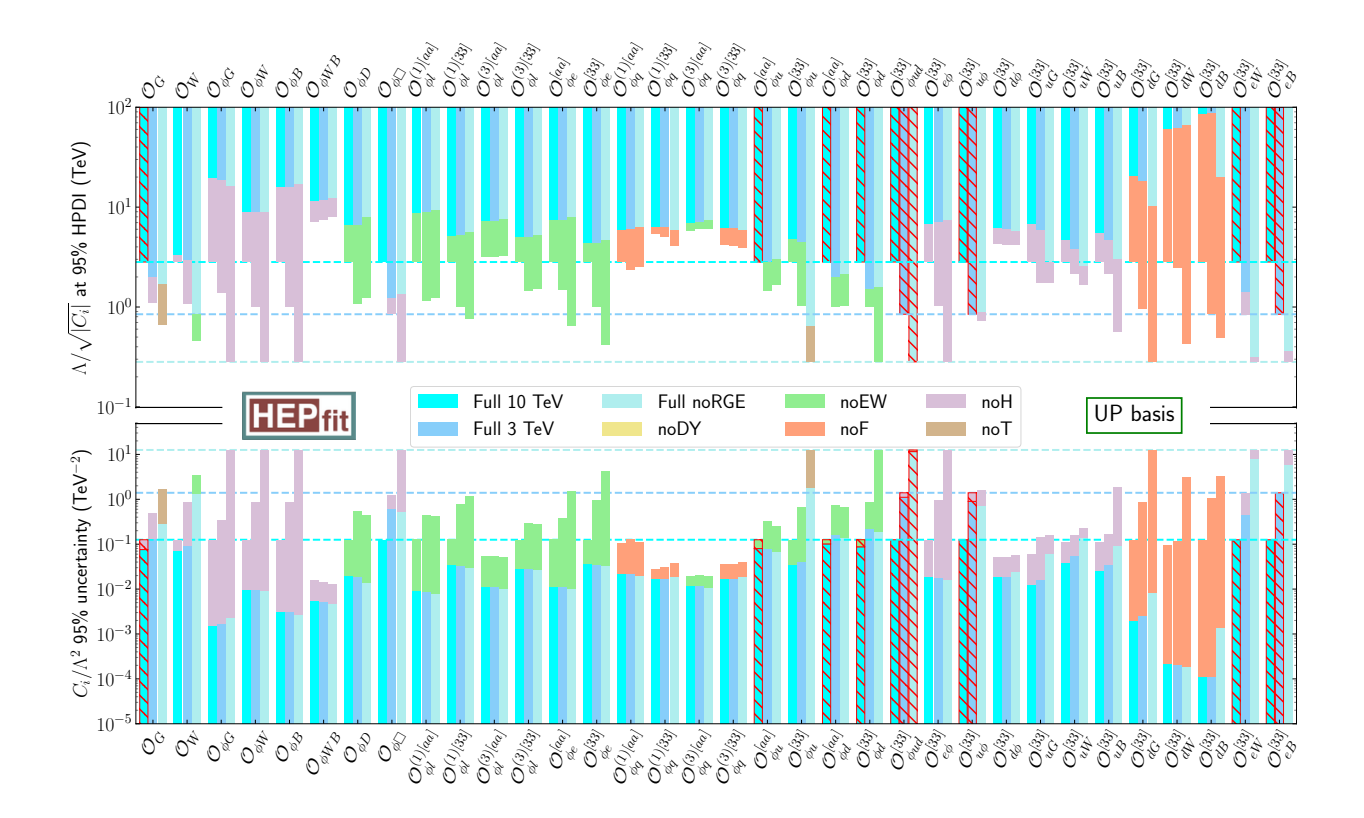


Figure 11.12: Results from a global fit in the $U(2)^5$ flavor-symmetric SMEFT (from Ref. [304]). For each coefficient C_i , the bottom panel shows the width of the 95% probability range divided by two, while the top panel shows the (normalized) scale of new physics allowed by the data at 95% probability. Each case includes results obtained for different values of Λ and removing the most constraining data set for that particular coefficient. The color code is as explained in the legend (see text for more details).

of SM effects, can be found in [277] (and references therein). Among them, several recent studies have presented individual and global fits of SMEFT Wilson coefficients that consider a broad spectrum of observables including Higgs-boson production and decay rates as well as STXS, top-quark rates and asymmetries, electroweak precision observables and diboson production, Drell-Yan observables, jet production cross sections, and flavor observables [304–312].

As an illustration, Fig. 11.12 shows the result of a global fit of SMEFT operators containing the SM scalar field ϕ , and hence directly affecting Higgs-boson observables, but also being constrained by electroweak, top-quark, Drell-Yan, and flavor observables through renormalization group evolution (RGE). The lower plot gives the 95% probability bounds obtained on the $C_i(\Lambda)/\Lambda^2$ coefficients, while the upper plot translates those bounds into a lower bound on the scale of new physics (normalized by the square root of the maximum of the 95% Highest Posterior Density Interval, or HPDI, for $|C_i|$). Both panels show results for the three cases $1)\Lambda = 10$ TeV with RGE, 2) $\Lambda = 3$ TeV with RGE, and 3) $\Lambda = 1$ TeV with no RGE. Furthermore, the horizontal lines indicate the maximum value allowed for each Wilson coefficient in the fit, corresponding to the perturbativity limit (4π) , for the different values chosen for the scale Λ . The cases in which the 95% HPDI interval touches the prior's edges are hatched with red diagonal lines, indicating that the fit is just returning what assumed in the prior and further precision in the determination of the most constraining observ-

ables is needed. When the posterior distribution of a coefficient is completely flat, indicating that more observables need to be included in the fit, the 95% HPDI interval is hatched with diagonal white lines. The role of Higgs-boson measurements of signal strengths and STXS on several new physics interaction is manifest (see difference between blue and purple bounds). More details can be found in Ref. [304].

Overall, several operators that directly affect leading Higgs-boson production or decay modes are strongly constrained by LHC measurements, while operators whose main role is to affect e.g. high- p_T^H distributions are still marginally constrained, due to limited statistics in the experimental measurements, but their effects will be within the reach of the HL-LHC sensitivity. At the same time, several correlations have emerged with operators that are mainly constrained by non-Higgs observables, such that precision measurements of SM parameters, top-quark couplings, and Drell-Yan cross sections will provide very constraining complementary information.

In addition to the global fits prepared by theoretical groups, ATLAS and CMS have published interpretations of the Higgs boson measurements discussed in this document in terms of EFT constraints. The studies range from interpretations of differential cross sections or of STXS measurements (see for instance Refs. [239,251,311]) to analyses based on the construction of dedicated observables sensitive to specific operators. Several examples of the latter, related to CP properties, will be discussed in Section 11.3.9. Finally, first attempts by the collaborations to perform global fits including data from LHC Higgs boson, EW vector boson, top quark, and multi-jet measurements, and also EWPO measurements from LEP and SLC, have been reported in Refs. [312,313].

11.3.6 Higgs-boson Self-Couplings

One of the most important open questions in the field is the precise mapping of the Higgs potential and the exploration of the inner workings of the EWSB mechanism. Probing the structure of the Higgs potential has deep implications in several areas of fundamental physics, including electroweak phase transitions, baryogenesis, and early universe cosmology (see Section 11.2.4).

As discussed in the introduction (see Eq. 11.8), in the SM the Higgs potential can be decomposed in a Higgs-field mass term and two self-interaction terms, one trilinear and one quadrilinear in the Higgs-boson field. In the SM they can both be expressed through the unique self-coupling $\lambda_{SM} = \frac{m_H^2}{2v^2}$, but in the presence of new physics they could be interpreted as independent effective interactions expressed through different self-coupling parameters λ_3 and λ_4 . In the spirit of the κ framework described in Section 11.3.5.1, these self-couplings can be parameterized by modifiers κ_3 and κ_4 , both equal to 1 in the SM:

$$\kappa_3 = \frac{\lambda_3}{\lambda_3^{\text{SM}}}, \quad \kappa_4 = \frac{\lambda_4}{\lambda_4^{\text{SM}}}.$$
 (11.21)

Probing these couplings is one of the central goals of the HL-LHC program. Current datasets do not yet provide sufficient sensitivity to directly measure κ_3 or κ_4 . However, κ_3 can already be constrained through studies of Higgs pair production $(pp \to HH)$. See Figure 11.4 for the main Feynman diagrams for HH production at the LHC. Single Higgs production processes also provide indirect sensitivity to κ_3 through global fits. In contrast, probing κ_4 directly requires access to triple Higgs production $(pp \to HHH)$, which has an extremely low cross section in the SM and is out of reach even for the HL-LHC. Nevertheless, recent analyses have begun placing first experimental constraints on κ_4 .

i. Higgs Pair Production at the LHC

The theory of double-Higgs (HH) production is discussed in Section 11.2.5.1. This process has not been observed yet at the LHC due to its very small production cross section in the SM. We recall

that the N3LO+N3LL prediction for $\sigma^{HH}_{\rm ggF}$ is 33.46^{+0.88%}, fb at the 13 TeV LHC (see Sec. 11.2).

Experimentally, the most sensitive final states are $HH \to \gamma \gamma bb$, $HH \to \tau \tau b\bar{b}$, $HH \to b\bar{b}b\bar{b}$, which benefit from the larger branching fraction of $b\bar{b}$ decays and the identification of the diphoton or ditau pair. Other decay modes, such as $VVb\bar{b}$, multilepton final states, and other final states involving tau leptons, are more limited in sensitivity, though they can provide complementary information and can help to constrain specific regions of phase space in a combined HH global fit.

The study of HH production provided the best avenue to access the trilinear self-coupling κ_3 at the LHC. Variations in the value of the κ_3 affect not only the total yield of HH events produced, but also the shape of key kinematical distributions such as the mass of the HH system. These changes need to be taken into account in the analysis for an optimal sensitivity to the self-coupling. Furthermore, a precise knowledge of the top-Yukawa coupling is needed. The best measurements of the HH production and of κ_3 require different optimizations that probe different regimes in p_T^H : lower for the measurement of κ_3 and higher for the observation of HH production.

ATLAS Ref. [183] and CMS Ref. [184] have placed limits at 95% CL on HH production cross section through the combination of all available Run-2 analyses, for an integrated luminosity of up to 140 fb⁻¹ at 13 TeV. The results target the dominant ggF production and the subleading qqHH production, which provides access to the VVHH vertex and enables constraints on the κ_{2V} parameter. The experiments are starting to explore also rarer production modes, like VHH [314,315] or ttHH production modes [316].

The latest observed and expected upper limits on the HH production signal strength at 95% CL for ATLAS Ref. [183] and CMS Ref. [184] are:

ATLAS:
$$\mu_{\rm HH} < 2.9$$
 (expected : 2.4),
CMS: $\mu_{\rm HH} < 3.5$ (expected : 2.5).

For the VBF production mode the upper limits are $\mu_{\text{VBFHH}} < 44$ (47) (ATLAS) and $\mu_{\text{VBFHH}} < 79$ (91) (CMS) also at 95% CL. These HH combinations yield the following constraints on the coupling modifiers κ_3 and κ_{2V} :

ATLAS:
$$-1.2 < \kappa_3 < 7.2 \quad (-1.6 < \kappa_3 < 7.2 \quad \text{expected}),$$

 $0.6 < \kappa_{2V} < 1.5 \quad (0.4 < \kappa_{2V} < 1.6 \text{ expected}).$
CMS: $-1.39 < \kappa_3 < 7.02 \quad (-1.02 < \kappa_3 < 7.19 \quad \text{expected}),$
 $0.62 < \kappa_{2V} < 1.42 \quad (0.69 < \kappa_{2V} < 1.35 \quad \text{expected}).$ (11.23)

These results have been combined in a joint ATLAS and CMS study of HH production using Run-2 data [317], including the most sensitive channels from each experiment, with integrated luminosities ranging between 126 and 140 fb⁻¹. An observed 95% CL upper limit on $\mu_{HH} < 2.5$ is set, with an expected value of 1.7 (2.8) assuming the absence (presence) of the SM HH signal. The HH signal strength is measured to be $0.8^{+0.9}_{-0.7}$, for an observed significance of 1.1 standard deviations (1.3 expected for the SM HH signal). Corresponding constraints are set on the couplings, also at 95% CL: $-0.71 < \kappa_3 < 6.1$ and $0.73 < \kappa_{2V} < 1.3$.

ATLAS and CMS have extended the study of HH production to new physics scenarios using the HEFT frameworks [184,318]. The results are interpreted in terms of constraints on HEFT operators and the correlation between them. They are also presented in terms of upper limits on specific benchmarks proposed by the LHC Higgs Working Group. In Ref. [318], constraints on individual SMEFT operators are also proposed, while in Refs. [184,318] the possibility of constraining HEFT operators whose coefficients, at the lowest order, are in direct correspondence with κ modifiers, is also explored. Overall, the results are consistent with the SM predictions. For more details, see the original references.

The Higgs pair searches can be combined with single-Higgs coupling measurements. We can exploit the complementarity between single-Higgs and di-Higgs processes to simultaneously probe multiple Higgs boson couplings, including the self-coupling and the top-quark Yukawa coupling. A joint fit enables the simultaneous constraint of key Higgs boson couplings such as κ_t , κ_V , κ_3 , and κ_{2V} , and the study of their correlation. For the latest experimental H + HH constraints see Refs. [319, 320].

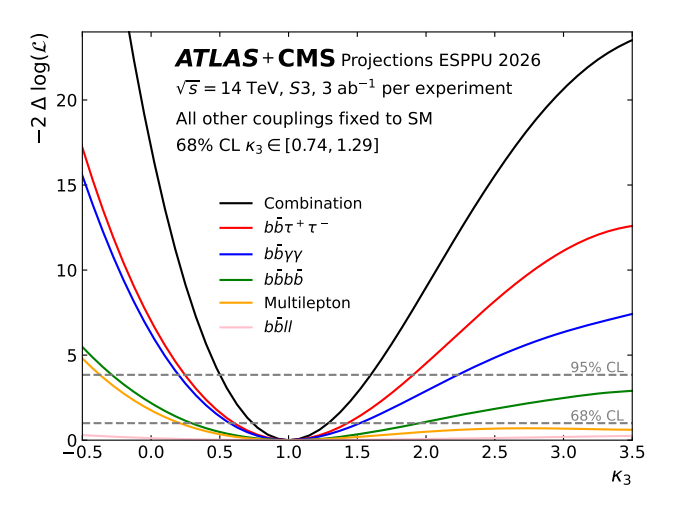
Given the statistically limited nature of the Higgs boson pair production analyses and the ongoing advancements in experimental techniques, incorporating data from the LHC Run 3 is of particular importance. The first analysis utilizing the Run 3 dataset is presented in Ref. [321], where ATLAS presents a search for HH production in the $b\bar{b}\gamma\gamma$ final state using a combined dataset of 140 fb $^{-1}$ at 13 TeV and 168 fb $^{-1}$ at 13.6 TeV. This search sets a 95% CL upper limit on the signal strength of $\mu_{HH} < 3.8$, and constrains the Higgs boson self-coupling to $-1.7 < \kappa_3 <$ 6.6. CMS has recently made public their first Run 3 search for this final state, for an integrated luminosity of $61.9~{\rm fb^{-1}}$ at $13.6~{\rm TeV}$ (2022-2023) [322]. They report a limit on the signal strength of $\mu_{HH} < 11.0$ (7.3) and a constraint on the self-coupling of $-5 < \kappa_3 < 12$ using a two-dimensional fit to the diphoton and dijet mass observables. CMS has also released a study of the $HH \rightarrow 4b$ final state using the same dataset [323]. The analysis sets observed (expected) upper limits of μ_{HH} < 4.4 (4.4), as well as couplings constraints of -3.3 < κ_3 < 9.7, and 0.63 < κ_{2V} < 1.43. Compared to previous LHC results in this final state, the sensitivity for an equivalent integrated luminosity shows a very significant improvement. Although these results do not yet exceed the sensitivity of the full Run 2 combinations, they clearly demonstrate the power of the Run 3 dataset and its potential to significantly improve κ_3 constraints already in the near term.

Projections for the HL-LHC, shown in Figure 11.13, indicate that each experiment can achieve a sensitivity better than 4σ by the end of the HL-LHC [266]. The combined ATLAS+CMS significance will result in an expected $> 5\sigma$ observation of the process already with 2 ab⁻¹. The uncertainty on the κ_3 parameter is projected to be better than 30% at $3ab^{-1}$, with the statistical uncertainty expected to remain dominant. Ongoing improvements in analysis techniques are likely to outperform this expectation. Projections for κ_{2V} based on the performance of the ATLAS boosted VBF 4b analysis [324] search yield a precision of about 13% with 3 ab⁻¹.

ii. The Hunt for Triple Higgs Boson Production

Recent studies have focused on the extremely rare HHH production. Although the SM cross section for this process is far below the LHC sensitivity, its direct access to the Higgs quartic self-coupling λ_4 has motivated the first experimental attempts to constrain potential deviations from the SM prediction.

ATLAS placed a first 95% upper limit of 59 fb on the cross section for SM HHH production through the 6b final state, using the full Run-2 dataset [325]. This limit is equivalent to 760 times the SM cross section (750 expected). Assuming $\kappa_3 = 1$ then κ_4 is constrained to $-230 < \kappa_4 < 240$ at 95% CL (both for expected and observed limits). CMS has searched for HHH in the final states with four b jets and two photons [326] and six b jets [327] with the full Run-2 dataset. The observed (expected) 95% CL upper limits on the inclusive HHH production cross section are found to be 244 (152) fb and 44 (43) fb, respectively. They can be translated to constraints of $-533 < \kappa_4 < 541$ ([-397,406] expected) and $-190 < \kappa_4 < 190$ ([-190,190] expected), also at 95% CL. In these analyses simultaneous constraints of κ_3 and κ_4 are also explored. The ATLAS 4b results have been projected to the end of the HL-LHC, yielding a limit on HHH production that amounts to 86 times the SM expectation. This is a conservative estimation, since more final states will be explored in the future.



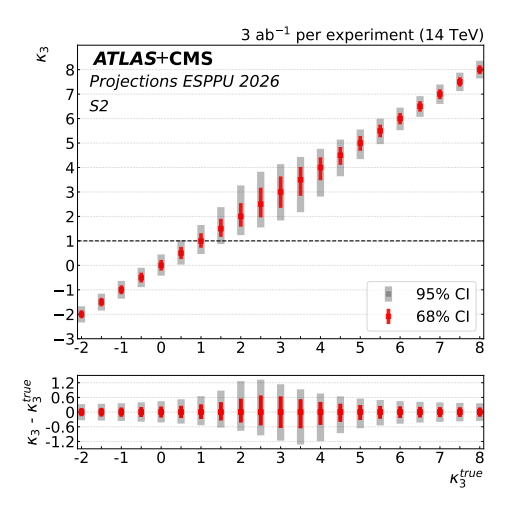


Figure 11.13: (Left) Expected ATLAS+CMS κ_3 likelihood scans for single decay channels and the combination for $3ab^{-1}$, fixing $\kappa_3 = 1$ (Right) Precision on κ_3 as a function of its value [266].

11.3.7 Higgs-Boson Mass Measurements

The mass of the Higgs boson is not predicted by the SM and must be determined experimentally. A precise determination of its value is therefore an essential input to all theoretical predictions of Higgs boson production cross sections and decay branching ratios. And, as discussed in Section 11.2, the Higgs boson mass not only plays a key role in Higgs phenomenology but also has fundamental consequences for the structure and long-term stability of the electroweak vacuum.

The precision measurements of the Higgs boson mass at the LHC are based on two decay channels: $\gamma\gamma$ and $ZZ^*/4\ell$. These channels allow for a complete reconstruction of the decay products and provide mass resolutions that range from 1.4 GeV to 2 GeV for ATLAS and from 1.0 GeV to 2.8 GeV for CMS (see Ref. [328] and the reconstruction-performance references therein). The diphoton channel provides a larger sample of Higgs bosons but with a much larger background. The four-lepton channel has less signal events, but a much smaller background and better mass resolution. The measurements require a precise calibration of the energy and momentum scales for electrons, muons, and photons. The electron and muon calibrations are based primarily on the large $Z \to ee$ and $Z \to \mu\mu$ data samples, taking advantage of the precisely known mass of the Z boson. Since photons interact differently from electrons, an extrapolation from the electron calibration is necessary, which introduces additional systematic uncertainties.

ATLAS and CMS have published many Higgs boson mass measurements using both the Run 1 and Run 2 datasets. The most precise results from both experiments are summarized below:

• The most precise measurement of the Higgs boson mass was obtained by ATLAS using the Run 1 and Run 2 datasets by combining the diphoton and ZZ channels [329]. This yielded a mass of:

$$m_H = 125.11 \pm 0.09 \, (\text{stat.}) \pm 0.06 \, (\text{syst.}) \, \text{GeV}.$$

• The most precise diphoton channel measurement was obtained by ATLAS [330], combining their Run 1 and Run 2 measurements. The mass was measured to be:

$$m_H = 125.22 \pm 0.11 \, (\text{stat.}) \pm 0.09 \, (\text{syst.}) \, \text{GeV}.$$

The systematic uncertainty of 90 MeV is worth noting, as it results from a highly challenging calibration procedure and the estimation of the material upstream of the calorimeter, which is required to extrapolate the calorimeter energy response from electrons in Z boson decays to photons. This result is promising for future precision measurements in this channel. In addition, ATLAS estimated the expected effect of the interference between the signal and the gluon fusion continuum di-photon background to be about 24 MeV (Ref. [330]).

• The most precise four-lepton channel result was obtained by CMS [231], combining the Run 1 and Run 2 measurements. This yielded a mass of:

$$m_H = 125.08 \pm 0.10 \, (\text{stat.}) \pm 0.05 \, (\text{syst.}) \, \text{GeV}.$$

It is the most precise single-channel measurement at the LHC. Since the result is dominated by the statistical uncertainty of 100 MeV, this channel will very likely continue to yield the most precise measurements in the future as the sizes of the data sets increase.

The ATLAS and CMS collaborations combined their mass measurements using the Run-1 dataset [328] yielding

$$m_H = 125.09 \pm 0.21 \, (\mathrm{stat.}) \pm 0.11 \, (\mathrm{syst.}) \, \mathrm{GeV}.$$

The mass combination using the full Run-2 datasets of the two collaborations will significantly improve our knowledge of the Higgs boson mass, given the doubling of the signal sample and the fact that most uncertainties are uncorrelated. It will be a useful input to future SM predictions and for the LHC combination of current and future Higgs boson measurements.

11.3.8 Higgs-boson Width

In the SM, the Higgs boson width is very precisely predicted once the Higgs boson mass is known. For a mass of 125 GeV, the Higgs boson has a very narrow width of 4.1 MeV [59]. It is dominated by the fermionic decays partial width at approximately 75%, while the vector boson modes are suppressed and contribute 25% only.

In proton-proton collisions such as the ones at the LHC only the cross sections times branching fractions can be measured in all production modes. As a consequence, the total width of the Higgs boson cannot be directly derived form the measurements of Higgs boson rates without additional assumptions. Direct constraints on the Higgs boson width are much larger than the expected width of the SM Higgs boson. Indirect constraints, subject to assumptions, with all the statistics of the HL-LHC will constrain the measurement only to the $\approx 20\%$ level. In contrast, a future Higgs factory would be able to constrain the width to the level of 1% through the recoil against a Z boson in $e^+e^- \rightarrow ZH$ events [194]. The different approaches at LHC and the latest experimental measurements are discussed in the following.

11.3.8.1 Direct constraints

Analyses of the reconstructed mass line-shape in the two channels with a good mass resolution, the $H \to \gamma \gamma$ and $H \to ZZ^{(*)} \to 4\ell$ channels, allow for a direct measurement of the width of the SM Higgs boson. The intrinsic mass resolution in these channels is much larger than the expected width of the SM Higgs boson. As a result, only upper limits on the Higgs boson width have been set by ATLAS [331] and CMS [231]. The two main challenges of direct constraints on the width through the measurement of the line-shape are: (i) the modeling of resolution uncertainties and (ii) the modeling of the interference between the signal and the continuum background which can be sizeable for large widths, in particular in the range where direct constraints are set. These challenges affect mostly the diphoton channel. Given that these interference effects are small with respect to the individual channels sensitivity, they are usually neglected in deriving constraints on the total width. The combined constraints, however, being more precise, could be affected by the

interference. Direct lineshape measurements provide the most unambiguous access to the Higgs boson width, however constraints are still much larger than the expected SM width. The current results are fully compatible with the SM hypothesis.

CMS reported an upper limit on the total width of $\Gamma_H < 50$ MeV at 68% CL (330 MeV at 95% CL) [231] for the $H \to ZZ^{(*)} \to 4\ell$ channel, using the 138 fb⁻¹ collision dataset at 13 TeV. This is the most stringent constraint to date in this final state. Recently CMS followed this result with a new constraint in the diphoton channel [332] which considers the effect of the interference with the continuum, for the first time at the LHC. See more details in the following section.

11.3.8.2 Constraints in the diphoton channel

In the diphoton channel, it was noticed in Refs. [236,333–335] that the effect of the interference between the main signal $gg \to H \to \gamma \gamma$ and the continuum irreducible background $gg \to \gamma \gamma$, taking into account detector resolution effects, is responsible for a non negligible mass shift. A similar interference effect is found between $q\gamma \to \gamma \gamma$ and $q\gamma \to H \to \gamma \gamma$. The size of the mass shift depends on the total width of the Higgs boson and it was suggested that measuring this mass shift could provide a constraint on the width [333]. It was further noticed that the mass shift has a dependence also on the diphoton transverse momentum. The total width of the Higgs boson could therefore be constrained using the diphoton channel alone.

Furthermore, Ref. [336], reported that the interference between the main signal $qq \to H \to \gamma\gamma$ amplitude and the continuum irreducible background $gg \to \gamma \gamma$ amplitude generates non-negligible change in the on-shell cross sections, as a result of the existence of a relative phase between these amplitudes. The size of this on-shell interference effect depends on the total width of the Higgs boson and it was suggested that measuring this on-shell cross section precisely could provide a constraint on the Higgs total width. This interference effect yields a reduction of around 2% for the $qq \to H \to \gamma \gamma$ cross section measurement in the SM. The current evaluation of this interference effect is performed at NLO and has a $^{+50\%}_{-30\%}$ uncertainty, due to the fact that the large relative phase is driven by the two-loop $gg \to \gamma \gamma$ background amplitude [236, 333, 336]. This on-shell interference effect has a dependence on the p_T of the diphoton system and the photon polar angle in the diphoton rest frame, which can be further exploited to improve the measurement to constrain the Higgs total width. Taking the ratios of the on-shell cross section of the Higgs boson to diphoton channel and the cross section of the Higgs boson to four-leptons channel where the interference effect is negligible could put a bound on the Higgs boson total width. This ratio is free from many dominant sources of systematic uncertainties for cross section measurements, i.e., PDF uncertainty and luminosity uncertainty, and can be further improved by the accumulation of the LHC data.

Experimental studies were performed to estimate the size of these effects [330,337]. As discussed in Section 11.3.7, the estimation of the expected mass shift in the diphoton channel in ATLAS is 24 MeV. Very preliminary studies of the sensitivity of the mass shift method to estimate the width of the Higgs boson in the HL-LHC were made by ATLAS [338] and yielded an expected 95% CL upper limit on the total width of approximately 200 MeV from 3 ab⁻¹ of 14 TeV data. Similarly, a preliminary estimation of the current limit from the cross section ratio measurement and the the interference effect set constraints of 60 MeV for 3 ab⁻¹ of 14 TeV data [339].

These projections are superseded by a new Run-2 result by CMS that reports the first Higgs width constraint in the diphoton channel exploiting the effect of interference [332]. It uses the $H \to \gamma \gamma$ lineshape and studies the distortions in the mass spectrum caused by the interference between $gg \to H \to \gamma \gamma$ and the continuum $gg \to \gamma \gamma$ background. The measurement yields an upper limit of $\Gamma_H < 92$ (138) MeV at 95% CL and is the most stringent Γ_H constraint to date using measurements of on-shell Higgs boson final states.

11.3.8.3 Indirect constraints from off-shell couplings

The total width of the Higgs boson can also be constrained through the simultaneous analysis of on-shell and off-shell production measurements in the VV channel [232,233]. In the off-shell regime, introduced in Section 11.2.5.3, production in the VV final state is enhanced when the invariant mass exceeds $2m_V$ and both vector bosons become on-shell. This enhancement partially offsets the decline in Higgs boson production away from its mass peak and enables the measurement described

The signal strength measurements for on-shell $\mu_{\text{on-shell}}$ and off-shell $\mu_{\text{off-shell}}$ for a given production mechanism j can be expressed in terms of coupling modifiers g_p and g_d for production and decay respectively. The corresponding cross-sections are given by Eq. 11.12, repeated here for completeness:

$$\sigma_j^{\text{on-shell}} \propto \frac{g_p^2 g_d^2}{\Gamma_H} \propto \mu_j^{\text{on-shell}} \quad \text{and} \quad \sigma_j^{\text{off-shell}} \propto g_p^2 g_d^2 \propto \mu_j^{\text{on-shell}} \Gamma_H$$
 (11.24)

Assuming that the coupling modifiers are identical in both regimes, the total Higgs boson width Γ_H can be extracted from the ratio of the measured on-shell and off-shell signal strengths. This measurement relies on the assumption that the ratio of couplings in the off-shell and on-shell regimes follows the SM prediction, that ggF is the dominant production mechanism, and that there are no significant contributions from BSM particles to the ggH loop within the mass range considered in the analysis. Another important aspect to consider is the sizable destructive interference between the Higgs boson signal and the non-resonant VV production in the off-shell region. This interference scales with $\sqrt{\mu_i^{on-shell}}$.

ATLAS and CMS have studied off-shell production in the $H \to ZZ \to 4\ell$ channel, and are able to exclude the background-only hypothesis $\mu_{\text{off-shell}} = 0$ with a significance of 3.7 σ (2.4 σ) observed (expected) for ATLAS [340] and 3.8σ (2.4 σ expected) for CMS [231]. This corresponds to evidence for the off-shell production of a Higgs boson, through the measurement of a significant deficit in the overall $gg \to VV$ production. The measured total off-shell signal strengths $\mu_{\text{off-shell}}$, combining the 4ℓ and $2\ell 2\nu$ final states and the ggF, VBF and VH production modes, are the following:

(ATLAS)
$$\mu_{\text{off-shell}} = 1.06^{+0.62}_{-0.45} \text{ (obs)} [1.00^{+0.83}_{-0.83} \text{ (exp)}],$$

(CMS) $\mu_{\text{off-shell}} = 0.67^{+0.42}_{-0.32} \text{ (obs)} [1.00^{0.83}_{-0.84} \text{ (exp)}].$ (11.25)

These off-shell production analyses exploit kinematic event characteristics to further gain in sensitivity to discriminate between the signal and background. From these measurements of the cross-section a constraint on the total width can be derived as mentioned above, following 11.24. The sensitivity to the Higgs width already reached at Run 2 is remarkable:

(ATLAS)
$$\Gamma_H = 4.3^{+2.7}_{-1.9} \ [4.1^{+3.5}_{-3.4} \ (exp)] \text{ MeV},$$
 (11.26)
(CMS) $\Gamma_H = 3.0^{+2.0}_{-1.5} \ [4.1 \pm 3.5 \ (exp)] \text{ MeV}.$ (11.27)

(CMS)
$$\Gamma_H = 3.0^{+2.0}_{-1.5} [4.1 \pm 3.5 \text{ (exp)}] \text{ MeV}.$$
 (11.27)

CMS has also derived results allowing for anomalous couplings of the Higgs boson [341], reducing the discriminating power of the kinematic variables used in the analysis but also mitigating the model dependence. Neither the results nor the sensitivities are significantly affected by allowing specific anomalous coupling parameters to float in the fits. The best fit of Γ_H in the anomalous couplings scenario ranges from $\Gamma_H = 2.7^{+2.1}_{-1.4}$ MeV to $\Gamma_H = 3.4^{+2.3}_{-1.8}$ MeV, depending on the coupling addressed. CMS has also investigated the impact of heavy particles in the ggH loop, through the introduction of a new heavy quark with an unconstrained coupling strength κ_Q [231]. This scenario results in less stringent limits on Γ_H , though largely consistent with the previous quoted values. The resulting Γ_H measurement in this case is $\Gamma_H = 2.7^{+2.7}_{-1.8}$ MeV (expected $4.1^{+5.5}_{-4.1}$). More details can be found in Refs. [341] and [231], respectively.

ATLAS has recently applied the "on-shell to off-shell" technique to constrain the total width of the Higgs boson in the $H \to WW \to 2\ell 2\nu$ decay mode the 140 fb⁻¹ Run-2 dataset [342]. The analysis sets an observed (expected) 95% CL upper limit on the rate of off-shell Higgs boson production at 3.4 (4.4) times the SM prediction. This translates into an observed (expected) upper limit on the Higgs boson total width of 13.1 (17.3) MeV. ATLAS has applied a similar on-sell to off-shell logic to $t\bar{t}H$ production, assuming the tree-level Higgs-top Yukawa coupling is the same in the on-sell and off-sell regimes. The measurements of on-shell $t\bar{t}H$ production and four-top-quark production, which includes contributions from off-shell processes, are combined to yield an observed (expected) 95% CL upper limit of 450 MeV (75 MeV). Considering as well the constraint on the Higgs-top Yukawa coupling from loop-induced Higgs boson production and decay processes improves this result down to 160 MeV (55 MeV) [343].

Finally, ATLAS and CMS performed a study of the prospects for HL-LHC for measuring the Higgs boson width in the four lepton channel using the on-shell to off-shell method. Within assumptions similar to the ones mentioned above for the Run-2 measurements and assuming the SM central value, the width of the Higgs boson could be constrained with a $\approx 20\%$ precision with a luminosity of $3 \, \text{ab}^{-1}$ [344]:

$$\Gamma_H = 4.1_{-0.8}^{+0.7} \,\text{MeV}.$$
 (11.28)

11.3.9 Higgs-boson Spin and CP Properties

In the SM, the Higgs boson has quantum numbers $J^{PC}=0^{++}$, meaning that it is a spin-0 particle, with even charge-parity (CP). The determination of the spin and CP quantum numbers of the observed Higgs boson is therefore an essential test of the theory. Alternative spin and parity hypotheses can be tested through measurements of the kinematic distributions of the particles produced in association with the Higgs boson or resulting from the Higgs boson's decay. The charge conjugation quantum number can be inferred by the fact that the observed particle decays to two photons: since charge conjugation is multiplicative and since photons are C-odd eigenstates, the observation of the decay to two photons implies that the observed neutral particle is C-even, if we assume C conservation.

The spin of a particle directly impacts the angular distributions and relative momenta of its decay products. For example, in the decay of a spin-0 particle, the matrix element does not depend on the production and decay angles in its rest frame, which results in isotropic distributions. In contrast, a spin-2 boson would generate characteristic angular modulations and correlations among final-state momenta.

Channels in which the Higgs boson decays can be fully or partially reconstructed provide sensitivity to spin-parity assignments, anomalous couplings, and possible CP-violating contributions. The most powerful channel in this respect is $H \to ZZ^* \to 4\ell$, where all final-state momenta are measured with high precision. The fully differential decay rate depends on seven observables: the invariant masses of the two lepton pairs, and five angles defined in the Higgs boson rest frame [345, 346]. These include the decay angles θ_1 and θ_2 (the angles between the negatively charged leptons and the directions of the Z_1 and Z_2 bosons in their respective rest frames), Φ (the angle between the decay planes of the two Z bosons), Φ_1 (the angle between the Z_1 decay plane and the production plane defined by the beam axis), and θ^* (the polar angle of the Z_1 boson relative to the beam axis). These observables, illustrated in Fig. 11.14, provide detailed information on the spin and CP structure of the Higgs boson and are used in both model-specific and effective field theory interpretations.

In this channel, both ATLAS and CMS have used matrix element-based kinematic discriminants and multivariate techniques to test alternative J^P hypotheses. The results show excellent agreement with the scalar (0^+) hypothesis and exclude a pure pseudoscalar (0^-) interpretation, as well as a wide range of spin-1 and spin-2 models, at high confidence levels [40].

Complementary information is provided by the $H \to WW^* \to \ell\nu\ell\nu$ decay channel. Although a full kinematic reconstruction is not possible due to the presence of neutrinos, spin correlations induced by the V-A structure of the W boson decay lead to distinctive patterns in the final-state leptons. In particular, for a scalar Higgs boson, the charged leptons tend to be emitted close together in the transverse plane, have a small invariant mass $m_{\ell\ell}$, and the transverse mass of the reconstructed Higgs boson candidate has a distinctive distribution. These kinematic features provide discrimination power between scalar, pseudoscalar, and higher-spin hypotheses. Both experiments have excluded spin-1 alternatives in this channel at the 95% confidence level or higher.

The $H\to\gamma\gamma$ channel contributes useful constraints on alternative spin-CP scenarios. For example, the production angle of the photons in the Collins–Soper frame is sensitive to the spin of the decaying boson. Spin-2 hypotheses predict markedly different distributions from spin-0 and have been excluded with high significance. Moreover, spin-1 hypotheses are strongly disfavored on theoretical grounds: the Landau–Yang theorem forbids the decay of a spin-1 particle into two identical massless vector bosons. While exotic models involving intermediate decays to collimated photons can evade this constraint, they are not consistent with global fits to the data and are tightly constrained by existing measurements.

In addition to information from the decay kinematics, production observables sensitive to the structure of the Higgs-vector boson and Higgs-fermion couplings have been exploited in channels such as vector boson fusion (VBF), and associated production channels (VH) and (VH).

In summary, the combined data from ATLAS and CMS have excluded a pure pseudoscalar (CP-odd) Higgs boson and a range of spin-1 and spin-2 models at confidence levels that exceed 99%. These results are covered in more detail in previous reviews [40].

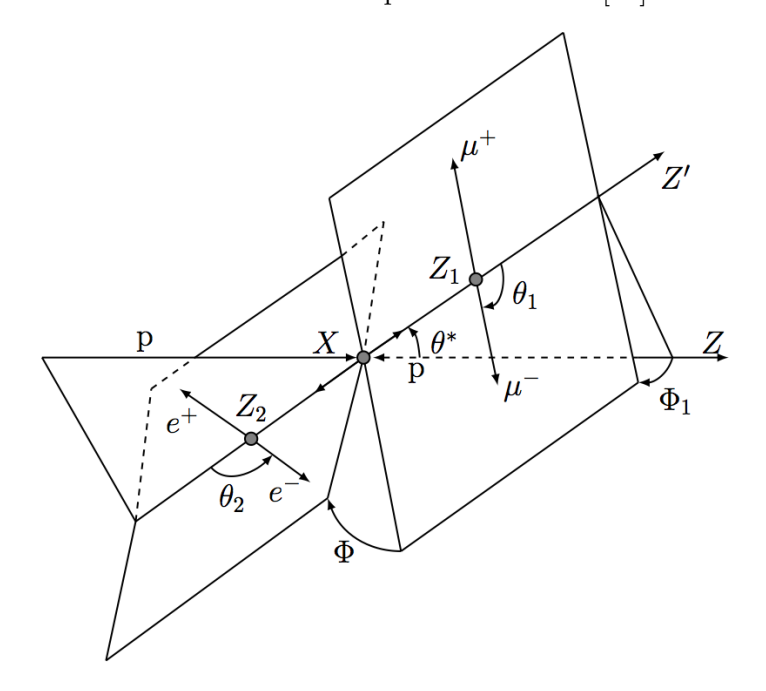


Figure 11.14: Definition of the production and decay angles defined for the $H \to ZZ^{(*)} \to 4\ell$ final state.

11.3.9.1 CP-odd interactions and CP-mixing

While a pure CP-odd hypothesis for the observed Higgs boson has been excluded at high confidence level, the presence of a small CP-odd admixture, which would signal CP violation in the Higgs sector, remains experimentally allowed. CP-odd interactions can be expressed in the framework of the SMEFT, formulated in various operator bases (as discussed in Section 11.3.5.2). This formalism aligns naturally with global analyses of a broader set of observables probing the Standard Model and its possible extensions. The CP properties inferred for the Higgs boson depend on the coupling being probed, since different interactions can exhibit different CP-mixing structures. In the context of Higgs boson interactions with electroweak bosons, the effective Lagrangian includes higher-dimensional operators constructed from the gauge-invariant combination $\Phi^{\dagger}\Phi$ and the electroweak field-strength tensors $W^I_{\mu\nu}$ and $B_{\mu\nu}$, defined prior to electroweak symmetry breaking. The CP-odd interactions are then encoded in three dimension-six operators: $\Phi^{\dagger}\Phi \tilde{W}^I_{\mu\nu}W^{I\mu\nu}$, $\Phi^{\dagger}\Phi \tilde{W}^I_{\mu\nu}B^{\mu\nu}$, and $\Phi^{\dagger}\Phi \tilde{B}_{\mu\nu}B^{\mu\nu}$, with corresponding Wilson coefficients $c_{H\tilde{W}}$, $c_{H\tilde{W}B}$, and $c_{H\tilde{B}}$, respectively.

It is important to note that CP-odd couplings of the Higgs boson to vector bosons are not allowed at tree level [347] and are therefore suppressed by Λ , the scale of new physics. However, CP-odd couplings of the Higgs boson to fermions are allowed at tree level, and these can be parametrised in a somewhat simpler way with the following Lagrangian, which accounts only for an additional pseudo-scalar term:

$$\mathcal{L}_0^{\psi_f} \supset \frac{\lambda_f}{\sqrt{2}} \left(\kappa_f H \overline{\psi}_f \psi_f + i \tilde{\kappa}_f H \overline{\psi}_f \gamma_5 \psi_f \right). \tag{11.29}$$

This formulation is equivalent to the definition of the CP-mixing angle $\varphi_f = \tan \frac{\tilde{\kappa}_f}{\kappa_f}$.

It is interesting to note that CP-odd Higgs couplings to fermions can have sizable effects on low-energy observables, such as the electron electric dipole moment (EDM), which is both precisely measured and theoretically well understood [348,349]. In particular, due to the large value of the top Yukawa coupling, CP-violating interactions involving the top quark are subject to stringent indirect limits. Current bounds on the electron EDM constrain the CP-odd top Yukawa coupling to values below $\tilde{\kappa}_t < 0.001$ [348], a level of precision that is extremely challenging to surpass with direct measurements at the LHC. It should be emphasized, however, that EDM experiments constrain the product of Yukawa couplings, in this case $\kappa_e \times \tilde{\kappa}_t$. As a result, assumptions must be made about the value of κ_e , which is itself not experimentally accessible at present.

By contrast, the constraints on the CP-odd Yukawa coupling of the tau lepton are considerably weaker. The current electron EDM bounds allow values as large as $\tilde{\kappa}_{\tau} < 0.3$ [348], leaving significant room for potential CP violation in the Higgs-tau sector. This makes direct searches for CP-odd or mixed CP Higgs couplings to taus particularly compelling. Such effects can be probed using kinematic observables sensitive to tau polarization in Higgs decays, as will be discussed in Sec. 11.3.9.3 of this review. For a discussion of searches for CP-odd couplings to vector bosons, we refer the reader to previous editions of this review [40].

With the full Run 2 dataset, analyses began to simultaneously exploit both the production and decay kinematics of the Higgs boson for CP measurements. This strategy is exemplified by the analysis of the $H \to ZZ^* \to 4\ell$, $H \to \gamma\gamma$, and $H \to WW^{(*)} \to \ell\nu\ell\nu$ channels, in both ATLAS and CMS, which combine information from the production and decay angles of the process with observables sensitive to VBF production [350,351]. In addition, studies of off-shell Higgs boson production have provided complementary information on the CP structure of the Higgs–electroweak boson interaction [341].

Some of these studies make use of "optimal observables" constructed from matrix elements within the SMEFT framework. Specifically, they are defined as the ratio of the interference term

between the SM and SMEFT amplitudes to the squared SM matrix element, evaluated for given values of the Wilson coefficients $c_{H\tilde{W}}$, $c_{H\tilde{W}B}$, and $c_{H\tilde{B}}$. Tests of CP in the HVV coupling can also

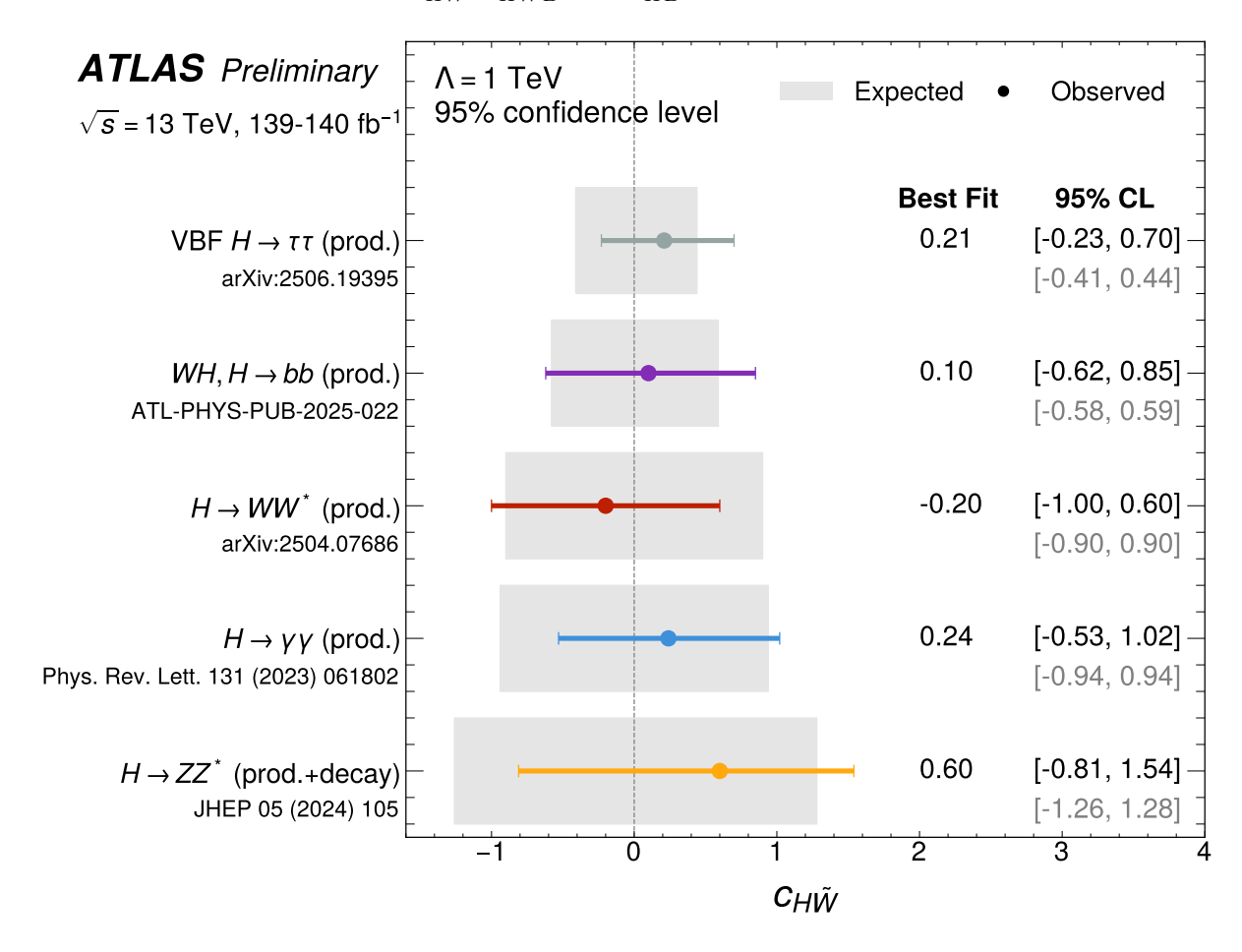


Figure 11.15: Comparison of results for the expected and observed measurements of the CP-odd Wilson coefficient $c_{H\tilde{W}}$ by ATLAS using the Run 2 dataset. The data and 95% confidence level (CL) bars show the observed values with statistical and systematic uncertainties, and the grey bands centered at zero show the expected 95% CL intervals. The test fit values and 95% CL observed (expected) limits are also explicitly listed on the right-most side of the plot in black (gray). All couplings scale as $1/\Lambda^2$ with the assumed value of $\Lambda = 1$ TeV.

be probed with the VBF production process in the $H \to \tau^+\tau^-$ channel or in the WH($b\bar{b}$) channels. Some examples of such measurements performed by ATLAS [352] are shown in Fig. 11.15. All results are found to be in agreement with the SM expectations. CMS has performed an analysis using the VBF and VH production channels and has combined its results with the aforementioned ZZ^* channel using the same dataset [353].

These results emphasize the complementarity between production and decay observables and the power of a global strategy that combines all accessible experimental information to test the Higgs boson's properties.

11.3.9.2 Probing the $Hf\bar{f}$ coupling CP properties in $pp \to t\bar{t}H$ production

As mentioned above, although EDM experiments provide stringent constraints on CP-violating effects in the top Yukawa sector, these limits are subject to model-dependent uncertainties. It is therefore important to probe such CP-violating effects through direct measurements. The associ-

ated production of a Higgs boson with a top-quark pair $(pp \to t\bar{t}H)$ offers a powerful channel for this purpose. In particular, Run 2 data have provided enhanced sensitivity to the CP structure of the top Yukawa coupling, especially in final states where the Higgs boson decays to two photons. In this channel, angular and kinematic correlations between the Higgs boson and the top quarks offer sensitivity to possible CP-odd contributions.

Using the full Run 2 dataset, several Higgs boson decay channels have been studied in this context. In the $H\to\gamma\gamma$ channel, ATLAS excludes CP-mixing angles $\varphi_t>43^\circ$ and $\varphi_t<-43^\circ$ at 95% confidence level [354]. More recently, constraints from the $H\to b\bar{b}$ channel have been reported, with a measured value of $\varphi_t=11^\circ{}^{+52^\circ}_{-73^\circ}$ [355].

Using the full Run 2 dataset, CMS [356] measured the CP-odd fraction of the top Yukawa coupling in the diphoton channel, defined as:

$$f_{CP} = \frac{|\tilde{\kappa}_t|^2}{|\kappa_t|^2 + |\tilde{\kappa}_t|^2} \times \operatorname{sign}\left(\frac{\tilde{\kappa}_t}{\kappa_t}\right), \tag{11.30}$$

and obtained a value of $|f_{CP}| = 0.00 \pm 0.33$. A complementary constraint on the CP-odd fraction was also derived using the $H \to 4\ell$ channel [357]. More recently, CMS has analyzed the $t\bar{t}H$ multilepton channel, which is sensitive to both $H \to WW$ and $H \to \tau^+\tau^-$ decays, to further probe the CP properties of the top Yukawa interaction [358]. Combining this analysis with those from the diphoton and four-lepton channels, CMS obtained an updated constraint on the CP-odd fraction:

$$|f_{CP}| = 0.28_{-0.28}^{+0.27}. (11.31)$$

In these analyses, events with both leptonic and hadronic top-quark decays were included to maximize acceptance and statistical power.

11.3.9.3 Probing $Hf\overline{f}$ coupling CP properties in $H \to \tau^+\tau^-$ decays

As discussed in Section 11.3.9.1, the decay of the Higgs boson to tau leptons provides opportunities to probe the CP properties of the $Hf\bar{f}$ coupling, thanks to the sensitivity of certain observables to tau polarization.

Using the full Run 2 dataset, CMS performed the first analysis of transverse spin correlations between the tau leptons in this final state [359]. These correlations are sensitive to the CP-mixing angle, which characterizes the relative contributions of scalar and pseudoscalar components in the Higgs—tau coupling. The transverse spin correlations manifest themselves through the angular distributions of the visible tau decay products, which are experimentally accessible.

In the case of the two-body decay of a tau lepton into a charged pion and a neutrino, the transverse momenta of the two charged pions tend to be anti-aligned for a scalar Higgs boson and aligned for a pseudoscalar. Consequently, the angle between the decay planes of the two tau leptons, as illustrated in Fig. 11.16 (left), is sensitive to the CP-mixing of the Higgs-tau coupling.

Since the tau direction cannot be reconstructed directly, the direction of the impact parameter is used as a proxy. The impact parameter is defined as the vector pointing from the interaction point to the point of closest approach of the charged pion track. In the Higgs boson rest frame, these directions are denoted by λ^{\pm} , as shown in Fig. 11.16 (center).

For multi-body tau decays—such as those proceeding via intermediate vector mesons like the ρ or $a_1(1260)$, the decay planes are constructed from the visible final-state particles. In the case of $\rho \to \pi^+\pi^0$, the decay plane is defined by the charged and neutral pion momenta. For $a_1 \to \pi^+\pi^0\pi^0$, the plane is typically defined using the charged pion and the combined momentum of the two neutral pions. These angular correlations provide sensitivity to the CP structure of the Higgs—tau interaction. The separation between pure scalar and pure pseudoscalar scenarios is illustrated in Fig. 11.16 (right).

A similar analysis was performed by ATLAS [360]. The observed (expected) results are summarized below:

ATLAS
$$\varphi_{\tau} = 9^{o} \pm 16^{o} \quad (0^{o} \pm 28^{o}) \quad [359],$$

CMS $\varphi_{\tau} = -1^{o} \pm 19^{o} \quad (0^{o} \pm 21^{o}) \quad [360].$

The current experimental precision achieved by ATLAS and CMS is already comparable to the targets originally foreseen for the HL-LHC, as outlined in Ref. [361], which projected an angular resolution between $\pm 18^{\circ}$ and $\pm 30^{\circ}$.

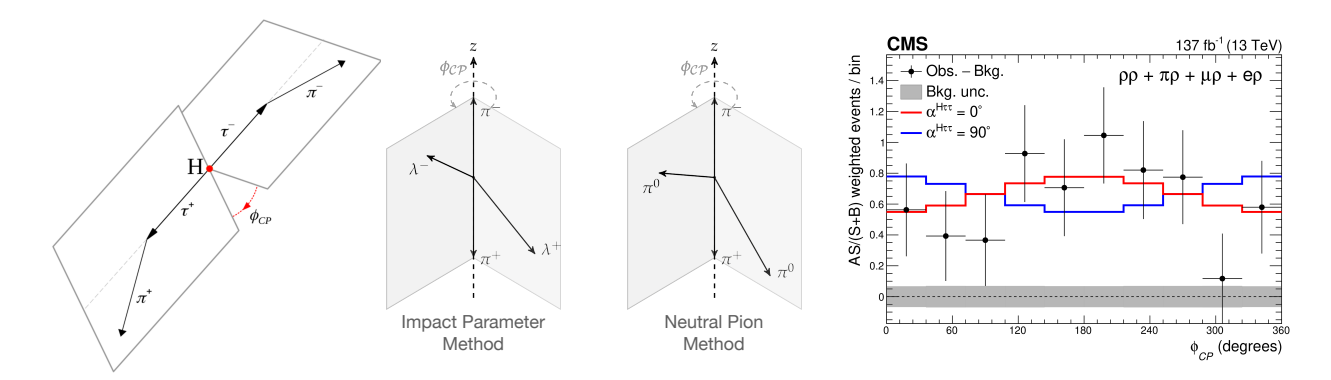


Figure 11.16: Sketch of the definition of the φ_{CP} angle for for the decays $\tau^{\pm} \to \pi^{\pm} \nu_{\tau}$ (left) and the definition at reconstruction level of φ_{CP} observables (center). The rightmost plot shows the distribution weighted per tau decay categories of the φ_{CP} observables, including the expected distributions for the expected pure scalar or pure pseudo scalar cases.

11.3.9.4 Implications of Higgs boson measurements on its CP properties

Beyond the hypothesis testing performed in specific final states, the global consistency of measured Higgs production and decay kinematics, which assumes a spin-0, CP-even boson, provides compelling evidence for this assignment. Kinematic features, including transverse momentum spectra, jet correlations, and angular observables, have been measured with high precision across various production and decay channels. The excellent agreement with SM expectations implies that large deviations from the spin-0, CP-even scenario are highly disfavored. While small admixtures of non-SM CP-odd components in the coupling structure remain experimentally allowed, the data strongly support the conclusion that the observed particle is dominantly a spin-0 scalar with positive parity.

11.4 Beyond the Standard Model (BSM) Higgs boson

The discovery of a light scalar with couplings to gauge bosons and fermions that are consistent with SM predictions, together with the slow running of the Higgs boson self-coupling at high energies allow one to consider the SM as a valid perturbative description of nature all the way to the Planck scale. This picture is admittedly very attractive, but it posits that the Higgs boson is an elementary scalar field, whose mass has quantum sensitivity to possible new physics scales. As discussed in Section 11.1.3 this EW/Higgs naturalness problem [23] has become much more definite after the Higgs boson discovery at $m_H = 125$ GeV. Finding a more fundamental explanation of the origin of EWSB and of the EW scale is by itself a strong motivation to explore BSM theories that could induce the existence of the scalar sector of the SM as it has now been experimentally confirmed.

There are two broad classes of models addressing the naturalness problem⁹, that we can in full generality classify as based on a weakly coupled or strongly coupled approach to EWSB. The first one is based on SUSY [24] (for comprehensive reviews, see Refs. [25, 26]). This is a weakly coupled approach to EWSB, maintaining the perturbativity of the SM. The Higgs boson remains elementary and the corrections to its mass are screened at the scale at which SUSY is broken, generically identified with the soft SUSY breaking parameter, $M_{\rm SUSY}$. Provided $M_{\rm SUSY}$ is of order of a few TeV, the fine-tuning problem is solved, in the sense that the low energy mass parameters of the Higgs sector become insensitive to physics at the GUT or Planck scale. Another interesting feature of SUSY theories is related to the dynamical generation of EWSB [363]. While in the SM a negative Higgs-boson mass parameter μ^2 (see Eq. 11.2) needs to be inserted by hand to induce EWSB, in SUSY, even if the relevant Higgs mass parameter is positive in the ultraviolet, it may become negative and induce EWSB radiatively through the strong effect of the top quark-Higgs boson coupling in its renormalization group evolution [363]. The scalar sector of SUSY-based theories is a particular realization of a Two Higgs-Doublet Model (2HDM) that only extend the scalar sector of the SM by one extra complex SU(2) doublet, under certain additional symmetry conditions. It predicts three neutral and a pair of charged Higgs particles [39]. One of the neutral Higgs bosons, most often the lightest CP-even one, has properties that can resemble those of the SM Higgs boson (at least in some regions of the parameter space referred to as the alignment limit [364, 365], which in the case of sufficiently heavy additional Higgs bosons is dubbed the decoupling limit [366, 367]). Such scalar is referred to as a SM-like Higgs boson, meaning that its couplings are close to the ones predicted in the SM.

The other approach invokes the existence of strong interactions at a scale of the order of one TeV or above and these new interactions induce the breaking of the electroweak symmetry [368]. In the original incarnation, dubbed technicolor, the strong interactions themselves trigger EWSB without the need of a Higgs boson. Another possibility, compatible with the ATLAS and CMS discovery, is that the strong interactions produce four light resonances identified with the Higgs-field doublet and EWSB proceeds through vacuum misalignment [27] (see also Refs. [28, 29] for recent reviews). In that case, the Higgs boson itself has a finite size and thus never feels the UV degrees of freedom that would otherwise have dragged its mass to much higher scales. The Higgs boson could also correspond to the Goldstone boson associated with the spontaneous breaking of scale invariance, see Ref. [369] and references therein. However, this dilaton/radion scenario now requires a jumbled model-building to be consistent with the constraints from the coupling measurements. The idea that the Higgs boson itself could be a composite bound state emerging from a new strongly-coupled sector has been also reconsidered thanks to the insights gained from the AdS/CFT duality. The composite Higgs boson idea is a realization of EWSB via strong dynamics that smoothly interpolates between the standard technicolor approach and the true SM limit. To avoid the usual conflict with EW data, it is sufficient, if not necessary, that a mass gap separates the Higgs resonance from the other resonances of the strong sector. Such a mass gap can naturally follow from dynamics if the strongly-interacting sector exhibits a global symmetry, G, broken dynamically to a subgroup H at the scale f, such that, in addition to the three Nambu-Goldstone bosons of SO(4)/SO(3)that describe the longitudinal components of the massive W and Z, the coset G/H contains a fourth Nambu-Goldstone boson that can be identified with the physical Higgs boson. Modern incarnations of composite Higgs models have been recently investigated in the framework of 5D warped models where, according to the principles of the AdS/CFT correspondence, the holographic composite Higgs boson then originates from a component of a gauge field along the 5th dimension with appropriate boundary conditions. A last proposed ingredient in the construction of viable

⁹Another solution to the naturalness problem is to lower the fundamental scale of quantum gravity, like for instance in models with large extra-dimensions, see Ref. [362].

composite Higgs-boson models is the concept of partial compositeness [370], i.e., the idea that there are only linear mass mixings between elementary fields and composite states. After diagonalization of the mass matrices, the SM particles, fermions and gauge bosons, are admixtures of elementary and composite states and thus they interact with the strong sector, and in particular with the Higgs boson through their composite component. This setup has important consequences on the flavor properties, chiefly the suppression of large flavor-changing neutral currents involving light fermions. It also plays an important role in dynamically generating a potential for the would-be Goldstone bosons. Partial compositeness also links the properties of the Higgs boson to the spectrum of the fermionic resonances, i.e., the partners of the top quark. The bounds from the direct searches for the top partners, in addition to the usual constraints from EW precision data, force the minimal composite Higgs models into some unnatural corners of their parameter spaces [371].

Beyond models that directly address the problem of naturalness and the origin of the EWSB, NP explorations through the Higgs portal can be more agnostic and test the existence of exotic particles from unknown extensions of the SM. Among weakly-interactive theories derived from extended gauge symmetry groups (e.g. grand-unified theories [372]), many include extended scalar sectors, that involve scalar singlets, extra doublets, triplets, or even more complicated scalar multiplet structures. In these models, as for SUSY-inspired models, EWSB is realized in such a way to generate a physical scalar mass eigenstate with the property of the SM Higgs boson. However, the spectrum of physical scalars also includes a variety of extra heavier CP-even scalars, both neutral and charged, as well as CP-odd pseudoscalars, that can be searched for at the LHC. At the same time, many NP scenarios involve light scalar degrees of freedom, such as axion-like-particles [373].

All these BSM scenarios can have important effects on the phenomenology of the discovered Higgs boson and reveal themselves through precision measurements of its branching ratios, width, mass, and couplings. For instance, deviations from the SM Higgs-boson pattern of couplings, explored through the κ or EFT frameworks described in Section 11.3.5, could point to specific classes of BSM theories. At the same time, direct search for heavy scalar resonances decaying into SM particles or for exotic decays of the SM Higgs boson become essential to identify evidence of NP. Furthermore, in all cases, the role of the Higgs boson in the unitarization of scattering amplitudes is shared by other particles, not just scalar particles, which remain targets of experimental searches, both in the heavy and light mass regime [29, 373–375].

In the following, we will briefly recall the most relevant phenomenological implications of NP models that motivates existing BSM Higgs searches at the LHC. Because of their distinct phenomenology, they will be grouped into weakly- and strongly-coupled models, discussed in Sections 11.4.1 and 11.4.2 respectively. Constraints on exotic decays of the discovered Higgs boson will be presented in Section 11.4.3 and a comprehensive summary of existing searches for BSM scalars will be the subject of Section 11.4.4.

11.4.1 Weakly coupled approach to EWSB

11.4.1.1 Higgs bosons in the Minimal Supersymmetric Standard Model (MSSM)

The simplest realistic model of low-energy SUSY is the minimal SUSY extension of the SM (MSSM) [26, 376], that associates a SUSY partner to each gauge boson and chiral fermion of the SM, and provides a realistic model of physics at the weak scale. Of the more than 100 new parameters that are introduced in the general MSSM [26] only a subset of them impact the Higgs-boson phenomenology either directly at tree-level or through quantum effects.

The MSSM contains the particle spectrum of a 2HDM extension of the SM and the corresponding SUSY partners (see Section 11.4.1.2 for a brief overview of 2HDM). Two Higgs doublets, Φ_1 and Φ_2 , with hypercharge Y = -1 and Y = 1, respectively, are required to ensure an anomaly-free SUSY extension of the SM and to generate mass for down-type quarks/charged leptons (Φ_1) and

up-type quarks (Φ_2) [39]. The Higgs potential reads

$$V = m_1^2 \Phi_1^{\dagger} \Phi_1 + m_2^2 \Phi_2^{\dagger} \Phi_2 - m_3^2 (\Phi_1^T i \sigma_2 \Phi_2 + \text{h.c.})$$

$$+ \frac{1}{2} \lambda_1 (\Phi_1^{\dagger} \Phi_1)^2 + \frac{1}{2} \lambda_2 (\Phi_2^{\dagger} \Phi_2)^2 + \lambda_3 (\Phi_1^{\dagger} \Phi_1) (\Phi_2^{\dagger} \Phi_2) + \lambda_4 |\Phi_1^T i \sigma_2 \Phi_2|^2$$

$$+ \frac{1}{2} \lambda_5 \left[(\Phi_1^T i \sigma_2 \Phi_2)^2 + \text{h.c.} \right] + \left[[\lambda_6 (\Phi_1^{\dagger} \Phi_1) + \lambda_7 (\Phi_2^{\dagger} \Phi_2)] \Phi_1^T i \sigma_2 \Phi_2 + \text{h.c.} \right],$$
(11.32)

where $m_i^2 = \mu^2 + m_{H_i}^2$ (i = 1, 2), with μ being the supersymmetric Higgsino mass parameter and m_{H_i} the soft supersymmetric breaking mass parameters of the two Higgs doublets; $m_3^2 \equiv B\mu$ is associated to the B-term soft SUSY breaking parameter; and λ_i , for i = 1 to 7, are all the Higgs quartic couplings.

After the spontaneous breaking of the electroweak symmetry, five physical Higgs particles are left in the MSSM spectrum: one charged Higgs pair, H^{\pm} , one CP-odd neutral scalar, A, and two CP-even neutral states, H and h, with h being the lightest. The Higgs sector at tree level depends on the electroweak gauge coupling constants and the vacuum expectation value v – or equivalently the Z gauge boson mass – and is determined by only two free parameters: $\tan \beta$ - the ratio of the two Higgs doublets' vacuum expectation values v_2/v_1 - and one Higgs boson mass, conventionally chosen to be the CP-odd Higgs boson mass, m_A . The other tree-level Higgs boson masses are then given in terms of these parameters. The tree level value of m_h is maximized not only for $m_A \gg m_Z$ but also for $\tan \beta \gg 1$. For $m_A \gg m_Z$ it acquires a maximum value $m_h = m_Z \cos 2\beta$. Radiative corrections have a significant impact on the values of Higgs boson masses and couplings in the MSSM. They have been computed using a number of techniques, with a variety of approximations, see Ref. [377] for a recent review. The discovered SM-like Higgs boson, if interpreted as the lightest MSSM Higgs boson with a mass of about 125 GeV, provides information on the possible MSSM parameter space [26].

The phenomenology of the Higgs sector depends on the couplings of the Higgs bosons to gauge bosons and fermions 11 . At tree-level, the couplings of the two CP-even Higgs bosons to W and Z bosons are given in terms of the angles α , that diagonalizes the CP-even Higgs boson squared-mass matrix, and β

$$g_{hVV} = g_V m_V \sin(\beta - \alpha), \quad g_{HVV} = g_V m_V \cos(\beta - \alpha),$$
 (11.33)

where $g_V \equiv 2m_V/v$, for V=W or Z ($g_V m_V$ is the SM hVV coupling). Observe that in the limit $\cos(\beta-\alpha)\to 0$, the lightest CP-even Higgs boson h behaves as the SM Higgs boson. This situation is called alignment and is achieved in specific regions of parameter space for $m_A \geq m_Z$ [366] or in the large $m_A\gg m_Z$ limit, in which alignment is achieved through decoupling [366, 367]. There are no tree-level couplings of A or H^\pm to VV. The couplings of the Z boson to two neutral Higgs bosons are given by $g_{\phi AZ}(p_\phi-p_A)$, where $\phi=H$ or h, the momenta p_ϕ and p_A point into the vertex, and

$$g_{hAZ} = g_Z \cos(\beta - \alpha)/2, \quad g_{HAZ} = -g_Z \sin(\beta - \alpha)/2. \tag{11.34}$$

The expressions of the couplings between a charged Higgs boson, a neutral Higgs boson and the W boson as well as the expressions of the four-point couplings of vector bosons and Higgs bosons can be found in Ref. [39].

 $^{^{10}}$ Observe that in the SM sections of this review, H denotes the SM Higgs boson, whereas in the sections about SUSY, or extensions of the SM with two Higgs doublets, H is used for the heaviest CP-even Higgs boson, since this is the standard notation in the literature, and the 125 GeV SM-like light Higgs boson will be denoted by h. Generically, in the MSSM, the lightest CP-even Higgs boson is indeed SM-like and thus it is naturally identified with the 125 GeV Higgs boson discovered by ATLAS and CMS, while in general 2HDM extensions, with or without SUSY, there could still be lighter scalar states below 125 GeV. To avoid confusion we will keep denoting the SM-like Higgs boson by h in the entire BSM Higgs section.

¹¹Reviews of the properties and phenomenology of the Higgs bosons of the MSSM can be found for example in Refs. [26, 378, 379].

The tree-level Higgs boson couplings to fermions obey the following property: the neutral components of one Higgs doublet, Φ_1 , couple exclusively to down-type fermion pairs while the neutral components of the other doublet, Φ_2 , couple exclusively to up-type fermion pairs [39]. This Higgs-fermion coupling structure corresponds to a Type-II 2HDM (see Section 11.4.1.2). In the MSSM, fermion masses are generated when both neutral Higgs components acquire a vacuum expectation value, and the relations between Yukawa couplings and fermion masses are (in third-generation notation)

$$y_{b,\tau} = \sqrt{2} \, m_{b,\tau} / (v \cos \beta), \quad y_t = \sqrt{2} \, m_t / (v \sin \beta).$$
 (11.35)

The couplings of the neutral Higgs bosons to $f\bar{f}$, relative to their SM values, $g m_f/(2m_W)$, are therefore given by

$$hb\bar{b}: -\sin\alpha/\cos\beta, \qquad ht\bar{t}: \cos\alpha/\sin\beta, Hb\bar{b}: \cos\alpha/\cos\beta, \qquad Ht\bar{t}: \sin\alpha/\sin\beta, Ab\bar{b}: \gamma_5 \tan\beta, \qquad At\bar{t}: \gamma_5 \cot\beta.$$
 (11.36)

In each relation above, the factor listed for $b\bar{b}$ also pertains to $\tau^+\tau^-$. The charged Higgs boson couplings to fermion pairs, normalized to $g/(\sqrt{2}m_W)$, are given by

$$g_{H^-t\bar{b}}: m_t \cot \beta \frac{1+\gamma_5}{2} + m_b \tan \beta \frac{1-\gamma_5}{2}, \quad g_{H^-\tau^+\nu}: m_\tau \tan \beta \frac{1-\gamma_5}{2}.$$
 (11.37)

The non-standard neutral Higgs bosons have significantly enhanced couplings to down-type fermions at sizable $\tan \beta$. Radiative corrections can modify significantly the values of the Higgs boson couplings to fermion pairs and to vector boson pairs, through a radiatively-corrected value for $\cos(\beta - \alpha)$ as well as from the one-loop vertex corrections to tree-level Higgs-fermion Yukawa couplings, see Ref. [26] and references therein, for a detailed discussion.

Given the outlined structure of the MSSM Higgs bosons couplings to SM fermions and gauge bosons the MSSM parameters have to be arranged such that the mass, the CP properties, as well as the decay and production properties of one of the neutral Higgs bosons agree with the LHC Higgs data. Given that present data allows only for moderate departures from the SM predictions, it implies that some degree of alignment is necessary.

The SM-like branching ratios of h can be modified if decays into SUSY particles are kinematically allowed, and, in particular, decays into a pair of the lightest SUSY particles – i.e., the lightest neutralinos, $\tilde{\chi}_1^0$, can become dominant and would be invisible if R-parity is conserved [380]. Moreover, if light superpartners exist and couple to photons and/or gluons, the h loop-induced coupling to gg and $\gamma\gamma$ could deviate sizeably from the corresponding SM predictions (see for instance the review [379]), and would be in conflict with present data (see Section 11.3.5). For the heavier Higgs states, there are two possibilities to be considered 12 :

- i) Alignment triggered by decoupling, hence $m_A \geq$ several hundred GeV: the HWW and HZZ couplings are very small. The dominant H, A decay branching ratios strongly depend on $\tan \beta$. The decay modes $H, A \rightarrow b\bar{b}, \ \tau^+\tau^-$ dominate when $\tan \beta$ is large (this holds even away from decoupling). For small $\tan \beta$, the $t\bar{t}$ decay mode dominates above its kinematic threshold. For the charged Higgs boson, $H^+ \rightarrow t\bar{b}$ dominates.
- ii) Some degree of alignment without decoupling, hence $m_A \leq$ a few hundred GeV: the main difference with the previous case is that, in the low tan β regime (tan $\beta \leq 5$), additional decay channels may be allowed which involve decays into the lightest SM-like Higgs boson; $A \to Zh$,

 $^{^{12}}$ In very special regions of the parameter space, there is still the possibility that the heavier CP-even Higgs state is identified with the 125 GeV Higgs boson discovered by ATLAS and CMS, see for instance the discussion in Ref. [381] and the benchmark M_H^{125} defined in Ref. [382].

 $H \to hh$ as well as $H \to WW/ZZ$ decay modes are available (they are suppressed in the strict alignment limit). When kinematically open, the decays $A/H \to t\bar{t}$ become relevant or even dominant for sufficiently small tan β . For the charged Higgs boson, $H^+ \to \tau^+\nu_{\tau}$ dominates below the $t\bar{b}$ threshold, and also $H^{\pm} \to W^{\pm}h$ may be searched for.

In both cases i) and ii), the heavier Higgs states, H, A and H^{\pm} , are roughly mass degenerate (with masses \pm 20 GeV or less apart). If kinematically allowed, the heavy Higgs boson decays into charginos, neutralinos and third-generation squarks and sleptons can be important [383].

At hadron colliders, the dominant neutral Higgs boson production mechanism at moderate values of $\tan \beta$ is gluon fusion, mediated by loops containing heavy top and bottom quarks and the corresponding SUSY partners. The effect of light stops that may contribute to the gluon fusion production can be partially cancelled by mixing effects. Higgs boson radiation off bottom quarks becomes important for large $\tan \beta$, where at least two of the three neutral Higgs bosons have enhanced couplings to bottom-type fermions [384, 385]. Detailed discussions of the impact of radiative corrections in these search modes are presented for instance in Ref. [386]. The vector boson fusion and Higgs-strahlung production of the CP-even Higgs bosons as well as the associated production of neutral Higgs bosons with top quark pairs have lower production cross sections by at least an order of magnitude with respect to the dominant ones, depending on the precise region of MSSM parameter space [56–59]. Higgs boson pair production of non-standard MSSM Higgs bosons has been studied in Ref. [387, 388]. For a discussion of charged Higgs boson production at LHC, see Refs. [57,58,389]. Strong production of a heavy neutral Higgs boson followed by its decay into top-quark pairs is a challenging channel, only most recently being searched for by ATLAS and CMS. Interference effects between the signal and the SM $t\bar{t}$ background need to be carefully taken into account [390, 391].

In summary, the additional Higgs bosons are sought for mainly via the following channels:

$$\begin{split} pp &\to A/H \to \tau^+\tau^- \text{ (inclusive)}, \\ b\bar{b}A/H, A/H &\to \tau^+\tau^- \text{ (with b-tag)}, \\ b\bar{b}A/H, A/H &\to b\bar{b} \text{ (with b-tag)}, \\ pp &\to t\bar{t} \to H^\pm W^\mp b\bar{b}, \ H^\pm \to \tau^+\nu_\tau(\tau^-\bar{\nu}_\tau) \text{ or } t\bar{b} \ (b\bar{t}) \ , \\ gb &\to H^-t \text{ or } g\bar{b} \to H^+\bar{t}, \ H^\pm \to \tau^+\nu_\tau(\tau^-\bar{\nu}_\tau) \text{ or } t\bar{b} \ (b\bar{t}) \ . \end{split}$$

After the Higgs boson discovery, updated MSSM benchmarks scenarios have been defined to highlight interesting conditions for the MSSM Higgs boson searches [58,382] and are scrutinised by the LHC Higgs Working Group [392].

The compatibility between the predicted and measured Higgs boson mass sets stringent constraints on the parameter space of BSM models. As an example, Fig. 11.17 illustrates the constraints imposed on a specific scenario labeled as M_h^{125} [393] by Higgs-boson searches at the LHC. The M_h^{125} benchmark assumes that super partners are heavy, so that the phenomenology of the observed Higgs boson is not altered except in its couplings due to the existence of another doublet. Note that to use the predicted Higgs boson mass as a constraint (exclusion at nearly constant $\tan \beta$ at high M_A in the $(M_A, \tan \beta)$ plane), it is important to account for the theoretical uncertainty on the prediction which is in excess of an order of magnitude larger than the experimental uncertainty on the measured mass of the Higgs boson. The theoretical uncertainty depends itself on the specific SUSY spectrum for a given MSSM parameter set. It is therefore highly model-dependent and influenced by parameters that do not affect much the phenomenology of the heavy Higgs bosons. A more generic estimate of ± 3 GeV is made and found to be a conservative choice [377]. It should

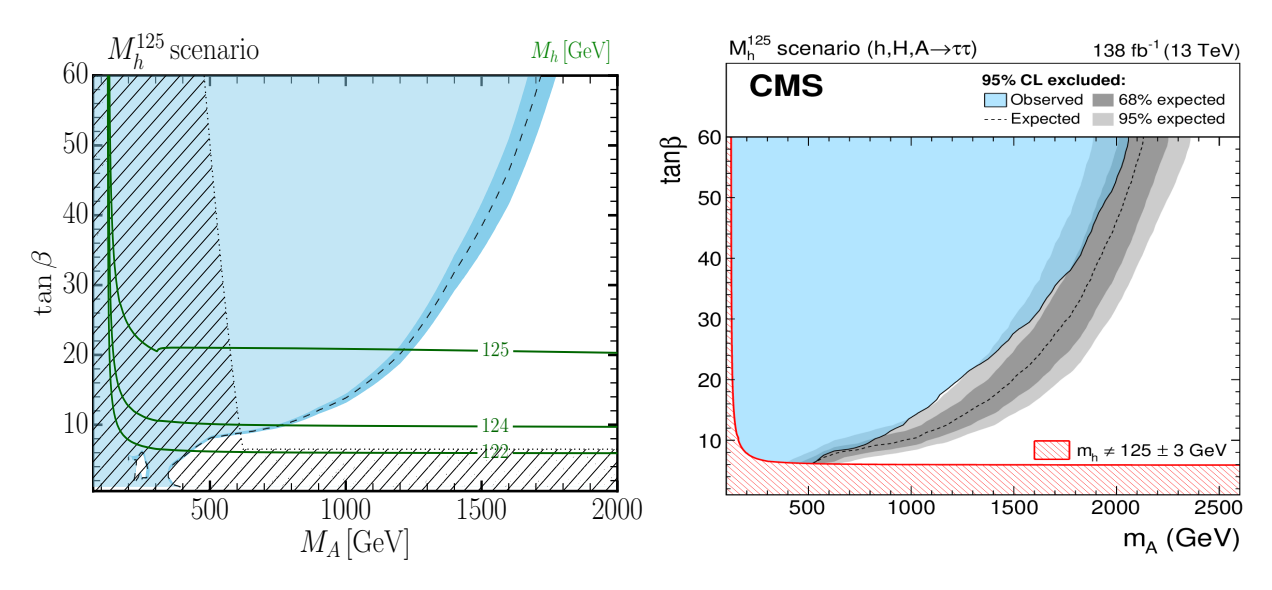


Figure 11.17: (Left) The predicted 95% CL exclusion contours in the $(M_A, \tan \beta)$ parameter space for the M_h^{125} benchmark scenarios [393]. The blue area represents the bounds from searches for heavy Higgs bosons (H and A), with the darker blue band indicating the theoretical uncertainty. The green solid lines are predictions for the mass of the lighter CP-even scalar h, the hatched area is excluded by a mismatch between the properties of h and those of the observed Higgs boson. The nearly vertical dotted line illustrates the lower limit on the mass of the A boson from precision measurements of the Higgs-boson couplings and the close-to horizontal dotted line represents the limit on $\tan \beta$ from the compatibility of the measured mass of the observed Higgs boson and the prediction using radiative corrections. (Right) Expected and observed 95% CL exclusion contours. The expected median in the absence of a signal is shown as a dashed black line. The dark and bright grey bands indicate the central 68% and 95% intervals of the expected exclusion. The observed exclusion contour is indicated by the colored blue area. Those parts of the parameter space where M_h deviates by more then ± 3 GeV from the mass of h(125) are indicated by a red hatched area [394].

also be noticed that the red region of parameter space is highly model-dependent and it depends on parameters that do not affect much the phenomenology of the heavy Higgs bosons.

The scalar sector of the MSSM can be also extended to include extra singlets. The addition of a singlet superfield to the MSSM may come along with additional symmetries imposed to the theory. Depending on such symmetries, different models with singlet extensions of the MSSM (xMSSM) have been proposed, see Ref. [395] for a general review. A singlet extended SUSY Higgs sector opens new avenues for discovery. Since the singlet pseudoscalar particle may be identified as the pseudo-Goldstone boson of a spontaneously broken Peccei-Quinn symmetry, it may become naturally light [396]. Generally, there is mixing of the singlet sector with the MSSM Higgs sector, and for a sufficiently light, singlet-dominated scalar or pseudoscalar, h_S or A_S , respectively, the SM-like Higgs boson h may decay to pairs of h_S or A_S . The light scalar and/or pseudoscalar may subsequently decay to $\tau\tau$ or $b\bar{b}$ pairs. Such cascade decays are more difficult to detect than in standard searches due to the potentially soft decay products. There is also a rich phenomenology for the decays of the heavy CP-even and CP-odd doublets, H and H into two lighter Higgs bosons such as $H \to hh_S$, hh, h_Sh_S or H and H as well as into a light Higgs boson and a gauge boson: $H \to A_SZ$; H and H is singlet-dominated scalar or pseudoscalar are somewhat heavier, the decays H and H or H is singlet-dominated scalar or pseudoscalar are somewhat heavier, the decays H is H into the decays H into the decays H is H into the decays H is H into the decay H is H into the decay H is H into the decay H into the decay H is H into the decay H is H into the decay H is H into the decay H into the decay H is H into the decay H into the decay H is H into the decay H into the decay H is H into the decay H into the decay H is H into the decay H into

 $A_S \to h_S Z$ will be allowed.

Additional extensions of the MSSM have been considered to either avoid phenomenological constraints or address phenomena not explained in the SM. For instance, SUSY scenarios with CP-violation (CPV) phases are theoretically appealing, since additional CPV beyond that observed in the K-, D-, and B-meson systems is required to explain the observed cosmic matter-antimatter asymmetry. In the MSSM, CPV effects in the Higgs sector appear at the quantum level, while in singlet extensions of the MSSM CPV effects can already be present at tree level. In general, CPV effects in the Higgs sector have significant constraints from electric dipole moments data [397]. Major variations to the Higgs-boson phenomenology occur in the presence of explicit CPV phases. In the CPV case, vector-boson pairs couple to all three neutral Higgs-boson mass eigenstates. The discovery of a 125 GeV Higgs boson has put strong constraints on the realization of the CPV scenario within the MSSM. This is partly due to the fact that the observed Higgs-boson rates are close to the SM values, and a large CPV component would necessarily induce a large variation in the rate of the SM-like Higgs-boson decays into the weak gauge bosons W^{\pm} and Z. The measured Higgs-boson mass imposes additional constraints on the realization of this scenario.

Future precision measurements of the Higgs-boson couplings to fermions and gauge bosons together with information on heavy Higgs-boson searches will provide powerful information on the SUSY parameter space [398]. Improvements in our understanding of B-physics observables put indirect constraints on additional Higgs bosons in mass ranges that would not be accessible in direct LHC searches. In particular, $BR(B_s \to \mu^+\mu^-)$, $BR(b \to s\gamma)$, and $BR(B_u \to \tau\nu)$ play an important role within minimal flavour-violating (MFV) models [399], in which flavour effects proportional to the CKM matrix elements are induced as in the SM [400].

11.4.1.2 Non-supersymmetric extensions of the Higgs sector

There are many ways to extend the minimal scalar sector of the SM. In the case of SUSY models illustrated in Section 11.4.1.1, the scalar sector consists of a constrained type-II 2HDM (see point i. below), with restrictions on the Higgs-boson masses and couplings induced by SUSY. In the following discussion, more generic 2HDM's are presented (for some comprehensive reviews, see [401]). These models are theoretically less compelling since they do not provide an explanation for the SM Higgs naturalness problem, but on the other hand they are agnostic about the overall theoretical framework they may derive from, and can lead to different patterns of Higgs-fermion couplings, hence, to different phenomenology. It is also possible to consider models with a SM Higgs boson and one or more additional scalar SU(2) doublets that acquire no VEV and hence play no role in the EWSB mechanism. Such models are dubbed Inert Higgs Doublet Models (IHD) [402]. Without a VEV associated to it, a Higgs boson from an inert doublet has no tree-level coupling to gauge bosons and hence cannot decay into a pair of them. Moreover, imposing a Z_2 symmetry that prevents them from coupling to the fermions, it follows that, if the lightest inert Higgs boson is neutral, it becomes a good DM candidate with interesting associated collider signals. Various studies of IHD models in the light of a 125 GeV Higgs boson have been performed, see for instance Ref. [403], showing an interesting interplay between collider and direct DM detection signals.

An interesting type of 2HDMs are those in which an Abelian flavour symmetry broken at the electroweak scale creates the fermion mass hierarchies and mixing angles [404]. This idea is based on the Froggatt–Nielsen model [405], where a flavon field couples differently to the SM fermions of different flavour charges. Such flavon acquires a vacuum expectation value, breaking the flavour symmetry but leaving both the flavour breaking and the new physics scales undetermined. In Refs. [406], it was proposed to relate the flavour breaking scale to the electroweak scale by identifying the flavon with the modulus square of the Higgs field. A 2HDM, however, provides a more compelling realisation of the electroweak scale flavour breaking idea. In the most ambitious con-

structions of two Higgs doublet flavour models (2HDFM), the textures of the Yukawa couplings are a result of an Abelian flavour symmetry that only allows renormalisable Yukawa couplings of the top quark to the Higgs bosons. All other Yukawa couplings are generated by higher dimensional operators that produce hierarchical entries of the Yukawa matrices, explaining the observed quark masses and mixing angles. Flavour observables, LHC Higgs signal strength measurements, electroweak precision measurements, unitarity and perturbativity bounds, as well as collider searches for new scalar resonances result in precise predictions for the parameters of these 2HDFMs. In particular, correlated departures from SM Higgs boson couplings, as well as additional Higgs bosons with masses < 700 GeV must be observed at the LHC. Other incarnations of 2HDFMs can aim at only partially explaining the fermion mass hierarchies but are therefore less restrictive.

Other extensions of the Higgs sector can include multiple copies of $SU(2)_L$ doublets [407], additional scalar singlets [408], triplets or more complicated combinations of scalar multiplets in the Higgs Lagrangian . It is also possible to enlarge the gauge symmetry beyond $SU(2)_L \times U(1)_Y$ along with the necessary Higgs-field structure to generate gauge boson and fermion masses. There are two main experimental constraints on these extensions: (i) precision measurements which constrain $\rho = m_W^2/(m_Z^2\cos^2\theta_W)$ to be very close to 1 and (ii) flavour changing neutral current (FCNC) effects. In electroweak models based on the SM gauge group, the tree-level value of ρ is determined by the Higgs multiplet structure. By suitable choices for the hypercharges, and in some cases the mass splitting between the charged and neutral Higgs sector or the vacuum expectation values of the Higgs fields, it is possible to obtain a richer combination of singlets, doublets, triplets and higher multiplets compatible with precision measurements.

In the following the case of 2HDMs and models with an additional Higgs triplet will be briefly discussed as the most common examples constrained by experiments. There is a lot of activity on the study of non-supersymmetric models with an extended Higgs sector, with an intense collaboration between theorists and experimentalists in particular inside the LHC Higgs Working Group [392].

i. Two-Higgs-doublet models

General two-Higgs-doublet models [401] can have a more diverse Higgs-fermion coupling structure than in SUSY, and can be viewed as a simple extension of the SM to realize the spontaneous breakdown of $SU(2)_L \times U(1)_Y$ to $U(1)_{em}$. Quite generally, if the two Higgs doublets contain opposite hypercharges, the scalar potential will contain mixing mass parameters of the kind $m_{12}^2 \Phi_1^T i \sigma_2 \Phi_2 + h.c.$. In the presence of such terms, both Higgs doublets will acquire vacuum expectation values, $v_1/\sqrt{2}$ and $v_2/\sqrt{2}$, respectively, and the gauge boson masses will keep their SM expressions with the Higgs VEV v replaced by $\sqrt{v_1^2 + v_2^2}$. Apart from the mass terms, the most generic renormalisable and gauge invariant scalar potential for two Higgs doublets with opposite hypercharges contains seven quartic couplings, as presented in Eq. (11.32).

Just as in the MSSM case, after electroweak symmetry breaking and in the absence of CP-violation in the scalar sector, the physical spectrum contains a pair of charged Higgs bosons H^{\pm} , a CP-odd Higgs boson A and two neutral CP-even Higgs bosons, h and H. The angles α and β diagonalize the CP-even, and the CP-odd and charged Higgs sectors, respectively. The complete 2HDM is defined only after considering the interactions of the Higgs fields to fermions. Yukawa couplings of the generic form

$$-y_{ij}^a \bar{\Psi}_L^i H_a \Psi_R^j + h.c. \tag{11.39}$$

may be added to the renormalisable Lagrangian of the theory. Contrary to the SM, the two Higgs doublet structure does not ensure the alignment of the fermion mass terms $m_{ij} = y_{ij}^a v_a / \sqrt{2}$ with the Yukawa couplings y_{ij}^a . This implies that quite generally the neutral Higgs bosons will mediate

flavour changing interactions between the different mass eigenstates of the fermion fields. Such flavour changing interactions should be suppressed in order to describe properly the Kaon, D and B meson phenomenology. Based on the Glashow-Weinberg criterion [409], according to which the tree-level FCNC's mediated by neutral Higgs bosons will be absent if all fermions of a given electric charge couple to no more than one Higgs doublet, the simplest way of avoiding such transitions is to assume the existence of a symmetry that ensures the couplings of the fermions of each given quantum number (up-type and down-type quarks, charged and neutral leptons) to only one of the two Higgs doublets. Different models may be defined depending on which of these fermion fields couple to a given Higgs boson. Conventionally, models of type-I are those in which all SM fermions couple to a single Higgs field, while in type-II models, down-type quarks and charged leptons couple to a common Higgs field, while the up-type quarks and neutral leptons couple to the other. Two other realizations of type-II models are commonly referred to as "lepton-specific", when quarks couple to one of the Higgs bosons while leptons couple to the other, or "flipped" when up-type quarks and charged leptons couple to one of the Higgs fields while down-quarks and neutral leptons couple to the other. Finally, alternative ways of suppressing tree-level scalar FCNC in a 2HDM through specific assumptions on the structure of the Yukawa mixing matrices have been proposed, the so-called type-III models [410,411], and shown to be phenomenologically viable [412].

The two Higgs doublet model phenomenology depends strongly on the size of the mixing angle α and therefore on the quartic couplings. For large values of m_A , $\sin \alpha \to -\cos \beta$, $\cos \alpha \to \sin \beta$, $\cos(\beta - \alpha) \to 0$, and the lightest CP-even Higgs boson h behaves as the SM Higgs boson. The same behaviour is obtained if the quartic couplings are such that $\mathcal{M}_{12}^2 \sin \beta = -(\mathcal{M}_{11}^2 - m_h^2) \cos \beta$. The latter condition represents a situation in which the couplings of h to fermions and weak gauge bosons become the same as in the SM, without decoupling the rest of the non-standard scalars and it is of particular interest due to the fact that the discovered Higgs boson has SM-like properties. This situation will be referred to as alignment, as in the MSSM case.

In type-II 2HDM, at large values of $\tan \beta$ and moderate values of m_A , the non-standard Higgs bosons H,A and H^{\pm} couple strongly to bottom quarks and τ leptons. Hence, the decay modes of the non-standard Higgs bosons tend to be dominated by the b-quark and τ -lepton modes, including top quarks or neutrinos in the case of the charged Higgs boson. However, for large and negative values of λ_4 (see Eq. 11.32), the charged Higgs boson mass may be sufficiently heavy to allow on-shell decays $H^{\pm} \to W^{\pm} + (H,A)$, via a trilinear coupling

$$g_{H^{\pm}W^{\mp}H,A} \simeq \frac{M_W}{v} \sin(\beta - \alpha)(p_{H^+} - p_{H,A}),$$
 (11.40)

where p_{H^+} and $p_{H,A}$ are the charged and neutral scalar Higgs-boson momenta pointing into the vertex. On the other hand, for large and positive values of λ_5 (see Eq. 11.32), the above charged Higgs-boson decay into a W^{\pm} and the CP-odd Higgs boson may be allowed, but the heavy Higgs boson H may be sufficiently heavy to decay into a CP-odd Higgs boson and an on-shell $Z, H \to Z + A$, via

$$g_{HZA} \simeq \frac{M_Z}{v} \sin(\beta - \alpha)(p_H - p_A).$$
 (11.41)

The decay $H^{\pm} \to W^{\pm} + H$, on the other hand may be allowed only if $\lambda_4 < -\lambda_5$. The couplings controlling all the above decay modes are proportional to $\sin(\beta - \alpha)$ and therefore they are unsuppressed in the alignment limit. Moreover, these could still be the dominant decay modes at moderate values of $\tan \beta$, offering a way to evade the current bounds obtained assuming a dominant decay into b-quarks or τ -leptons. The quartic couplings are restricted by the condition of stability of the effective potential as well as by the restriction of obtaining the proper value of the lightest

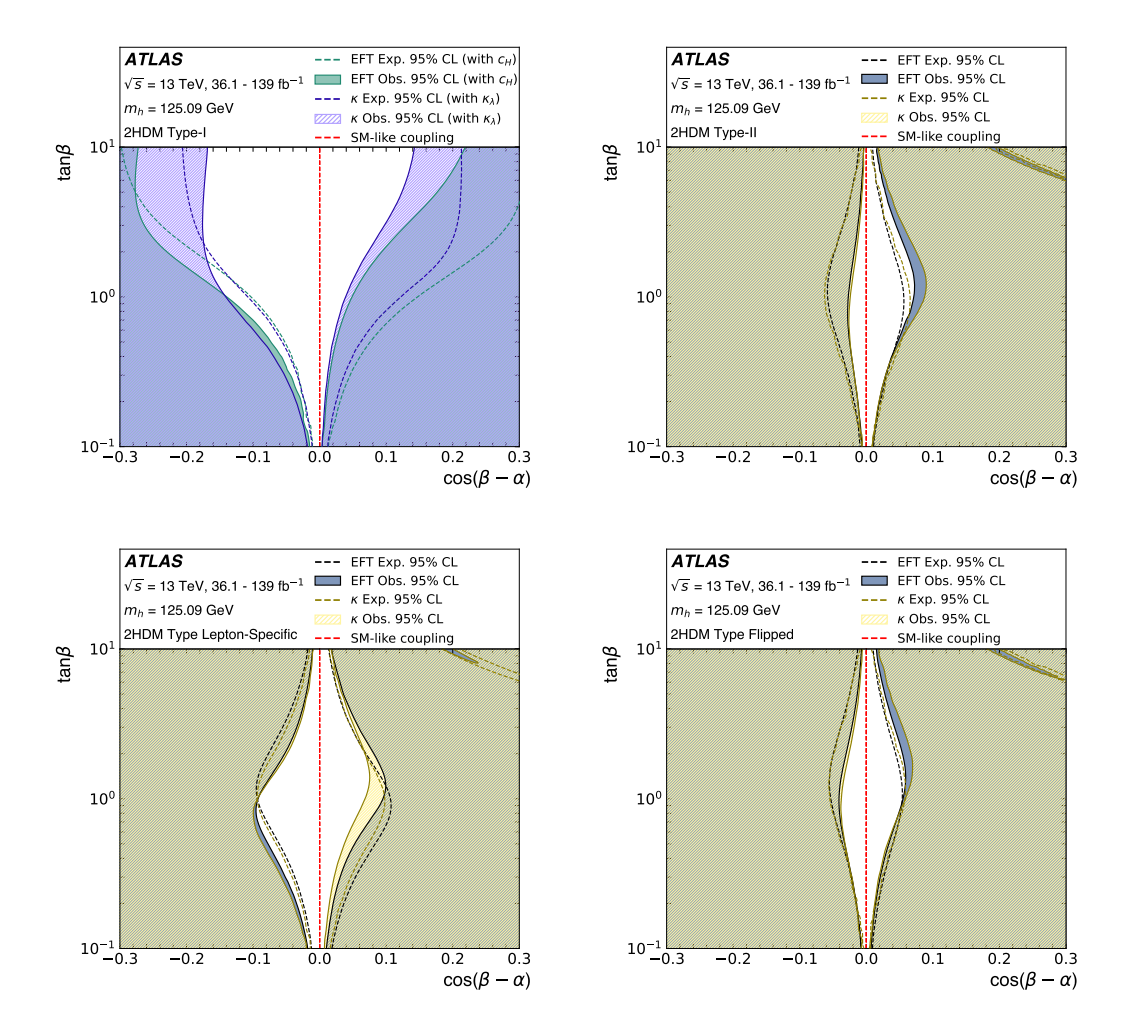


Figure 11.18: Constraints on the parameters space of 2HDM of Type I and II, based on either the κ or SMEFT approach to the parametrization of NP effects in the SM Higgs boson couplings. See Ref. [311] for more details.

CP-even Higgs boson mass. LHC measurements of Higgs-boson couplings are already constraining the 2HDM parameter space, as illustrated in Fig. 11.18 for the case of models of Type I and II.

As discussed in the case of the SUSY 2HDM, additional effects of explicit CPV can be introduced by allowing some of the parameters of the Higgs potential to be complex. As for the SUSY case, the three neutral mass eigenstates mix with each other and give origin to a different phenomenology. For a comprehensive detailed discussions of 2HDM phenomenology, see for example Refs. [59,401].

ii. Higgs-boson triplets

Electroweak triplet scalars are the simplest non-doublet extension of the SM that can participate in the spontaneous breakdown of $SU(2)_L \times U(1)_Y$ to $U(1)_{em}$. Two types of model have been developed in enough detail to make a meaningful comparison to LHC data: the Higgs triplet model (HTM) [413] and the Georgi–Machacek model (GM) [414].

The Higgs triplet model extends the SM by the addition of a complex $SU(2)_L$ triplet scalar field Δ with hypercharge Y=2, and a general gauge-invariant renormalisable potential $V(\Phi, \Delta)$ for Δ

and the SM Higgs doublet Φ . The components of the triplet field can be parameterised as

$$\Delta = \frac{1}{\sqrt{2}} \begin{pmatrix} \Delta^+ & \sqrt{2}\Delta^{++} \\ v_{\Delta} + \delta + i\xi & -\Delta^+ \end{pmatrix}, \tag{11.42}$$

where Δ^+ is a singly-charged field, Δ^{++} is a doubly-charged field, δ is a neutral CP-even scalar, ξ is a neutral CP-odd scalar, and v_{Δ} is the triplet VEV. The general scalar potential mixes the doublet and triplet components. After electroweak symmetry breaking there are seven physical mass eigenstates, denoted $H^{\pm\pm}$, H^{\pm} , A, H, and h.

A distinguishing feature of the HTM is that it violates the custodial symmetry of the SM (see Sec. 11.2.3); thus the ρ parameter deviates from 1 even at tree level. Letting x denote the ratio of triplet and doublet VEVs, the tree level expression is

$$\rho = \frac{1+2x^2}{1+4x^2} \,. \tag{11.43}$$

The measured value of the ρ parameter then limits the triplet VEV to be quite small, $x \lesssim 0.03$, or $v_{\Delta} < 8$ GeV. This constraint severely limits the role of the triplet scalar in the EWSB mechanism.

The small VEV of the Higgs triplet in the HTM is a virtue from the point of view of generating neutrino masses without the necessity for introducing right-handed neutrino fields. The gauge invariant dimension four interaction

$$h_{\nu_{ij}} \ell_i^T C^{-1} i \sigma_2 \Delta \ell_j , \qquad (11.44)$$

where ℓ_i are the lepton doublets, C is the charge conjugation matrix, and $h_{\nu_{ij}}$ is a complex symmetric coupling matrix, generates a Majorana mass matrix for the neutrinos:

$$m_{\nu_{ij}} = \sqrt{2}h_{\nu_{ij}}v_{\Delta} . \tag{11.45}$$

This can be combined with the usual neutrino seesaw to produce what is known as the type-II seesaw [415].

The HTM suggests the exciting possibility of measuring parameters of the neutrino mass matrix at the LHC. If the doubly-charged Higgs boson is light enough and/or its couplings to W^+W^+ are sufficiently suppressed, then its primary decay is into same-sign lepton pairs: $H^{++} \to \ell_i^+ \ell_j^+$; from Eq. (11.44) and Eq. (11.45), it is apparent that these decays are in general lepton-flavour violating with branchings proportional to elements of the neutrino mass matrix [416].

Precision electroweak data constrain the mass spectrum as well as the triplet VEV of the HTM [417]. These constraints favor a spectrum where H^{++} is the lightest of the exotic bosons, and where the mass difference between H^{+} and H^{++} is a few hundred GeV. The favored triplet VEV is a few GeV, which also favors H^{++} decays into $W^{+}W^{+}$ over same-sign dileptons.

The GM model addresses the ρ parameter constraint directly by building in a custodial symmetry (it was however argued that large corrections to $\rho=1$ are generated at one-loop [418], requiring some fine-tuning to preserves agreement with EW precision data). Writing the complex scalar doublet of the SM as a (2,2) under $\mathrm{SU}(2)_L \times \mathrm{SU}(2)_R$, it is obvious that the next simplest construction respecting custodial symmetry is a scalar transforming like a (3,3) [419]. These nine real degrees of freedom correspond to a complex electroweak triplet combined with a real triplet, with the scalar potential required to be invariant under $\mathrm{SU}(2)_R$. Under the custodial $\mathrm{SU}(2)_{L+R}$, they transform as $1 \oplus 3 \oplus 5$, with a CP-even neutral scalar as the custodial singlet (thus matching the SM Higgs

boson), a CP-odd neutral scalar in the custodial triplet, and another CP-even neutral scalar in the custodial 5-plet. The scalar components can be decomposed as

$$\Xi = \begin{pmatrix} \chi_3^* & \xi_1 & \chi_1 \\ -\chi_2^* & \xi_2 & \chi_2 \\ \chi_1^* & -\xi_1^* & \chi_3 \end{pmatrix},\tag{11.46}$$

where ξ_2 is a real scalar and the others are complex scalars. Linear combinations of these scalars account for the neutral custodial singlet, a neutral and singly-charged field making up the custodial triplet, and neutral, singly-charged, and doubly-charged fields making up the custodial 5-plet.

When combined with the usual SM doublet field Φ , the electroweak scale v is now related to the doublet and triplet VEVs by

$$v^2 = v_{\varPhi}^2 + 8v_{\Xi}^2 \ . \tag{11.47}$$

Note that the GM triplets by themselves are sufficient to explain electroweak symmetry breaking and the existence of a 125 GeV neutral boson along with a custodial triplet of Goldstone bosons; the complex doublet field in the GM model is required to generate fermion masses via the usual dimension four Yukawa couplings. This raises the question of whether one can rule out the possibility that the 125 GeV boson is the neutral member of a custodial 5-plet rather than a custodial singlet, without invoking decays to fermions. A conclusive answer is given by observing that the ratio of the branching fractions to W versus Z bosons is completely determined by the custodial symmetry properties of the boson. For a custodial 5-plet, the ratio of the signal strength to WW over that to ZZ is predicted to be 1/4 that of a SM Higgs boson [419], and thus already ruled out by the experimental results presented in Section 11.3.5.

Another interesting general feature of Higgs triplet models is that, after mixing, the SM-like neutral boson can have stronger couplings to WW and ZZ than predicted by the SM [420]; this is in contrast to mixing with additional doublets and singlet, which can only reduce the WW and ZZ couplings versus the SM. This emphasises that LHC Higgs data cannot extract model independent coupling strengths for the Higgs boson [256].

Because of the built-in custodial symmetry, the triplet VEV in the GM model can be large compared to the doublet VEV. The custodial singlet neutral boson from the triplets mixes with the neutral boson from the doublet. Two interesting special cases are (i) the triplet VEV is small and the 125 GeV boson is SM-like except for small deviations, and (ii) the 125 GeV boson is mostly the custodial singlet neutral boson from the electroweak triplets. The phenomenology of the doubly-charged and singly-charged bosons is similar to that of the HTM. The constraints on the GM model from precision electroweak data, LEP data, and current LHC data are summarised in Ref. [59].

11.4.2 EWSB induced by strong dynamics

11.4.2.1 Little Higgs models

The idea behind the Little Higgs boson models [421] is to identify the Higgs doublet as a (pseudo) Nambu–Goldstone boson while keeping some sizeable non-derivative interactions, in particular a larger Higgs-boson quartic interaction. By analogy with QCD where the pions $\pi^{\pm,0}$ appear as Nambu–Goldstone bosons associated to the breaking of the chiral symmetry $SU(2)_L \times SU(2)_R/SU(2)$, switching on some interactions that break explicitly the global symmetry will generate masses for the would-be massless Nambu–Goldstone bosons of the order of $g\Lambda_{G/H}/(4\pi)$, where g is the coupling of the symmetry breaking interaction and $\Lambda_{G/H} = 4\pi f_{G/H}$ is the dynamical scale of the global symmetry breaking G/H. In the case of the Higgs boson, the top Yukawa interaction or the gauge interactions themselves will certainly break explicitly (part of) the global symmetry since they act non-linearly on the Higgs boson. Therefore, obtaining a Higgs boson mass around 125 GeV would demand a dynamical scale $\Lambda_{G/H}$ of the order of 1 TeV, which is known to lead to too

large oblique corrections. Raising the strong dynamical scale by at least one order of magnitude requires an additional selection rule to ensure that a Higgs boson mass is generated at the 2-loop level only

$$m_h^2 = \frac{g^2}{16\pi^2} \Lambda_{G/H}^2 \to m_h^2 = \frac{g_1^2 g_2^2}{(16\pi^2)^2} \Lambda_{G/H}^2.$$
 (11.48)

The way to enforce this selection rule is through a "collective breaking" of the global symmetry:

$$\mathcal{L} = \mathcal{L}_{G/H} + g_1 \mathcal{L}_1 + g_2 \mathcal{L}_2. \tag{11.49}$$

Each interaction \mathcal{L}_1 or \mathcal{L}_2 individually preserves a subset of the global symmetry such that the Higgs boson remains an exact Nambu–Goldstone boson whenever either g_1 or g_2 is vanishing. A mass term for the Higgs boson can be generated only by diagrams involving simultaneously both interactions. At one-loop, such diagrams are not quadratically divergent, so the Higgs boson mass is not UV sensitive. Explicitly, the cancellation of the SM quadratic divergences is achieved by a set of new particles around the Fermi scale: gauge bosons, vector-like quarks, and extra massive scalars, which are related, by the original global symmetry, to the SM particles with the same spin. Contrary to SUSY, the cancellation of the quadratic divergences is achieved by same-spin particles. These new particles, with definite couplings to SM particles as dictated by the global symmetries of the theory, are perfect goals for the LHC.

The simplest incarnation of the collective breaking idea, the so-called littlest Higgs boson model, is based on a non-linear σ -model describing the spontaneous breaking SU(5) down to SO(5). A subgroup SU(2)₁ × U(1)₁ × SU(2)₂ × U(1)₂ is weakly gauged. This model contains a weak doublet, that is identified with the Higgs doublet, and a complex weak triplet whose mass is not protected by collective breaking. Other popular little Higgs models are based on different coset spaces: minimal moose (SU(3)²/SU(3)), the simplest little Higgs (SU(3)²/SU(2)²), the bestest little Higgs (SO(6)²/SO(6)). For comprehensive reviews, see Ref. [422].

11.4.2.2 Models of partial compositeness

As in all composite-Higgs models the Higgs boson appears as a pseudo Nambu–Goldstone boson: the new strongly coupled sector is supposed to be invariant under a global symmetry G spontaneously broken to a subgroup H at the scale f (the typical mass scale of the resonances of the strong sector is $m_{\rho} \sim g_{\rho} f$ with g_{ρ} the characteristic coupling of the strong sector). To avoid conflict with EW precision measurements, the strong interactions themselves should better not break the EW symmetry. Hence the SM gauge symmetry itself should be contained in H. The SM (light) fermions and gauge bosons cannot be part of the strong sector itself since LEP data have already put stringent bounds on the compositeness scale of these particles far above the TeV scale. The gauge bosons couple to the strong sector by a weak gauging of a $SU(2) \times U(1)$ subgroup of the global symmetry G. The couplings of the SM fermions to the strong sector could a priori take two different forms:

- (i) a bilinear coupling of two SM fermions to a composite scalar operator, \mathcal{O} , of the form $\mathcal{L} = y \bar{q}_L u_R \mathcal{O} + h.c.$, in simple analogy with the SM Yukawa interactions. This is the way fermion masses were introduced in technicolor theories and it generically comes with severe flavour problems and calls for extended model-building gymnastics [29] to circumvent them;
- (ii) a linear mass mixing with fermionic vector-like operators: $\mathcal{L} = \lambda_L \, \bar{q}_L \mathcal{Q}_R + \lambda_R \, \bar{\mathcal{U}}_L u_R$. \mathcal{Q} and \mathcal{U} are two fermionic composite operators of mass M_Q and M_U .

Being part of the composite sector, the composite fermionic operators can have a direct coupling of generic order Y_* to the Higgs boson. In analogy with the photon- ρ mixing in QCD, once the linear

mixings are diagonalised, the physical states are a linear combination of elementary and composite fields. Effective Yukawa couplings are generated and read for instance for the up-type quark

$$y = Y_* \sin \theta_L \sin \theta_R \tag{11.50}$$

where $\sin \theta_i = \lambda_i / \sqrt{M_{Q,U}^2 + \lambda_i^2}$, i = L, R, measure the amount of compositeness of the SM leftand right-handed up-type quark. If the strong sector is flavour-anarchic, i.e., if the couplings of the Higgs boson to the composite fermions does not exhibit any particular flavour structure, the relation Eq. (11.50) implies that the light fermions are mostly elementary states ($\sin \theta_i \ll 1$), while the third generation quarks need to have a sizable degree of compositeness. The partial compositeness paradigm offers an appealing dynamical explanation of the hierarchies in the fermion masses. In fact, if the UV scale at which the linear mixings are generated is large, then $\mathcal{O}(1)$ differences in the anomalous dimensions can generate naturally large hierarchies in the fermion masses via renormalisation group running [423].

Another nice aspect of the partial compositeness structure is the dynamical generation of the Higgs potential that is not arbitrary like in the SM. The Higgs boson being a pseudo-Nambu–Goldstone boson, its mass does not receive any contribution from the strong sector itself but it is generated at the one-loop level via the couplings of the SM particles to the strong sector since these interactions are breaking the global symmetries under which the Higgs doublet transforms non-linearly. Obtaining $v \ll f$, as required phenomenologically, requires some degree of tuning, which scales like $\xi \equiv v^2/f^2$. A mild tuning of the order of 10% ($\xi \approx 0.1$) is typically enough to comply with electroweak precision constraints.

As in SUSY scenarios, the top sector is playing a crucial role in the dynamics of EWSB and can provide the first direct signs of new physics. The direct searches for these top partners, in particular the ones with exotic electric charges 5/3, are already exploring the natural parameter spaces of these models [424].

The main physics properties of a pseudo Nambu–Goldstone Higgs boson can be captured in a model-independent way by a small number of higher-dimensional operators. Indeed, the strong dynamics at the origin of the composite Higgs boson singles out a few operators among the complete list discussed earlier in Section 11.3.5: these are the operators that involve extra powers of the Higgs doublets, and they are therefore generically suppressed by a factor $1/f^2$ as opposed to the operators that involve extra derivatives or gauge bosons that are suppressed by a factor $1/(g_{\rho}^2 f^2)$. Typically, these new interactions induce deviations in the Higgs boson couplings that scale like $\mathcal{O}(v^2/f^2)$. Hence, the measurements of the Higgs boson couplings can be translated into some constraints on the compositeness scale, $4\pi f$, of the Higgs boson. The peculiarity of these composite models is that, due to the Goldstone nature of the Higgs boson, the direct couplings to photons and gluons are further suppressed and generically the coupling modifiers defined in Section 11.3.5 scale like

$$\kappa_{W,Z,f} \sim 1 + \mathcal{O}\left(\frac{v^2}{f^2}\right), \quad \kappa_{Z\gamma} \sim \mathcal{O}\left(\frac{v^2}{f^2}\right), \quad \kappa_{\gamma,g} \sim \mathcal{O}\left(\frac{v^2}{f^2} \times \frac{y_t^2}{g_\rho^2}\right), \quad (11.51)$$

where g_{ρ} denotes the typical coupling strength among the states of the strongly coupled sector and y_t is the top Yukawa coupling, the largest interaction that breaks the Goldstone symmetry. The coupling modifiers also receive additional contributions from the other resonances of the strong sector, in particular the fermionic resonances of the top-quark sector that are required to be light to generate a 125 GeV Higgs-boson mass. Some indirect information on the resonance spectrum could thus be inferred by a precise measurement of the Higgs boson coupling deviations. Measurable effects of the top-quark partner have been predicted for differential distribution, like the Higgs boson p_T distribution [425]. The off-shell channel $gg \to h^* \to 4\ell$ [235] and the double Higgs boson production $gg \to hh$ [426] can also help to resolve the gluon loop and separate the top and top-partner contributions.

11.4.2.3 Minimal composite Higgs models

The minimal composite Higgs models (MCHM) are concrete examples of the partial compositeness paradigm. The Higgs doublet is described by the coset space SO(5)/SO(4) where a subgroup $SU(2)_L \times U(1)_Y$ is weakly gauged and under which the four Goldstone bosons transform as a doublet of hypercharge 1. There is some freedom on how the global symmetry is acting on the SM fermions, and the Higgs boson couplings to the fermions depend on the representation which the SM fermions are embedded into [427]. The non-linearly realised symmetry acting on the Goldstone bosons leads to general predictions of the coupling of the Higgs boson to the EW gauge bosons. For instance, it can be shown that the quadratic terms in the W and Z bosons read

$$m_W^2(h)\left(W_\mu W^\mu + \frac{1}{2\cos^2\theta_W}Z_\mu Z^\mu\right),$$
 (11.52)

with $m_W(h) = \frac{gf}{2} \sin \frac{H}{f}$. Expanding around the EW vacuum, the expression of the weak scale is $v = f \sin(\langle H \rangle/f)$. And the values of the modified Higgs boson couplings to the W and Z become:

$$g_{hVV} = \frac{2m_V^2}{v} \sqrt{1 - v^2/f^2}, \quad g_{hhVV} = \frac{2m_V^2}{v^2} (1 - 2v^2/f^2).$$
 (11.53)

Note that the Higgs boson couplings to gauge bosons is always suppressed compared to the SM prediction. This is a general result [428] that holds as long as the coset space is compact.

The (κ_V, κ_f) experimental fit of the Higgs boson couplings can be used to derive a lower bound on the Higgs boson compositeness scale $4\pi f \gtrsim 9 \,\text{TeV}$, which is less stringent than the indirect bound obtained from EW precision data, $4\pi f \gtrsim 15 \,\text{TeV}$ [429] but more robust and less subject on assumptions [430].

11.4.2.4 Twin Higgs models

In all composite models presented above, the particles responsible for canceling the quadratic divergences in the Higgs boson mass are charged under the SM gauge symmetries. In particular, the top partner carries color charge, implying a reasonably large minimal production cross section at the LHC. An alternative scenario, which is experimentally quite challenging and might explain the null result in various new physics searches, is the case nowadays referred to as "neutral naturalness" [30, 31, where the particles canceling the 1-loop quadratic divergences are neutral under the SM. The canonical example for such theories is the Twin Higgs model of Ref. [30]. This is an example of a pseudo-Goldstone boson model with an approximate global SU(4) symmetry broken to SU(3). The Twin Higgs model is obtained by gauging the $SU(2)_A \times SU(2)_B$ subgroup of SU(4), where $SU(2)_A$ is identified with the SM $SU(2)_L$, while $SU(2)_B$ is the twin SU(2) group. Gauging this subgroup breaks the SU(4) symmetry explicitly, but quadratically divergent corrections do not involve the Higgs boson when the gauge couplings of the two SU(2) subgroups are equal, $g_A = g_B$. The SU(4) \rightarrow SU(3) breaking will also result in the breaking of the twin $SU(2)_B$ group and, as a result, three of the seven Goldstone bosons will be eaten, leaving 4 Goldstone bosons corresponding to the SM Higgs doublet. In fact, imposing the Z_2 symmetry on the full model will ensure the cancellation of all 1-loop quadratic divergences to the Higgs boson mass. Logarithmically divergent terms can, however, arise for example from gauge loops, leading to a Higgs boson mass of order $q^2f/4\pi$, which is of the order of the physical Higgs boson mass for $f \sim 1 \text{ TeV}$. The quadratic divergences from the top sector can be eliminated if the Z_2 protecting the Higgs boson mass remains unbroken by the couplings that result in the top Yukawa coupling. This can be achieved by introducing top partners charged under a twin $SU(3)_C$. In this case, the quadratic divergences are canceled by top partners that are neutral under the SM gauge symmetries. For more details about the composite twin Higgs models, see Refs. [431].

11.4.3 Exotic Higgs-boson decays

While the measured properties of the Higgs boson are roughly consistent with SM predictions, the Higgs-boson total width remains only loosely constrained as discussed in Section 11.3.8. This leaves ample room for BSM decays, often referred to as "exotic Higgs decays". These include invisible decays into dark matter candidates, non-standard signatures like lepton-flavor-violating (LFV) modes, and decays into new light scalars or pseudoscalars, which may decay promptly or be long-lived. They probe a broad spectrum of models, including for instance Higgs portal dark matter and dark photons, two-Higgs-doublet plus singlet (2HDM+S) frameworks, and axion-like particle scenarios. For a theoretical review of exotic signatures, see for instance Ref. [432,433] and the documents of the LHC Higgs Working Group WG3 [392]. In the following we discuss some of these cases and their current experimental status.

11.4.3.1 Invisible Higgs Decays

A hypothetical coupling of the Higgs to dark matter candidates is motivated in many theoretical models [392, 434]. Higgs-boson decay modes in which the decay products escape detection are commonly named "invisible" Higgs decays, first proposed in Ref. [435]. Experimentally they are characterized by signatures dominated by a large imbalance of the transverse momentum in the detector (missing transverse energy, MET). These decays are possible in the SM through the very rare $h \to ZZ \to 4\nu$ final state (Br $\approx 0.1\%$), which is far below the reach of the LHC. An observation of a Higgs invisible decay rate would therefore signify new physics, such as a coupling of the Higgs boson to dark matter candidates.

Direct searches for invisible decays are performed in multiple Higgs production modes, including vector boson fusion (VBF), associated production with a Z or W boson (Zh, Wh), $t\bar{t}h$, and inclusive gluon fusion (jet+ $E_{\rm T}^{\rm miss}$ -based signatures). The VBF mode dominates the sensitivity due to its distinctive topology of forward jets which leads to reduced background contamination, and its larger production cross section when compared to VH production. Current Run 2 results yield 95% CL upper limits on the invisible branching fraction at $\mathcal{B}(h \to \text{inv}) < 10.7\%$ (7.7% expected) in ATLAS [436] and < 15% (8% expected) in CMS [437]. These direct bounds are incorporated into the global Higgs coupling fits discussed in Section 11.3.5.1, Eq.(11.19).

Invisible Higgs-boson decays can also be interpreted in the context of "Higgs portal" models, where the Higgs boson mediates interactions between the SM and a dark sector. A more detailed discussion of such models and their connection to direct dark matter searches can be found in this volume's dark matter review [438].

11.4.3.2 Flavor violating decays

The measurement of the Yukawa couplings of the Higgs boson to quarks and leptons is an important piece in the puzzle of flavor and its connection to the mechanism of EWSB. The lepton-flavor-violating (LFV) decays $h \to e\mu$, $h \to e\tau$, and $h \to \mu\tau$ are forbidden in the SM but can arise in a variety of BSM scenarios, including 2HDM models or composite Higgs models. These LFV Higgs decays probe off-diagonal Yukawa couplings $Y_{e\mu}$, $Y_{e\tau}$, or $Y_{\mu\tau}$, which couple the Higgs boson to leptons of different flavors.

The analysis of the full 13 TeV Run 2 datasets collected by ATLAS and CMS has set stringent 95% confidence level (CL) upper limits on the branching ratios of LFV decays of the Higgs in the $h \to \mu \tau$, $h \to e \tau$, and $h \to e \mu$ channels. For $h \to \mu \tau$, the observed (expected) limits are $\mathcal{B}(h \to \mu \tau) < 0.18\%$ (0.09%) from ATLAS [439] and < 0.15% (0.15%) from CMS [440]. For $h \to e \tau$, the corresponding limits are $\mathcal{B}(h \to e \tau) < 0.20\%$ (0.12%) from ATLAS [439] and < 0.22% (0.16%)

from CMS [440]. In the $h \to e\mu$ channel, the limits are $\mathcal{B}(h \to e\mu) < 6.2 \times 10^{-5}$ (5.9 × 10⁻⁵) from ATLAS [273] and $< 4.4 \times 10^{-5}$ (4.7 × 10⁻⁵) from CMS [441]. These numbers correspond to exotic decays of a 125 Higgs boson. The CMS search in the $e\mu$ channel was expanded to a wider mass range between 110 GeV and 160 GeV. A mild excess with a global significance of 2.8 standard deviations is observed for a mass hypothesis of approximately 146 GeV.

The presence of these off-diagonal LFV Yukawa couplings may enhance processes such as $\mu \to 3e$, $\mu \to e\gamma$, $\tau \to 3\mu$, $\tau \to \mu\gamma$ that can proceed via a virtual Higgs boson exchange. The direct limits derived by ATLAS and CMS on $Br(h \to \mu\tau)$ and $Br(h \to e\tau)$ are more than an order of magnitude stronger than limits derived from tau decays. On the other hand, the most stringent constraint on the $h \to e\mu$ branching ratio is derived indirectly from the results of searches for $\mu \to e\gamma$ [442], which yield a bound of $B(h \to e\mu) < O(10^{-8})$ [443].

Flavor-violating interactions of the Higgs boson may also involve quarks. These are studied in the context of top-quark flavor changing decays, such as $t \to hq$ (q = u, c), which provide complementary constraints on flavor-violating Yukawa couplings in the quark sector. ATLAS and CMS have searched for these processes with Run-1 and Run-2 data. Focusing on the Run-2 results, ATLAS has searched for FCNC top decays with subsequent decays of the Higgs boson to a pair of photons [444], yielding a 95% CL upper limit on BR $(t \to hc) < 0.22\%$ with an expected sensitivity of 0.16%. CMS has searched for FCNC top decays with subsequent decays of the Higgs boson to a pair of b-quarks [445], yielding a 95% CL upper limit on BR $(t \to hu) < 0.079\%$ with an expected sensitivity of 0.011% and on BR $(t \to hc) < 0.094\%$ with an expected sensitivity of 0.086%.

11.4.3.3 Other exotic decays: prompt and long-lived decays

Higgs decays into pairs of light scalars or pseudoscalars ($h \to ss$ or $h \to aa$) are particularly well motivated in extended Higgs sectors such as the 2HDM+S and axion-like particle models. These provide a very rich phenomenology, with different final states favored depending on the intermediate particle and its mass (4μ , 4τ , $2\mu 2\tau$, $2b2\mu$, $2b2\tau$, 4b, 4γ , $2\gamma 2\tau$...). They include both prompt decays of the mediator and long lived signatures. Experimental results on $h \to ss/aa$ signatures and their references can be found in the general summary of BSM Higgs searches presented in Table 11.6. An recent overview of the different decays from the point of view of ATLAS can also be found in Ref. [446]. For decays into axion-like particles, see the PDG review on the topic, Ref. [373].

Another class of models explores the connection between the Higgs boson and a "dark" sector of matter that does not interact directly with SM particles, and manifests itself only through mixing effects. A well known example is the hidden Abelian Higgs model (HAHM) [447], which introduces a dark photon, Z_D , that mediates a dark $U(1)_D$ gauge symmetry spontaneously broken by a dark Higgs mechanism. The Z_D can couple to SM particles via a hypercharge portal through kinetic mixing or via a Higgs portal through mixing with the SM Higgs. Higgs exotic decay searches in this framework have been performed by ATLAS and CMS, targeting both $h \to ZZ_D$ and $h \to Z_DZ_D$ decays [448–450], and probing both prompt and displaced signatures. Other examples of searches for dark photons in Higgs boson decays target final states with a visible photon and an undetected dark photon [451–453]. Further discussion on the dark sector comparing different search approaches can be found in Refs. [446, 454], and from a more general perspective in the dark matter PDG review [438].

Long lived signatures are an area in particularly rapid development in the current LHC Run 3 and with great room for improvement in HL-LHC. These searches involve non-standard objects that require dedicated reconstructed algorithms for displaced objects, both at trigger and at reconstruction level as shown for example in Ref. [455] from the point of view of CMS. Although no deviations from SM expectations have yet been observed, the HL-LHC will clearly expand the discovery potential, with sensitivities to exotic branching fractions as low as 10^{-5} – 10^{-6} in some

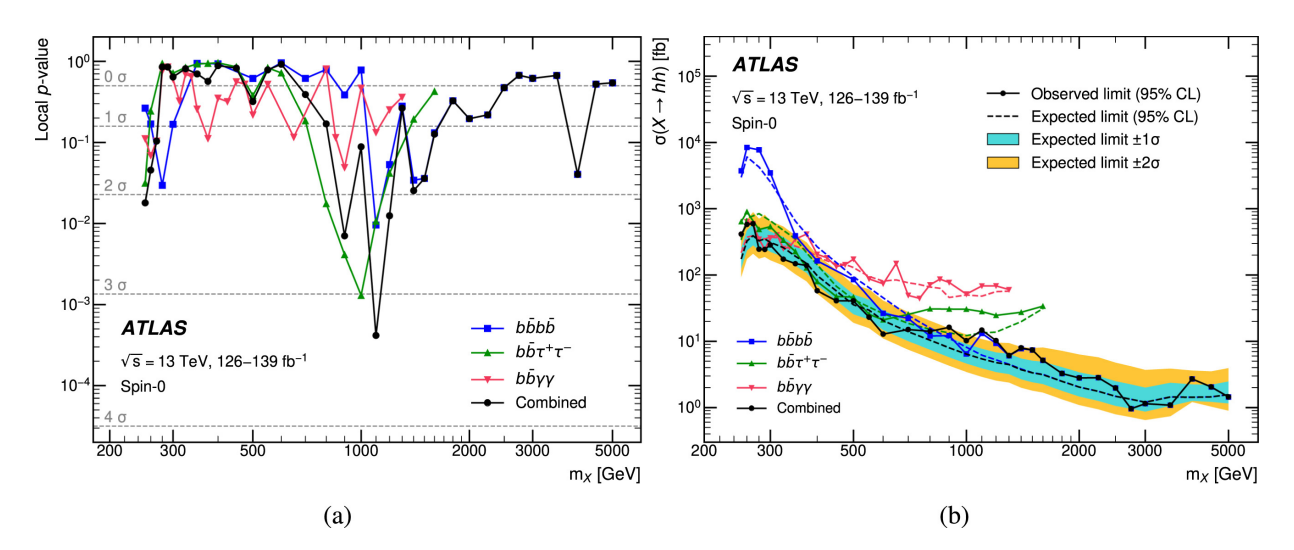


Figure 11.19: (left) Local p-value and (right) observed and expected upper limits at the 95% CL on the resonant Higgs boson pair production cross section as a function of the resonance mass m_X . The symbol h denotes a SM Higgs boson with a mass of 125 GeV. The results are taken from Ref. [456].

channels [344].

11.4.4 Summary of BSM Higgs boson search results

The measurements presented in Sections 11.3.3–11.3.9 have established the existence of a single scalar particle in the electroweak symmetry-breaking sector, consistent with the SM Higgs boson. However, they do not exclude the possibility of additional scalar particles. As discussed above, many classes of models beyond the SM predict extended Higgs sectors. The corresponding searches are typically designed to be as model-independent as possible ¹³, and can be grouped into the following categories (in the following, "h" refers to the 125 GeV scalar):

- (i) Searches for an additional CP-even state, primarily in the high-mass region, decaying to vector bosons. This could correspond either to the heavy CP-even state in a generic 2HDM, with the lighter state being the 125 GeV Higgs boson, or to an additional scalar singlet.
- (ii) Searches for an additional CP-even state, decaying to a pair of 125 GeV Higgs bosons $(H \to hh)$, or a pair of heavier scalars $(X \to YY)$. Examples of results obtained by ATLAS in the search for $X \to hh$ given in Figure 11.19.
- (iii) Searches for an additional scalar state X, with cascade decays to the 125 GeV Higgs boson and another scalar $(X \to Yh)$. An example of results obtained by CMS in the search for $X \to Yh$ is given in Figure 11.20.
- (iv) Searches for a heavy state decaying to fermion pairs, such as the CP-odd A or the heavy CP-even H in a generic 2HDM.
- (v) Searches for charged Higgs bosons, also predicted in generic 2HDMs.
- (vi) Searches for a light CP-odd state a in the low-mass region, as predicted in the NMSSM (an extension of the MSSM by one singlet chiral superfield containing a scalar), in a variety of final states. These include decays with one or two a bosons to photon, muon, tau, or b-quark pairs.

¹³Nevertheless, most non-SUSY models are expected to include additional states and dynamics above the weak scale to stabilize the scalar sector. Such new, unknown physics may influence the searches described in this section in ways that are difficult to quantify.

(vii) Searches for doubly charged Higgs bosons, expected in Higgs sector extensions with triplet representations.

A concise overview of the most recent searches at the LHC and elsewhere is given in Table 11.6. It summarizes these searches by final state, with the corresponding references provided for further details. Comprehensive reviews of Run-2 searches can be found in Refs. [446, 457] and references for Run-1 searches are available in Ref. [263].

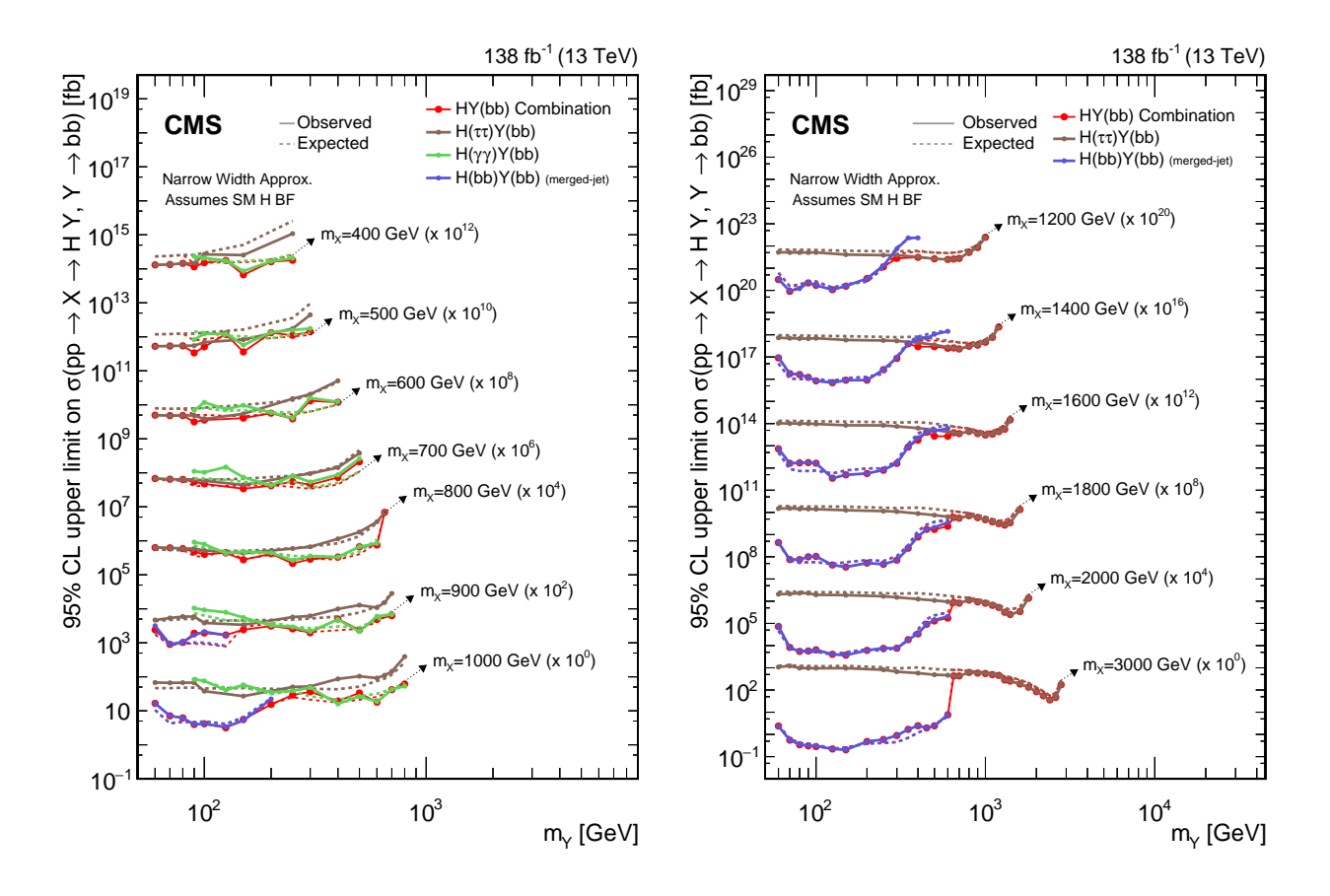


Figure 11.20: Search for $X \to YH$ where "H" is the 125 GeV Higgs boson: Observed and expected upper limits, at 95% CL, on the product of the cross section σ for the production of a resonance X via gluon–gluon fusion and the branching fraction \mathcal{B} for the $X \to Y(b\bar{b})H$ decay. For the branching fractions of the $H \to \tau^+\tau^-$, $H \to \gamma\gamma$ and $H \to b\bar{b}$ decays, the SM values are assumed. The results derived from the individual analyses presented here and the result of their combined likelihood analysis are shown as functions of m_Y and m_X for $m_X \le 1$ TeV (left), and $m_X \ge 1.2$ TeV (right). Observed limits are indicated by markers connected with solid lines, expected limits by dashed lines. For presentation purposes, the limits have been scaled in successive steps by two orders of magnitude, each. For each set of graphs, a black arrow points to the m_X -related legend. The results are taken from Ref. [457].

11.5 Summary and Outlook

Summary—The discovery of the Higgs boson is a major milestone in the history of particle physics as well as an extraordinary achievement of the LHC machine and the ATLAS and CMS experiments. Thirteen years after the discovery, substantial progress in the field of Higgs-boson

Table 11.6: Summary of references to the searches for additional states from extended Higgs sectors. (BBr) denotes the BaBar experiment and (TeV) the Tevatron experiments. V denotes either the W or the Z boson.

	ATLAS	CMS	Other experiments
CP-even H			
$H \to \gamma \gamma$	[458-460]	[461, 462]	_
$H \to \gamma \gamma \text{ (low mass)}$	[463]	[464-466]	_
$H o Z\gamma$	[467, 468]	[469]	_
$H \to ZZ \to 4\ell$	[470]	[471, 472]	_
$H o ZZ o \ell\ell u u$	[470]	[473]	_
$H \to WZ \to \ell\ell\ell\nu$	_	[474]	_
$H o ZZ o \ell\ell q \overline{q}$	[475]	[476, 477]	_
$H o ZZ o u u q \overline{q}$	[478]	_	_
$H \to WW \to \ell\nu\ell\nu$	[479, 480]	[481]	_
$H o WW o \ell u q \overline{q'}$	[482]	[481]	
$H o VV o q\overline{q'}q\overline{q'}(JJ)$	[483, 484]	[485]	_
$H \to VV$ combination	[486]	_	
$H \to hh \to b\bar{b}\tau\tau, b\bar{b}\gamma\gamma, bbWW^*, bbZZ^*, 4$	b [407 401]	[477 400 404]	
$\gamma \gamma WW^*, WW^*\tau \tau, WW^*WW^*, 4\tau$	[487-491]	[477, 492 - 494]	_
\overline{CP} -odd A (and/or CP -even H)			
$H, A \to \tau^+ \tau^-$	[495]	[394, 496]	[497, 498] (TeV)
,			[499] (LHCb)
$A \to \tau^+ \tau^- \text{ (low mass)}$	[500]	[501]	_
$H, A \rightarrow \mu^+\mu^-$	[502]	[503]	
$H/h \to \mu \tau, e \tau \text{ LFV}$	[439]	[504]	
$H/h \rightarrow e\mu \text{ LFV}$	[273]	[441]	
H,A o t ar t	[484, 505-507]	[508, 509]	
$H,A o bar{b}$	[510]	[511, 512]	[513, 514] (TeV)
$A \to hZ \to bbq\overline{q'}, bb\ell\ell, \ell\ell\tau\tau, \nu\overline{\nu}bb, bbbb$	[515, 516]	[517–519]	_
A o ZH	[520–522]	[523, 524]	_
$H \to ZA \to b\bar{b}\ell^+\ell^-$	[525]	[526]	_
Charged H^{\pm}		F7	
$H^{\pm} \rightarrow \tau^{\pm} \nu$	[527–529]	[530]	_
$H^{\pm} \rightarrow cs$	[531, 532]	[533]	_
$H^{\pm} ightarrow tb$	[534]	[535]	_
$H^{\pm} \rightarrow W^{\pm}Z$	[536, 537]	[538, 539]	_
$H^{\pm} \rightarrow W^{\pm}A$	_	[540]	_
$H^{\pm} \rightarrow HW^{\pm}$	[541]	[542]	_
$H^{\pm} \rightarrow cb$	[543]	[544]	
CP-odd a		[= ,=1	
$a \to \mu^+ \mu^-, \tau^+ \tau^-$	[545, 546]	[547]	[EGE] (I ED)
$h \to aa \to 4\mu, 4\tau, 2\mu 2\tau, 2\gamma 2\tau, 4\gamma$	[548 – 552]	[553 – 564]	[565] (LEP) [566] (TeV)
$h \to aa \to bb\mu\mu, bb\tau\tau, 4b$	[567-570]	[571–575]	[] ()
H o Za	[576, 577]	[578]	_
$\Upsilon_{1s,3s} o a\gamma$			[579, 580] (BBr)
$X \to YY \text{ and } X \to hY$			/
$\overline{X o YY}$	[581]	[582]	_
$X \to hY$	[583–586]	[587 - 592]	_
Doubly charged $H^{\pm\pm}$	[537, 593–595]	[539, 596]	

physics has been accomplished and a significant number of measurements probing the nature of this unique particle have been made. They are revealing an increasingly precise profile of the Higgs boson.

The LHC has concluded its Run 2 in 2018, delivering a dataset of 13 TeV pp collisions corresponding to an integrated luminosity of more than 150 fb⁻¹ of which more than 140 fb⁻¹ have been collected by ATLAS and CMS. The Run 3 started in 2022 at 13.6 TeV and has already delivered more than the total Run 2 integrated luminosity. With the substantial increase in production rates at the higher center-of-mass energy (mostly from Run 1 to Run 2) and the larger datasets, the LHC collaborations have delivered detailed studies of not only inclusive but also differential cross sections that are essential to probe the structure of the scalar sector of the SM and identify potential deviations from SM predictions.

Results of fundamental importance have been achieved with Run-2 datasets by ATLAS and CMS independently [255, 265], such as the clear and unambiguous observation of the Higgs-boson decay to τ leptons and to b quarks, as well as the clear and unambiguous observation of the production of the Higgs boson through the ttH process. These results provide direct evidence for the Yukawa coupling of the Higgs boson to fermions of the third generation: taus, bottom quarks and top quarks, at rates compatible with those expected in the SM. The most recent combination of Run 2 results has established all Higgs-boson couplings to gauge bosons and third-generation fermions with a precision between 5 and 10%. In addition, data analyzed so far have already brought evidence for the $H \to \mu^+\mu^-$ rare decay above the 3σ level for each experiment, and at the 3σ level for the $H \to Z\gamma$ rare decay when ATLAS and CMS combine their Run 2 results. The challenging study of the Higgs-charm coupling is a good example of LHC performance exceeding original expectations, with constraints on κ_c already at about 3 at 95% CL, thanks to improvements in charm tagging. New ideas have been implemented to indirectly determine the Higgs-boson width from both onshell and off-shell measurements reaching a remarkable sensitivity of about 4 MeV. The Higgs-boson mass has been measured with per-mille-level precision. Last but not least, great progress has been made in constraining the Higgs-boson self-coupling via di-Higgs production, which will probe the SM scalar potential and the origin of EWSB. These, and all other experimental measurements, are consistent at the moment with the EWSB mechanism of the SM.

New theoretical calculations and developments in Monte-Carlo simulations pertaining to Higgs physics are occurring at a rapid pace. For example, the theoretical prediction for the dominant gluon fusion production mode now includes the latest N3LO result at the inclusive and differential levels, which is twice as precise as previous NNLO calculations. All Higgs-boson production modes are known at (a)NNLO of QCD and NLO of EW corrections at both the inclusive and differential level, as well as in several fiducial volumes that have often been explored by interfacing fixed-order calculation with parton shower event generators at NNLO in QCD. At the inclusive level VBF and VH associate production are also known at N3LO. With these improvements in the state-of-the-art theory predictions and the increase in luminosity and center-of-mass energy, Higgs physics has definitively entered a precision era. Its impact can already be seen on the latest Run-2 combined measurements of the Higgs boson couplings (see Section 11.3.5). This situation allows for new challenges to ultimately increase further the reach in precision and it also widens the possibilities of unveiling the true nature and the dynamics of the EWSB mechanism.

Many extensions of the SM at higher energies call for an enlargement of the EWSB sector. Hence, direct searches for additional scalar states can provide valuable insights on the dynamics of the EWSB mechanism. The ATLAS and CMS experiments have searched for additional Higgs bosons in the Run-2 data, and have imposed constraints in broad ranges of mass and couplings for various scenarios with an extended Higgs sector.

Outlook—The unitarization of the vector boson scattering (VBS) amplitudes, dominated at high

energies by their longitudinal polarization, has been the basis of the *no lose* theorem at the LHC, and was a determining consideration in the building of the accelerator and detectors. It motivated the existence of a Higgs boson or the observability of manifestations of strong dynamics at the TeV scale. Now that a Higgs boson has been found and its couplings to gauge bosons are - within current accuracy - consistent with the SM predictions, perturbative unitarity is preserved to a large extent with the sole exchange of the Higgs boson, and without the need for any additional states. VBS remains still an important channel to further investigate in order to better understand the nature of the Higgs sector and the possible completion of the SM at the TeV scale. In association with the double Higgs boson production channel by vector boson fusion, VBS could, for instance, confirm that the Higgs boson is part of a weak doublet and also establish whether it is an elementary object or a composite state that could emerge as a pseudo-Nambu–Goldstone boson from a new underlying broken symmetry.

The fermion-Higgs boson couplings are not governed by local gauge symmetry. Thus, in addition to a new particle, the LHC has also discovered a new force, different in nature from the other fundamental interactions since it is non-universal and distinguishes between the three families of quarks and leptons. The existence of the Higgs boson embodies the problem of an unnatural cancellation among the quantum corrections to its mass if new physics is present at scales significantly higher than the EW scale. The non-observation of additional states which could stabilise the Higgs boson mass is a challenge for natural scenarios like SUSY or models with a new strong interaction in which the Higgs boson is not a fundamental particle. This increasingly pressing paradox starts questioning the principle of naturalness and it also inspires new solutions tied to the cosmological evolution of the Universe.

The search for the Higgs boson has occupied the particle physics community for the last 50 years. Its discovery has shaped and sharpened the physics programs of the LHC and the HL-LHC and has been central to the discussion of prospective future accelerators [191,192,194,195,597,598]. Given the exceptional performance of the LHC so far, projections for the HL-LHC promise to establish a legacy Higgs-boson precision physics program that will test the SM at an unprecedented level and will serve to deepen our understanding of fundamental physics. In particular, with respect to current data, the HL-LHC with an integrated luminosity of 3 ab⁻¹ per experiment is expected to (i) determine the $H \to \mu^+\mu^-$ and $H \to Z\gamma$ couplings with 3-7% precision; (ii) measure the other main Higgs-boson couplings to SM fermions and vector bosons, including loop-induced couplings to gluons and photons, with precision ranging from 1.6% to 3.6%; (iii) reach a sensitivity to the charm Yukawa coupling of 1.5 times the SM value at 95% C.L.; (iv) observe SM di-Higgs production with a significance exceeding 7σ ; (v) measure the Higgs-boson trilinear coupling with a precision better than 30%; (vi) observe longitudinally polarized vector boson W_LW_L scattering and measure its cross section with precision better than 20%; and (vi) continue placing strong bounds on high-scale new physics models both through direct searches and precision measurements of EW, top-quark, and flavor-physics observables [266]. The projected experimental systematic uncertainties are similar to the statistical uncertainties, but the dominant source of uncertainty arises from theory, and this remains the case even after assuming that, by the end of the HL-LHC run, the theory uncertainties can be reduced by a factor two compared to the current uncertainties [266]. Theoretical progress is hard to predict, but given the progress witnessed in theoretical calculations during the lifetime of the LHC, as well as the wealth of new ideas that have been employed and are currently being considered, a progress in theoretical predictions by a factor of two or more appears realistic but still requires dedicated and concerted effort.

Based on these outstanding achievements, future colliders currently being considered will improve our present knowledge of Higgs-boson physics by either increasing the precision or the energy reach of the HL-LHC [191, 192, 598, 598, 599]. Proposed e^+e^- colliders, both circular and linear,

with center-of-mass energies between M_Z and about 350 GeV, the so called *Higgs factories*, will be able to measure all Higgs-boson couplings at percent and sub-percent level, including the couplings to charm and strange quarks, and put first bounds on the extremely small electron Yukawa coupling. Only the measurement of the top-quark Yukawa coupling will require energies of about 550-600 GeV to reach a precision higher than the HL-LHC. Such energy upgrade is part of the proposed plan for an e^+e^- linear collider. e^+e^- colliders will also deliver a largely model-independent measurements of the Higgs-boson width and, for the case of circular e^+e^- colliders, even obtain a meaningful upper bound on the Yukawa couplings of the electron, getting us closer to establishing the origin of the electron mass which lies at the core of all atomic structures. A different class of colliders referred to as Multi-TeV colliders, colliding either pp or $\mu^+\mu^-$ beams, will explore LHC center-of-mass energy by roughly one order of magnitude and, besides measuring all Higgs-boson properties in a new energy regime, search for evidence of NP between the EW scale and about 10 TeV as suggested by the Higgs portal.

For both hadron and lepton colliders, substantial theoretical progress is crucial to fully exploit and capitalize on the experimental data. In particular, the expected HL-LHC data together with rapid ongoing progress in theoretical calculations are defining a new era of precision Higgs boson measurements.

References

- S.L. Glashow, Nucl. Phys. 20, 579 (1961); S. Weinberg, Phys. Rev. Lett. 19, 1264 (1967);
 A. Salam, Elementary Particle Theory, eds.: Svartholm, Almquist and Wiksells, Stockholm, 1968;
 S. L. Glashow, J. Iliopoulos and L. Maiani, Phys. Rev. D2, 1285 (1970).
- [2] F. Englert and R. Brout, Phys. Rev. Lett. 13, 321 (1964), [,157(1964)]; P. W. Higgs, Phys. Lett. 12, 132 (1964); P. W. Higgs, Phys. Rev. 145, 1156 (1966); G. S. Guralnik, C. R. Hagen and T. W. B. Kibble, Phys. Rev. Lett. 13, 585 (1964), [,162(1964)].
- J. M. Cornwall, D. N. Levin and G. Tiktopoulos, Phys. Rev. Lett. 30, 1268 (1973), [Erratum: Phys. Rev. Lett. 31, 572 (1973)]; J. M. Cornwall, D. N. Levin and G. Tiktopoulos, Phys. Rev. D10, 1145 (1974), [Erratum: Phys. Rev. D11, 972 (1975)]; C. H. Llewellyn Smith, Phys. Lett. 46B, 233 (1973); B. W. Lee, C. Quigg and H. B. Thacker, Phys. Rev. D16, 1519 (1977).
- [4] R. Barate *et al.* (LEP Working Group for Higgs boson searches, ALEPH, DELPHI, L3, OPAL), Phys. Lett. B **565**, 61 (2003), [hep-ex/0306033].
- [5] CDF and D. collaborations (CDF and D0), Technical report, Fermilab (2011), [arXiv:1107.5518].
- [6] L. Evans and P. Bryant, JINST 3, S08001 (2008).
- [7] S. Schael et al. (ALEPH, DELPHI, L3, OPAL, SLD, LEP Electroweak Working Group, SLD Electroweak Group, SLD Heavy Flavour Group), Phys. Rept. 427, 257 (2006), [hepex/0509008].
- [8] ALEPH, CDF, D0, DELPHI, L3, OPAL, SLD Collaborations, LEP Electroweak Working Group, Tevatron Electroweak Working Group, and SLD Electroweak and Heavy Flavour Groups, "Precision electroweak measurements and constraints on the standard model," (2010), [arXiv:1012.2367].
- [9] S. Schael et al. (ALEPH, DELPHI, L3, OPAL, LEP Electroweak), Phys. Rept. 532, 119 (2013), [arXiv:1302.3415].
- [10] The LEP Electroweak Working Grouphttps://lepewwg.web.cern.ch/lepewwg/.
- [11] J. Beringer et al. (Particle Data Group), Phys. Rev. D 86, 010001 (2012).

- [12] ATLAS Collaboration, JINST 3, S08003 (2008).
- [13] CMS Collaboration, JINST **3**, S08004 (2008).
- [14] ATLAS Collaboration, Phys. Lett. B **716**, 1 (2012), [arXiv:1207.7214].
- [15] CMS Collaboration, Phys. Lett. B **716**, 30 (2012), [arXiv:1207.7235].
- [16] ATLAS Collaboration, Phys. Lett. B **726**, 120 (2013), [arXiv:1307.1432].
- [17] ATLAS Collaboration, Eur. Phys. J. C 75, 476 (2015), [arXiv:1506.05669].
- [18] CMS Collaboration, Phys. Rev. D **92**, 012004 (2015), [arXiv:1411.3441].
- [19] CMS Collaboration, Eur. Phys. J. C 75, 212 (2015), [arXiv:1412.8662].
- [20] ATLAS Collaboration, Phys. Rev. D **90**, 052004 (2014), [arXiv:1408.0017].
- [21] CMS Collaboration, Phys. Rev. D **92**, 072010 (2015), [arXiv:1507.06656].
- [22] ATLAS and CMS Collaborations, JHEP **08**, 045 (2016), [arXiv:1606.02266].
- [23] K. G. Wilson, Phys. Rev. D3, 1818 (1971); G. 't Hooft, in Proc. of 1979 Cargèse Institute on Recent Developments in Gauge Theories, p. 135 Press, New York 1980; For a modern discussion, see the GGI Tea Break's Seminar by G.F. Giudice and R. Rattazzi, https://is.gd/nUnjAr (2021).
- [24] J. Wess and B. Zumino, Phys. Lett. **49B**, 52 (1974).
- [25] S. P. Martin, Adv. Ser. Direct. High Energy Phys. 1–98 (1998), [hep-ph/9709356].
- [26] B.C. Allanach and H.E. Haber, Supersymmetry, Part I (Theory), in this volume.
- [27] D. B. Kaplan and H. Georgi, Phys. Lett. **136B**, 183 (1984).
- [28] B. Bellazzini, C. Csaki and J. Serra, Eur. Phys. J. C74, 5, 2766 (2014), [arXiv:1401.2457];
 G. Panico and A. Wulzer, Lect. Notes Phys. 913, pp.1 (2016), [arXiv:1506.01961];
 C. Csaki, C. Grojean and J. Terning, Rev. Mod. Phys. 88, 4, 045001 (2016), [arXiv:1512.00468].
- [29] K.M. Black, R.S. Chivukula and M. Narain, *Dynamical Electroweak Symmetry Breaking: Implications of the H0*, in this volume.
- [30] Z. Chacko, H.-S. Goh and R. Harnik, Phys. Rev. Lett. 96, 231802 (2006), [hep-ph/0506256];
 Z. Chacko, H.-S. Goh and R. Harnik, JHEP 01, 108 (2006), [hep-ph/0512088].
- [31] N. Craig et al., JHEP 07, 105 (2015), [arXiv:1501.05310]; N. Craig, S. Knapen and P. Longhi, Phys. Rev. Lett. 114, 6, 061803 (2015), [arXiv:1410.6808].
- [32] P. W. Graham, D. E. Kaplan and S. Rajendran, Phys. Rev. Lett. 115, 22, 221801 (2015), [arXiv:1504.07551]; J. R. Espinosa et al., Phys. Rev. Lett. 115, 25, 251803 (2015), [arXiv:1506.09217]; G. Dvali (2019), [arXiv:1908.05984].
- [33] C. Csaki et al., Phys. Rev. Lett. 126, 091801 (2021), [arXiv:2007.14396]; N. Arkani-Hamed, R. Tito D'agnolo and H. D. Kim (2020), [arXiv:2012.04652]; R. Tito D'Agnolo and D. Teresi (2021), [arXiv:2106.04591].
- [34] T. Flacke et al., JHEP 06, 050 (2017), [arXiv:1610.02025].
- [35] J. Khoury and O. Parrikar, JCAP 12, 014 (2019), [arXiv:1907.07693]; G. F. Giudice, M. Mc-Cullough and T. You (2021), [arXiv:2105.08617].
- [36] W. Altmannshofer and A. Greljo (2024), [arXiv:2412.04549].
- [37] J. R. Ellis, M. K. Gaillard and D. V. Nanopoulos, Nucl. Phys. **B106**, 292 (1976).
- [38] M. A. Shifman et al., Sov. J. Nucl. Phys. 30, 711 (1979), [Yad. Fiz.30,1368(1979)].
- [39] J. F. Gunion et al., The Higgs Hunter's Guide, Addison-Wesley (1990).
- [40] R. L. Workman et al. (Particle Data Group), PTEP 2022, 083C01 (2022).

- [41] S. Weinberg, Phys. Rev. Lett. 43, 1566 (1979).
- [42] P. Sikivie et al., Nucl. Phys. B173, 189 (1980); H. Georgi, Ann. Rev. Nucl. Part. Sci. 43, 209 (1993).
- [43] M. J. G. Veltman, Nucl. Phys. **B123**, 89 (1977).
- [44] F. Devoto et al., J. Phys. G 49, 10, 103001 (2022), [arXiv:2205.03140].
- [45] G. Degrassi et al., JHEP 08, 098 (2012), [arXiv:1205.6497]; S. Alekhin, A. Djouadi and S. Moch, Phys. Lett. B716, 214 (2012), [arXiv:1207.0980]; D. Buttazzo et al., JHEP 12, 089 (2013), [arXiv:1307.3536]; A. V. Bednyakov et al., Phys. Rev. Lett. 115, 20, 201802 (2015), [arXiv:1507.08833]; G. Hiller et al., Phys. Rev. D 110, 11, 115017 (2024), [arXiv:2401.08811].
- [46] V. Branchina, E. Messina and M. Sher, Phys. Rev. **D91**, 013003 (2015), [arXiv:1408.5302].
- [47] A. Hook et al., JHEP 01, 061 (2015), [arXiv:1404.5953]; J. Kearney, H. Yoo and K. M. Zurek, Phys. Rev. D91, 12, 123537 (2015), [arXiv:1503.05193].
- [48] J. R. Espinosa, D. Racco and A. Riotto, Phys. Rev. Lett. 120, 12, 121301 (2018), [arXiv:1710.11196].
- [49] J. R. Espinosa, D. Racco and A. Riotto, JCAP **1809**, 09, 012 (2018), [arXiv:1804.07732].
- [50] A. Andreassen, W. Frost and M. D. Schwartz, Phys. Rev. D97, 5, 056006 (2018), [arXiv:1707.08124].
- [51] S. Chigusa, T. Moroi and Y. Shoji, Phys. Rev. Lett. 119, 21, 211801 (2017), [arXiv:1707.09301].
- [52] M. Shaposhnikov and C. Wetterich, Phys. Lett. B683, 196 (2010), [arXiv:0912.0208];
 M. Holthausen, K. S. Lim and M. Lindner, JHEP 02, 037 (2012), [arXiv:1112.2415].
- [53] F. L. Bezrukov and M. Shaposhnikov, Phys. Lett. B659, 703 (2008), [arXiv:0710.3755]; F. L. Bezrukov, A. Magnin and M. Shaposhnikov, Phys. Lett. B675, 88 (2009), [arXiv:0812.4950].
- [54] C. P. Burgess, H. M. Lee and M. Trott, JHEP 09, 103 (2009), [arXiv:0902.4465]; J. L. F. Barbon and J. R. Espinosa, Phys. Rev. D79, 081302 (2009), [arXiv:0903.0355]; M. P. Hertzberg, JHEP 11, 023 (2010), [arXiv:1002.2995].
- [55] LHC Higgs Working Group, https://twiki.cern.ch/twiki/bin/view/LHCPhysics/LHCHWG.
- [56] S. Dittmaier et al. (LHC Higgs Cross Section Working Group), CERN Report 2011-002 (2011), [arXiv:1101.0593].
- [57] S. Dittmaier et al. (LHC Higgs Cross Section Working Group), CERN Report 2012-002 (2012), [arXiv:1201.3084].
- [58] S. Heinemeyer et al. (LHC Higgs Cross Section Working Group), CERN Report 2013-004 (2013), [arXiv:1307.1347].
- [59] D. de Florian et al. (LHC Higgs Cross Section Working Group), CERN Report 2017-002 (2016), [arXiv:1610.07922].
- [60] A. Karlberg et al. (2024), [arXiv:2402.09955].
- [61] T. Aaltonen et al. (CDF, D0), Phys. Rev. **D88**, 5, 052014 (2013), [arXiv:1303.6346].
- [62] H. M. Georgi et al., Phys. Rev. Lett. 40, 692 (1978).
- [63] D. Graudenz, M. Spira and P. M. Zerwas, Phys. Rev. Lett. 70, 1372 (1993).
- [64] M. Spira et al., Nucl. Phys. **B453**, 17 (1995), [hep-ph/9504378].
- [65] S. Dawson, Nucl. Phys. B359, 283 (1991); A. Djouadi, M. Spira and P. M. Zerwas, Phys. Lett. B264, 440 (1991).

- [66] R. V. Harlander and K. J. Ozeren, JHEP 11, 088 (2009), [arXiv:0909.3420]; A. Pak, M. Rogal and M. Steinhauser, JHEP 02, 025 (2010), [arXiv:0911.4662].
- [67] C. Anastasiou et al., Phys. Rev. Lett. 114, 212001 (2015), [arXiv:1503.06056]; C. Anastasiou et al., JHEP 05, 058 (2016), [arXiv:1602.00695].
- [68] B. Mistlberger, JHEP **05**, 028 (2018), [arXiv:1802.00833].
- [69] G. Das, S. Moch and A. Vogt, Phys. Lett. B 807, 135546 (2020), [arXiv:2004.00563].
- [70] R. N. Lee et al., Phys. Rev. D 104, 7, 074008 (2021), [arXiv:2105.11504].
- [71] R. N. Lee et al., Phys. Rev. Lett. 128, 21, 212002 (2022), [arXiv:2202.04660].
- [72] B. Mistlberger and A. Suresh (2025), [arXiv:2504.10574].
- [73] F. Dulat, A. Lazopoulos and B. Mistlberger, Comput. Phys. Commun. **233**, 243 (2018), [arXiv:1802.00827].
- [74] R. V. Harlander, S. Liebler and H. Mantler, Comput. Phys. Commun. 212, 239 (2017), [arXiv:1605.03190].
- [75] J. Davies et al., Phys. Rev. D100, 3, 034017 (2019), [arXiv:1906.00982]; M. Czakon et al. (2021), [arXiv:2105.04436].
- [76] F. Caola et al., JHEP **09**, 035 (2018), [arXiv:1804.07632].
- [77] K. Melnikov and A. Penin, JHEP **05**, 172 (2016), [arXiv:1602.09020].
- [78] C. Anastasiou and A. Penin, JHEP **07**, 195 (2020), [Erratum: JHEP 01, 164 (2021)], [arXiv:2004.03602].
- [79] M. Czakon et al., Phys. Rev. Lett. 132, 21, 211902 (2024), [arXiv:2312.09896].
- [80] M. Czakon et al., JHEP 10, 210 (2024), [arXiv:2407.12413].
- [81] R. V. Harlander and W. B. Kilgore, Phys. Rev. Lett. 88, 201801 (2002), [hep-ph/0201206];
 C. Anastasiou and K. Melnikov, Nucl. Phys. B646, 220 (2002), [hep-ph/0207004]; V. Ravindran, J. Smith and W. L. van Neerven, Nucl. Phys. B665, 325 (2003), [hep-ph/0302135].
- [82] M. Bonvini et al., JHEP 08, 105 (2016), [arXiv:1603.08000].
- [83] G. Billis et al., Phys. Rev. Lett. 127, 7, 072001 (2021), [arXiv:2102.08039].
- [84] A. Djouadi and P. Gambino, Phys. Rev. Lett. 73, 2528 (1994), [hep-ph/9406432]; S. Actis et al., Phys. Lett. B670, 12 (2008), [arXiv:0809.1301]; U. Aglietti et al., Phys. Lett. B595, 432 (2004), [hep-ph/0404071]; G. Degrassi and F. Maltoni, Phys. Lett. B600, 255 (2004), [hep-ph/0407249].
- [85] C. Anastasiou, R. Boughezal and F. Petriello, JHEP 04, 003 (2009), [arXiv:0811.3458].
- [86] C. Anastasiou et al., JHEP 03, 162 (2019), [arXiv:1811.11211].
- [87] M. Bonetti, K. Melnikov and L. Tancredi, Phys. Rev. D97, 5, 056017 (2018), [Erratum: Phys. Rev. D97, 9, 099906 (2018)], [arXiv:1801.10403]; M. Bonetti et al., JHEP 11, 045 (2020), [arXiv:2007.09813]; M. Becchetti et al., Phys. Rev. D 103, 5, 054037 (2021), [arXiv:2010.09451]; M. Becchetti, F. Moriello and A. Schweitzer, JHEP 04, 139 (2022), [arXiv:2112.07578]; M. Bonetti, E. Panzer and L. Tancredi, JHEP 06, 115 (2022), [arXiv:2203.17202].
- [88] J. McGowan et al., Eur. Phys. J. C 83, 3, 185 (2023), [Erratum: Eur.Phys.J.C 83, 302 (2023)], [arXiv:2207.04739].
- [89] R. D. Ball et al. (NNPDF), Eur. Phys. J. C 84, 7, 659 (2024), [arXiv:2402.18635].
- [90] T. Cridge et al., J. Phys. G 52, 6 (2025), [arXiv:2411.05373].

- [91] F. Dulat, B. Mistlberger and A. Pelloni, Phys. Rev. D **99**, 3, 034004 (2019), [arXiv:1810.09462].
- [92] L. Cieri et al., JHEP **02**, 096 (2019), [arXiv:1807.11501].
- [93] X. Chen et al., Phys. Rev. Lett. 127, 7, 072002 (2021), [arXiv:2102.07607].
- [94] X. Chen, X. Guan and B. Mistlberger (2025), [arXiv:2504.06490].
- [95] S. P. Jones, M. Kerner and G. Luisoni, Phys. Rev. Lett. 120, 16, 162001 (2018), [Erratum: Phys.Rev.Lett. 128, 059901 (2022)], [arXiv:1802.00349].
- [96] X. Chen et al., JHEP 03, 096 (2022), [arXiv:2110.06953].
- [97] R. Bonciani et al., Phys. Lett. B 843, 137995 (2023), [arXiv:2206.10490].
- [98] E. Braaten, H. Zhang and J.-W. Zhang, Phys. Rev. D 97, 9, 096014 (2018), [arXiv:1707.09857].
- [99] J. M. Lindert et al., Phys. Rev. Lett. 118, 25, 252002 (2017), [arXiv:1703.03886].
- [100] M. Niggetiedt and M. Wiesemann, Phys. Lett. B 858, 139043 (2024), [arXiv:2407.01354].
- [101] K. Hamilton et al., JHEP 10, 222 (2013), [arXiv:1309.0017].
- [102] S. Höche, Y. Li and S. Prestel, Phys. Rev. D **90**, 5, 054011 (2014), [arXiv:1407.3773].
- [103] P. F. Monni, E. Re and M. Wiesemann, Eur. Phys. J. C **80**, 11, 1075 (2020), [arXiv:2006.04133].
- [104] G. P. Salam and E. Slade, JHEP 11, 220 (2021), [arXiv:2106.08329].
- [105] A. Banfi, G. P. Salam and G. Zanderighi, JHEP 06, 159 (2012), [arXiv:1203.5773]; T. Becher, M. Neubert and D. Wilhelm, JHEP 05, 110 (2013), [arXiv:1212.2621]; A. Banfi et al., JHEP 04, 049 (2016), [arXiv:1511.02886]; J. K. L. Michel, P. Pietrulewicz and F. J. Tackmann, JHEP 04, 142 (2019), [arXiv:1810.12911]; P. F. Monni, L. Rottoli and P. Torrielli, Phys. Rev. Lett. 124, 25, 252001 (2020), [arXiv:1909.04704].
- [106] I. Moult and I. W. Stewart, JHEP **09**, 129 (2014), [arXiv:1405.5534].
- [107] P. Cal et al., JHEP **03**, 155 (2025), [arXiv:2408.13301].
- [108] V. D. Barger et al., Phys. Rev. **D44**, 1426 (1991).
- [109] F. A. Dreyer and A. Karlberg, Phys. Rev. Lett. 117, 7, 072001 (2016), [arXiv:1606.00840].
- [110] P. Bolzoni et al., Phys. Rev. Lett. 105, 011801 (2010), [arXiv:1003.4451].
- [111] M. Cacciari et al., Phys. Rev. Lett. 115, 8, 082002 (2015), [Erratum: Phys. Rev. Lett. 120, 13,139901 (2018)], [arXiv:1506.02660].
- [112] J. Cruz-Martinez et al., Phys. Lett. **B781**, 672 (2018), [arXiv:1802.02445].
- [113] T. Han, G. Valencia and S. Willenbrock, Phys. Rev. Lett. 69, 3274 (1992), [hep-ph/9206246].
- [114] T. Liu, K. Melnikov and A. A. Penin, Phys. Rev. Lett. **123**, 12, 122002 (2019), [arXiv:1906.10899].
- [115] C. Brønnum-Hansen, M.-M. Long and K. Melnikov, JHEP 11, 130 (2023), [arXiv:2309.06292].
- [116] F. A. Dreyer, A. Karlberg and L. Tancredi, JHEP 10, 131 (2020), [Erratum: JHEP 04, 009 (2022)], [arXiv:2005.11334].
- [117] M. Rauch and D. Zeppenfeld, Phys. Rev. **D95**, 11, 114015 (2017), [arXiv:1703.05676].
- [118] K. Asteriadis et al., JHEP **02**, 046 (2022), [arXiv:2110.02818].
- [119] A. Buckley et al. (2021), [arXiv:2105.11399].
- [120] A. Behring et al. (2025), [arXiv:2507.01448].

- [121] A. Denner et al., JHEP **03**, 075 (2012), [arXiv:1112.5142].
- [122] A. Denner et al., Comput. Phys. Commun. 195, 161 (2015), [arXiv:1412.5390].
- [123] B. Jäger and J. Scheller, JHEP **09**, 191 (2022), [arXiv:2208.00013].
- [124] G. Barone et al. (2025), [arXiv:2507.22574].
- [125] S. L. Glashow, D. V. Nanopoulos and A. Yildiz, Phys. Rev. D18, 1724 (1978); T. Han and S. Willenbrock, Phys. Lett. B273, 167 (1991); T. Han, G. Valencia, and S. Willenbrock, Phys. Rev. Lett. 69, 3274 (1992); H. Baer, B. Bailey and J. F. Owens, Phys. Rev. D47, 2730 (1993); J. Ohnemus and W. J. Stirling, Phys. Rev. D47, 2722 (1993).
- [126] A. Stange, W. J. Marciano and S. Willenbrock, Phys. Rev. **D49**, 1354 (1994), [hep-ph/9309294]; A. Stange, W. J. Marciano and S. Willenbrock, Phys. Rev. **D50**, 4491 (1994), [hep-ph/9404247].
- [127] M. L. Ciccolini, S. Dittmaier and M. Krämer, Phys. Rev. D68, 073003 (2003), [hep-ph/0306234].
- [128] R. Hamberg, W. L. van Neerven and T. Matsuura, Nucl. Phys. B359, 343 (1991), [Erratum: Nucl. Phys. B644, 403 (2002)].
- O. Brein, A. Djouadi and R. Harlander, Phys. Lett. **B579**, 149 (2004), [hep-ph/0307206];
 L. Altenkamp et al., JHEP **02**, 078 (2013), [arXiv:1211.5015].
- [130] J. Davies, G. Mishima and M. Steinhauser, JHEP **03**, 034 (2021), [arXiv:2011.12314].
- [131] L. Chen et al., JHEP **03**, 125 (2021), [arXiv:2011.12325].
- [132] L. Chen et al., JHEP 08, 056 (2022), [arXiv:2204.05225].
- [133] B. Campillo Aveleira et al. (2025), [arXiv:2508.09905].
- [134] O. Brein et al., Eur. Phys. J. C72, 1868 (2012), [arXiv:1111.0761].
- [135] O. Brein, R. V. Harlander and T. J. E. Zirke, Comput. Phys. Commun. 184, 998 (2013),
 [arXiv:1210.5347]; R. V. Harlander et al., JHEP 05, 089 (2018), [arXiv:1802.04817].
- [136] R. Gauld et al., Phys. Lett. B 817, 136335 (2021), [arXiv:2009.14209].
- [137] J. Baglio et al., JHEP 12, 066 (2022), [arXiv:2209.06138].
- [138] A. Denner et al., JHEP 03, 075 (2012), [arXiv:1112.5142].
- [139] G. Ferrera, M. Grazzini, and F. Tramontano, Phys. Rev. Lett. 107, 152003 (2011).
- [140] F. Caola et al., Phys. Rev. D97, 7, 074022 (2018), [arXiv:1712.06954]; G. Ferrera, G. Somogyi and F. Tramontano, Phys. Lett. B 780, 346 (2018), [arXiv:1705.10304]; R. Gauld et al., JHEP 10, 002 (2019), [arXiv:1907.05836].
- [141] G. Ferrera, M. Grazzini and F. Tramontano, Phys. Lett. B740, 51 (2015), [arXiv:1407.4747];
 J. M. Campbell, R. K. Ellis and C. Williams, JHEP 06, 179 (2016), [arXiv:1601.00658].
- [142] W. Astill et al., JHEP **06**, 154 (2016), [arXiv:1603.01620].
- [143] J. M. Butterworth *et al.*, Phys. Rev. Lett. **100**, 242001 (2008), [arXiv:0802.2470].
- [144] A. Behring et al., Phys. Rev. D 101, 11, 114012 (2020), [arXiv:2003.08321].
- [145] W. Bizon et al. (2021), [arXiv:2106.06328].
- [146] R. Raitio and W. W. Wada, Phys. Rev. **D19**, 941 (1979); Z. Kunszt, Nucl. Phys. **B247**, 339 (1984); J. N. Ng and P. Zakarauskas, Phys. Rev. D **29**, 876 (1984); J. F. Gunion, Phys. Lett. **B261**, 510 (1991); W. J. Marciano and F. E. Paige, Phys. Rev. Lett. **66**, 2433 (1991).

- [147] W. Beenakker et al., Phys. Rev. Lett. 87, 201805 (2001), [hep-ph/0107081]; L. Reina and S. Dawson, Phys. Rev. Lett. 87, 201804 (2001), [hep-ph/0107101]; L. Reina, S. Dawson and D. Wackeroth, Phys. Rev. D 65, 053017 (2002), [hep-ph/0109066]; S. Dawson et al., Phys. Rev. D67, 071503 (2003), [hep-ph/0211438]; W. Beenakker et al., Nucl. Phys. B653, 151 (2003), [hep-ph/0211352]; S. Dawson et al., Phys. Rev. D68, 034022 (2003), [hep-ph/0305087].
- [148] Y. Zhang et al., Phys. Lett. **B738**, 1 (2014), [arXiv:1407.1110]; S. Frixione et al., JHEP **09**, 065 (2014), [arXiv:1407.0823]; S. Frixione et al., JHEP **06**, 184 (2015), [arXiv:1504.03446].
- [149] T. Plehn, G. P. Salam and M. Spannowsky, Phys. Rev. Lett. 104, 111801 (2010), [arXiv:0910.5472].
- [150] W.-L. Ju and L. L. Yang, JHEP **06**, 050 (2019), [arXiv:1904.08744].
- [151] A. Kulesza et al., JHEP 03, 065 (2016), [arXiv:1509.02780]; A. Broggio et al., JHEP 03, 124 (2016), [arXiv:1510.01914]; A. Broggio et al., JHEP 02, 126 (2017), [arXiv:1611.00049]; A. Kulesza et al., Phys. Rev. D 97, 11, 114007 (2018), [arXiv:1704.03363]; A. Broggio et al., JHEP 08, 039 (2019), [arXiv:1907.04343]; A. Kulesza et al., Eur. Phys. J. C 80, 5, 428 (2020), [arXiv:2001.03031].
- [152] A. Denner and R. Feger, JHEP 11, 209 (2015), [arXiv:1506.07448].
- [153] A. Denner et al., JHEP **02**, 053 (2017), [arXiv:1612.07138].
- [154] R. Frederix et al., Phys. Lett. B701, 427 (2011), [arXiv:1104.5613]; H. B. Hartanto et al., Phys. Rev. D 91, 9, 094003 (2015), [arXiv:1501.04498].
- [155] S. Catani et al., Eur. Phys. J. C 81, 6, 491 (2021), [arXiv:2102.03256].
- [156] S. Catani et al., Phys. Rev. Lett. 130, 11, 111902 (2023), [arXiv:2210.07846].
- [157] S. Devoto et al., JHEP **03**, 189 (2025), [arXiv:2411.15340].
- [158] F. Febres Cordero et al., JHEP 07, 084 (2024), [arXiv:2312.08131].
- [159] G. Wang et al., JHEP 07, 121 (2024), [arXiv:2402.00431].
- [160] B. Agarwal et al., JHEP **05**, 013 (2024), [Erratum: JHEP 06, 142 (2024)], [arXiv:2402.03301].
- [161] R. Balsach et al. (2025), [arXiv:2503.15043].
- [162] C. Brancaccio et al., JHEP 08, 145 (2021), [arXiv:2106.06516].
- [163] G. Bevilacqua et al., Phys. Rev. D 107, 1, 014028 (2023), [arXiv:2202.11186].
- [164] F. Demartin et al., Eur. Phys. J. C75, 6, 267 (2015), [arXiv:1504.00611].
- [165] D. Pagani, I. Tsinikos and E. Vryonidou, JHEP 08, 082 (2020), [arXiv:2006.10086].
- [166] C. Duhr et al., JHEP 08, 08, 017 (2020), [arXiv:2004.04752].
- [167] K.A. Assamagan *et al.*, [Higgs Working Group, "Physics at TeV Colliders" workshop, Les Houches, 2003], arXiv:hep-ph/0406152 (2004).
- [168] R. V. Harlander and W. B. Kilgore, Phys. Rev. D68, 013001 (2003), [hep-ph/0304035];
 J. M. Campbell et al., Phys. Rev. D67, 095002 (2003), [hep-ph/0204093];
 S. Dawson et al., Phys. Rev. Lett. 94, 031802 (2005), [hep-ph/0408077];
 S. Dittmaier, M. Krämer and M. Spira, Phys. Rev. D70, 074010 (2004), [hep-ph/0309204];
 S. Dawson et al., Phys. Rev. D69, 074027 (2004), [hep-ph/0311067].
- [169] S. Badger et al., JHEP **03**, 066 (2025), [arXiv:2412.06519].
- [170] S. Badger et al., JHEP 11, 012 (2021), [arXiv:2107.14733].
- [171] C. Biello et al., JHEP **04**, 088 (2025), [arXiv:2412.09510].

- [172] D. Pagani, H.-S. Shao and M. Zaro, JHEP 11, 036 (2020), [arXiv:2005.10277].
- [173] C. Grojean, A. Paul and Z. Qian, JHEP **04**, 139 (2021), [arXiv:2011.13945].
- [174] S. Dawson, S. Dittmaier and M. Spira, Phys. Rev. **D58**, 115012 (1998), [hep-ph/9805244].
- [175] D. de Florian and J. Mazzitelli, Phys. Rev. Lett. 111, 201801 (2013), [arXiv:1309.6594].
- [176] L.-B. Chen et al., Phys. Lett. B 803, 135292 (2020), [arXiv:1909.06808].
- [177] S. Borowka et al., Phys. Rev. Lett. 117, 1, 012001 (2016), [Erratum: Phys. Rev. Lett. 117, 7, 079901 (2016)], [arXiv:1604.06447]; J. Baglio et al., Eur. Phys. J. C79, 6, 459 (2019), [arXiv:1811.05692]; J. Davies et al., JHEP 11, 024 (2019), [arXiv:1907.06408].
- [178] S. Jaskiewicz *et al.*, JHEP **09**, 015 (2025), [arXiv:2501.00587].
- [179] M. Grazzini et al., JHEP **05**, 059 (2018), [arXiv:1803.02463].
- [180] J. Davies, K. Schönwald and M. Steinhauser, Phys. Lett. B 845, 138146 (2023), [arXiv:2307.04796].
- [181] J. Davies et al., JHEP 08, 096 (2024), [arXiv:2405.20372].
- [182] J. Davies, K. Schönwald and M. Steinhauser, JHEP 08, 192 (2025), [arXiv:2503.17449].
- [183] G. Aad et al. (ATLAS), Phys. Rev. Lett. 133, 10, 101801 (2024), [arXiv:2406.09971].
- [184] CMS Collaboration, CMS-HIG-20-011 (2025), [arXiv:2510.07527].
- [185] F. A. Dreyer and A. Karlberg, Phys. Rev. D 98, 11, 114016 (2018), [arXiv:1811.07906].
- [186] F. A. Dreyer et al., Eur. Phys. J. C 80, 11, 1037 (2020), [arXiv:2005.13341].
- [187] L.-S. Ling et al., Phys. Rev. D 89, 7, 073001 (2014), [arXiv:1401.7754].
- [188] F. A. Dreyer and A. Karlberg, Phys. Rev. D 99, 7, 074028 (2019), [arXiv:1811.07918].
- [189] R. Frederix et al., Phys. Lett. B **732**, 142 (2014), [arXiv:1401.7340].
- [190] B. Jäger, A. Karlberg and S. Reinhardt, JHEP **06**, 022 (2025), [arXiv:2502.09112].
- [191] R. K. Ellis et al. (2019), [arXiv:1910.11775].
- [192] M. Narain et al. (2022), [arXiv:2211.11084].
- [193] A. Arbey et al., Eur. Phys. J. C75, 8, 371 (2015), [arXiv:1504.01726]; A. Freitas et al. (2019), [arXiv:1906.05379].
- [194] J. de Blas et al., JHEP **01**, 139 (2020), [arXiv:1905.03764].
- [195] S. Dawson et al., in "Snowmass 2021," (2022), [arXiv:2209.07510].
- [196] H. Al Ali et al., Rept. Prog. Phys. 85, 8, 084201 (2022), [arXiv:2103.14043].
- [197] J. de Blas, J. Gu and Z. Liu, Phys. Rev. D **106**, 7, 073007 (2022), [arXiv:2203.04324].
- [198] J. de Blas et al. (Muon Collider) (2022), [arXiv:2203.07261].
- [199] B.L. Ioffe and V.A. Khoze, Sov. J. Nucl. Phys. 9, 50 (1978).
- [200] D. R. T. Jones and S. T. Petcov, Phys. Lett. 84B, 440 (1979); R. N. Cahn and S. Dawson, Phys. Lett. 136B, 196 (1984), [Erratum: Phys. Lett. 138B, 464 (1984)]; G. L. Kane, W. W. Repko and W. B. Rolnick, Phys. Lett. 148B, 367 (1984); G. Altarelli, B. Mele and F. Pitolli, Nucl. Phys. B287, 205 (1987); W. Kilian, M. Krämer and P. M. Zerwas, Phys. Lett. B373, 135 (1996), [hep-ph/9512355].
- [201] B. A. Kniehl, Z. Phys. C55, 605 (1992); J. Fleischer and F. Jegerlehner, Nucl. Phys. B216, 469 (1983); A. Denner et al., Z. Phys. C56, 261 (1992); B. A. Kniehl, Int. J. Mod. Phys. A17, 1457 (2002), [hep-ph/0112023].

- [202] K. J. F. Gaemers and G. J. Gounaris, Phys. Lett. 77B, 379 (1978); A. Djouadi, J. Kalinowski and P. M. Zerwas, Z. Phys. C54, 255 (1992); B. A. Kniehl, F. Madricardo and M. Steinhauser, Phys. Rev. D66, 054016 (2002), [hep-ph/0205312]; S. Dittmaier et al., Phys. Lett. B441, 383 (1998), [hep-ph/9808433]; S. Dittmaier et al., Phys. Lett. B478, 247 (2000), [hep-ph/0002035]; S. Dawson and L. Reina, Phys. Rev. D59, 054012 (1999), [hep-ph/9808443].
- [203] X. Chen et al. (2022), [arXiv:2209.14953].
- [204] A. Freitas and Q. Song, Phys. Rev. Lett. **130**, 3, 031801 (2023), [arXiv:2209.07612].
- [205] S. Heinemeyer, S. Jadach and J. Reuter, Eur. Phys. J. Plus **136**, 9, 911 (2021), [arXiv:2106.11802].
- [206] A. Belloni et al. (2022), [arXiv:2209.08078].
- [207] S. Frixione et al. (2021), [arXiv:2108.10261].
- [208] A. Denner et al., Eur. Phys. J. C71, 1753 (2011), [arXiv:1107.5909].
- [209] A. Djouadi, J. Kalinowski, and M. Spira, Comp. Phys. Comm. 108, 56 (1998); A. Djouadi et al., arXiv:1003.1643 [hep-ph] (2010).
- [210] S. G. Gorishnii et al., Mod. Phys. Lett. A5, 2703 (1990); S. G. Gorishnii et al., Phys. Rev. D43, 1633 (1991); A. L. Kataev and V. T. Kim, Mod. Phys. Lett. A9, 1309 (1994); L. R. Surguladze, Phys. Lett. B341, 60 (1994), [hep-ph/9405325].
- [211] S. A. Larin, T. van Ritbergen and J. A. M. Vermaseren, Phys. Lett. B362, 134 (1995), [hep-ph/9506465]; K. G. Chetyrkin, Phys. Lett. B390, 309 (1997), [hep-ph/9608318]; P. A. Baikov, K. G. Chetyrkin and J. H. Kuhn, Phys. Rev. Lett. 96, 012003 (2006), [hep-ph/0511063].
- [212] K. G. Chetyrkin and A. Kwiatkowski, Nucl. Phys. **B461**, 3 (1996), [hep-ph/9505358].
- [213] A. Primo et al., Phys. Rev. D 99, 5, 054013 (2019), [arXiv:1812.07811].
- [214] W. Bernreuther, L. Chen and Z.-G. Si, JHEP **07**, 159 (2018), [arXiv:1805.06658].
- [215] A. Behring and W. Bizoń, JHEP **01**, 189 (2020), [arXiv:1911.11524].
- [216] G. Somogyi and F. Tramontano, JHEP 11, 142 (2020), [arXiv:2007.15015].
- [217] J. Wang, Y. Wang and D.-J. Zhang, JHEP **03**, 068 (2024), [arXiv:2310.20514].
- [218] J. Wang, X. Wang and Y. Wang, JHEP **03**, 163 (2025), [arXiv:2411.07493].
- [219] J. Fleischer and F. Jegerlehner, Phys. Rev. D23, 2001 (1981); D. Yu. Bardin, B. M. Vilensky and P. K. Khristova, Sov. J. Nucl. Phys. 53, 152 (1991), [Yad. Fiz.53,240(1991)]; A. Dabelstein and W. Hollik, Z. Phys. C53, 507 (1992); B. A. Kniehl, Nucl. Phys. B376, 3 (1992); A. Djouadi et al., in "In *Munich/Annecy/Hamburg 1991, Proceedings, e+ e- collisions at 500 GeV, pt. A* 11-30," (1991).
- [220] F. Herzog et al., JHEP 08, 113 (2017), [arXiv:1707.01044].
- [221] T. Inami, T. Kubota and Y. Okada, Z. Phys. C18, 69 (1983); K. G. Chetyrkin, B. A. Kniehl and M. Steinhauser, Phys. Rev. Lett. 79, 353 (1997), [hep-ph/9705240]; P. A. Baikov and K. G. Chetyrkin, Phys. Rev. Lett. 97, 061803 (2006), [hep-ph/0604194].
- [222] H.-Q. Zheng and D.-D. Wu, Phys. Rev. D42, 3760 (1990); A. Djouadi et al., Phys. Lett. B257, 187 (1991); S. Dawson and R. P. Kauffman, Phys. Rev. D47, 1264 (1993); A. Djouadi, M. Spira and P. M. Zerwas, Phys. Lett. B311, 255 (1993), [hep-ph/9305335]; K. Melnikov and O. I. Yakovlev, Phys. Lett. B312, 179 (1993), [hep-ph/9302281]; M. Inoue et al., Mod. Phys. Lett. A9, 1189 (1994).
- [223] P. Maierhöfer and P. Marquard, Phys. Lett. **B721**, 131 (2013), [arXiv:1212.6233].

- [224] U. Aglietti et al., Phys. Lett. B595, 432 (2004), [hep-ph/0404071]; G. Degrassi and F. Maltoni, Phys. Lett. B600, 255 (2004), [hep-ph/0407249]; S. Actis et al., Phys. Lett. B670, 12 (2008), [arXiv:0809.1301]; U. Aglietti et al., Phys. Lett. B600, 57 (2004), [hep-ph/0407162]; G. Degrassi and F. Maltoni, Nucl. Phys. B724, 183 (2005), [hep-ph/0504137]; U. Aglietti et al., FERMILAB-CONF (2006), [hep-ph/0612172].
- [225] A. Abbasabadi et al., Phys. Rev. D55, 5647 (1997), [hep-ph/9611209]; A. Abbasabadi and W. W. Repko, Phys. Rev. D71, 017304 (2005), [hep-ph/0411152]; A. Abbasabadi and W. W. Repko, JHEP 08, 048 (2006), [hep-ph/0602087]; D. A. Dicus and W. W. Repko, Phys. Rev. D87, 7, 077301 (2013), [arXiv:1302.2159]; L.-B. Chen, C.-F. Qiao and R.-L. Zhu, Phys. Lett. B726, 306 (2013), [arXiv:1211.6058]; Y. Sun, H.-R. Chang and D.-N. Gao, JHEP 05, 061 (2013), [arXiv:1303.2230]; G. Passarino, Phys. Lett. B727, 424 (2013), [arXiv:1308.0422].
- [226] M. Spira, A. Djouadi and P. M. Zerwas, Phys. Lett. **B276**, 350 (1992).
- [227] R. Bonciani et al., JHEP 08, 108 (2015), [arXiv:1505.00567].
- [228] T. Gehrmann, S. Guns and D. Kara, JHEP **09**, 038 (2015), [arXiv:1505.00561].
- [229] A. Bredenstein et al., Phys. Rev. D74, 013004 (2006), [hep-ph/0604011]; A. Bredenstein et al., JHEP 02, 080 (2007), [hep-ph/0611234]; A. Bredenstein et al., Prophecy4f: A Monte Carlo generator for a proper description of the Higgs decay into 4 fermions, http://omnibus.uni-freiburg.de/~sd565/programs/prophecy4f/prophecy4f.html.
- [230] A. Ghinculov, Phys. Lett. B337, 137 (1994), [Erratum: Phys. Lett. B346, 426 (1995)], [hep-ph/9405394]; L. Durand, B. A. Kniehl and K. Riesselmann, Phys. Rev. D51, 5007 (1995), [hep-ph/9412311]; L. Durand, K. Riesselmann and B. A. Kniehl, Phys. Rev. Lett. 72, 2534 (1994), [Erratum: Phys. Rev. Lett. 74, 1699 (1995)].
- [231] A. Hayrapetyan et al. (CMS), Phys. Rev. D 111, 9, 092014 (2025), [arXiv:2409.13663].
- [232] N. Kauer and G. Passarino, JHEP 08, 116 (2012), [arXiv:1206.4803].
- [233] F. Caola and K. Melnikov, Phys. Rev. D88, 054024 (2013), [arXiv:1307.4935]; J. M. Campbell, R. K. Ellis and C. Williams, JHEP 04, 060 (2014), [arXiv:1311.3589]; J. M. Campbell, R. K. Ellis and C. Williams, Phys. Rev. D89, 5, 053011 (2014), [arXiv:1312.1628].
- [234] C. Englert and M. Spannowsky, Phys. Rev. **D90**, 053003 (2014), [arXiv:1405.0285].
- [235] A. Azatov *et al.*, Zh. Eksp. Teor. Fiz. **147**, 410 (2015), [J. Exp. Theor. Phys.120,354(2015)], [arXiv:1406.6338]; A. Azatov *et al.*, JHEP **09**, 123 (2016), [arXiv:1608.00977].
- [236] P. Bargiela et al., Eur. Phys. J. C 83, 2, 174 (2023), [arXiv:2212.06287].
- [237] B. Agarwal et al., Phys. Rev. Lett. 134, 3, 031901 (2025), [arXiv:2404.05684].
- [238] R. C. L. de Sá et al. (2025), [arXiv:2506.17022].
- [239] CMS Collaboration, CMS-PAS-HIG-21-018 (2025).
- [240] ATLAS Collaboration, ATLAS-CONF-2025-006 (2025).
- [241] A. M. Sirunyan et al. (CMS), JHEP **01**, 148 (2021), [arXiv:2009.04363].
- [242] G. Aad et al. (ATLAS) (2025), [arXiv:2507.03595].
- [243] G. Aad et al. (ATLAS, CMS), Phys. Rev. Lett. 132, 2, 021803 (2024), [arXiv:2309.03501].
- [244] G. Aad et al. (ATLAS), Eur. Phys. J. C 84, 1, 78 (2024), [arXiv:2306.11379].
- [245] G. Cowan, Statistics, in this volume.
- [246] G. Aad et al. (ATLAS), Phys. Lett. B 816, 136204 (2021), [arXiv:2008.02508].
- [247] A. Hayrapetyan et al. (CMS), JHEP 12, 035 (2024), [arXiv:2407.08012].
- [248] A. Hayrapetyan et al. (CMS), Phys. Lett. B 857, 138964 (2024), [arXiv:2403.20201].

- [249] G. Aad et al. (ATLAS), JHEP 05, 028 (2023), [arXiv:2207.08615].
- [250] A. M. Sirunyan et al. (CMS), Phys. Lett. **B792**, 369 (2019), [arXiv:1812.06504].
- [251] V. Chekhovsky et al. (CMS), CMS-HIG-23-013 (2025), [arXiv:2504.13081].
- [252] N. Berger et al. (2019), [arXiv:1906.02754].
- [253] ATLAS Collaboration, ATLAS-CONF-2020-027 (2020).
- [254] ATLAS Collaboration, ATLAS-CONF-2020-053 (2020).
- [255] G. Aad et al. (ATLAS), Nature **607**, 7917, 52 (2022), [Erratum: Nature 612, E24 (2022)], [arXiv:2207.00092].
- [256] A. David *et al.* (LHC Higgs Cross Section Working Group), LHC HXSWG interim recommendations to explore the coupling structure of a Higgs-like particle (2012), [arXiv:1209.0040].
- [257] M. Dührssen, Prospects for the measurement of Higgs boson coupling parameters in the mass range from 110–190 GeV (2003); M. Duhrssen et al., Phys. Rev. D70, 113009 (2004), [hep-ph/0406323]; R. Lafaye et al., JHEP 08, 009 (2009), [arXiv:0904.3866].
- [258] J. R. Espinosa et al., JHEP 05, 097 (2012), [arXiv:1202.3697]; A. Azatov, R. Contino and J. Galloway, JHEP 04, 127 (2012), [Erratum: JHEP 04, 140 (2013)], [arXiv:1202.3415];
 D. Carmi et al., JHEP 07, 136 (2012), [arXiv:1202.3144]; J. R. Espinosa et al., JHEP 12, 045 (2012), [arXiv:1207.1717].
- [259] LHC Higgs Cross Section Working Group, https://twiki.cern.ch/twiki/bin/view/LHCPhysics/LHCHWG2KAPPA.
- [260] G. Aad et al. (ATLAS, CMS), JHEP 08, 045 (2016), [arXiv:1606.02266].
- [261] A. Hayrapetyan et al. (CMS), Phys. Lett. B 860, 139202 (2025), [arXiv:2405.16566].
- [262] G. Aad et al. (ATLAS), Phys. Rev. Lett. 133, 14, 141801 (2024), [arXiv:2402.00426].
- [263] M. Tanabashi et al. (Particle Data Group), Phys. Rev. **D98**, 3, 030001 (2018).
- [264] M. Farina et al., JHEP **05**, 022 (2013), [arXiv:1211.3736].
- [265] A. Tumasyan et al. (CMS), Nature 607, 7917, 60 (2022), [arXiv:2207.00043].
- [266] ATLAS and CMS Collaborations, CDS (2025), [arXiv:2504.00672], URL https://cds.cern.ch/record/2928907.
- [267] A. Hayrapetyan et al. (CMS), CMS-HIG-24-018 (2025), [arXiv:2509.22535].
- [268] G. Aad et al. (ATLAS) (2024), [arXiv:2410.19611].
- [269] A. Hayrapetyan et al. (CMS), Phys. Lett. B 865, 139462 (2025), [arXiv:2411.15000].
- [270] A. Hayrapetyan et al. (CMS) (2025), [arXiv:2508.14988].
- [271] V. Chekhovsky et al. (CMS) (2025), [arXiv:2503.08797].
- [272] V. Chekhovsky et al. (CMS) (2025), [arXiv:2502.05665].
- [273] G. Aad et al. (ATLAS), Phys. Lett. B 801, 135148 (2020), [arXiv:1909.10235].
- [274] A. Tumasyan et al. (CMS), Phys. Lett. B 846, 137783 (2023), [arXiv:2208.00265].
- [275] I. Brivio and M. Trott, Phys. Rept. **793**, 1 (2019), [arXiv:1706.08945].
- [276] G. Isidori, F. Wilsch and D. Wyler, Rev. Mod. Phys. 96, 1, 015006 (2024), [arXiv:2303.16922].
- [277] J. Aebischer, A. J. Buras and J. Kumar (2025), [arXiv:2507.05926].
- [278] A. Manohar and H. Georgi, Nucl. Phys. B234, 189 (1984); M. A. Luty, Phys. Rev. D57, 1531 (1998), [hep-ph/9706235]; D. Liu et al., JHEP 11, 141 (2016), [arXiv:1603.03064].
- [279] G. F. Giudice et al., JHEP **06**, 045 (2007), [hep-ph/0703164].

- [280] S. Alioli et al., Phys. Lett. B 809, 135703 (2020), [arXiv:2003.11615].
- [281] R. Boughezal, Y. Huang and F. Petriello, Phys. Rev. D **106**, 3, 036020 (2022), [arXiv:2207.01703].
- [282] S. Alioli et al., in "Snowmass 2021," (2022), [arXiv:2203.06771].
- [283] W. Buchmuller and D. Wyler, Nucl. Phys. **B268**, 621 (1986).
- [284] C. J. C. Burges and H. J. Schnitzer, Nucl. Phys. B228, 464 (1983); C. N. Leung, S. T. Love and S. Rao, Z. Phys. C31, 433 (1986).
- [285] B. Grzadkowski et al., JHEP 10, 085 (2010), [arXiv:1008.4884].
- [286] L. Lehman and A. Martin, JHEP **02**, 081 (2016), [arXiv:1510.00372]; B. Henning *et al.*, JHEP **08**, 016 (2017), [arXiv:1512.03433].
- [287] C. Hays et al., JHEP **02**, 123 (2019), [arXiv:1808.00442].
- [288] R. Alonso et al., JHEP **04**, 159 (2014), [arXiv:1312.2014].
- [289] D. A. Faroughy et al., JHEP 08, 166 (2020), [arXiv:2005.05366].
- [290] J. de Blas et al., JHEP **03**, 109 (2018), [arXiv:1711.10391].
- [291] I. Brivio et al., SciPost Phys. 12, 1, 036 (2022), [arXiv:2108.01094].
- [292] A. Carmona et al., SciPost Phys. 12, 6, 198 (2022), [arXiv:2112.10787].
- [293] J. Fuentes-Martín et al., Eur. Phys. J. C 83, 7, 662 (2023), [arXiv:2212.04510].
- [294] E. E. Jenkins, A. V. Manohar and M. Trott, JHEP 10, 087 (2013), [arXiv:1308.2627].
- [295] E. E. Jenkins, A. V. Manohar and M. Trott, JHEP **01**, 035 (2014), [arXiv:1310.4838].
- [296] J. C. Criado, Comput. Phys. Commun. 227, 42 (2018), [arXiv:1710.06445].
- [297] A. Celis et al., Eur. Phys. J. C 77, 6, 405 (2017), [arXiv:1704.04504].
- [298] J. Aebischer, J. Kumar and D. M. Straub, Eur. Phys. J. C **78**, 12, 1026 (2018), [arXiv:1804.05033].
- [299] S. Di Noi and L. Silvestrini, Eur. Phys. J. C 83, 3, 200 (2023), [arXiv:2210.06838].
- [300] J. Alwall et al., JHEP **07**, 079 (2014), [arXiv:1405.0301].
- [301] I. Brivio, Y. Jiang and M. Trott, JHEP 12, 070 (2017), [arXiv:1709.06492].
- [302] I. Brivio, JHEP **04**, 073 (2021), [arXiv:2012.11343].
- [303] C. Degrande et al., Phys. Rev. D 103, 9, 096024 (2021), [arXiv:2008.11743].
- [304] J. de Blas et al. (2025), [arXiv:2507.06191].
- [305] J. Ellis et al., JHEP **04**, 279 (2021), [arXiv:2012.02779].
- [306] J. J. Ethier et al. (SMEFiT), JHEP 11, 089 (2021), [arXiv:2105.00006].
- [307] L. Allwicher et al. (2023), [arXiv:2311.00020].
- [308] R. Bartocci, A. Biekötter and T. Hurth, JHEP **05**, 074 (2024), [arXiv:2311.04963].
- [309] R. Bartocci, A. Biekötter and T. Hurth, JHEP 05, 203 (2025), [arXiv:2412.09674].
- [310] E. Celada et al., JHEP **09**, 091 (2024), [arXiv:2404.12809].
- [311] G. Aad et al. (ATLAS), JHEP 11, 097 (2024), [arXiv:2402.05742].
- [312] V. Chekhovsky et al. (CMS), CMS-SMP-24-003 (2025), [arXiv:2504.02958].
- [313] ATLAS Collaboration, ATL-PHYS-PUB-2022-037 (2022).
- [314] A. Hayrapetyan et al. (CMS), JHEP 10, 061 (2024), [arXiv:2404.08462].
- [315] G. Aad et al. (ATLAS), Eur. Phys. J. C 83, 6, 519 (2023), [arXiv:2210.05415].

- [316] CMS Collaboration, CMS-PAS-HIG-23-004 (2025).
- [317] ATLAS and CMS Collaborations, CMS-PAS-HIG-25-014, ATLAS-CONF-2025-012 (2025).
- [318] ATLAS Collaboration, ATL-PHYS-PUB-2025-034 (2025), URL https://cds.cern.ch/record/2942493.
- [319] A. Hayrapetyan et al. (CMS), Phys. Lett. B 861, 139210 (2025), [arXiv:2407.13554].
- [320] G. Aad et al. (ATLAS), Phys. Lett. B 843, 137745 (2023), [arXiv:2211.01216].
- [321] ATLAS Collaboration, ATLAS-CONF-2025-005 (2025).
- [322] CMS Collaboration, CMS-PAS-HIG-25-007 (2025).
- [323] CMS Collaboration, CMS-PAS-HIG-24-010 (2025).
- [324] ATLAS Collaboration, ATL-PHYS-PUB-2025-005 (2025).
- [325] G. Aad et al. (ATLAS), Phys. Rev. D 111, 3, 032006 (2025), [arXiv:2411.02040].
- [326] CMS Collaboration, CMS-PAS-HIG-24-015 (2025).
- [327] CMS Collaboration, CMS-PAS-HIG-24-012 (2025).
- [328] G. Aad et al. (ATLAS, CMS), Phys. Rev. Lett. 114, 191803 (2015), [arXiv:1503.07589].
- [329] G. Aad et al. (ATLAS), Phys. Rev. Lett. 131, 25, 251802 (2023), [arXiv:2308.04775].
- [330] G. Aad et al. (ATLAS), Phys. Lett. B 847, 138315 (2023), [arXiv:2308.07216].
- [331] G. Aad et al. (ATLAS), Phys. Rev. **D90**, 5, 052004 (2014), [arXiv:1406.3827].
- [332] CMS Collaboration, CMS-PAS-HIG-25-004 (2025).
- [333] L. J. Dixon and M. S. Siu, Phys. Rev. Lett. **90**, 252001 (2003), [hep-ph/0302233].
- [334] S. P. Martin, Phys. Rev. **D86**, 073016 (2012), [arXiv:1208.1533].
- [335] L. J. Dixon and Y. Li, Phys. Rev. Lett. 111, 111802 (2013), [arXiv:1305.3854].
- [336] J. Campbell *et al.*, Phys. Rev. Lett. **119**, 18, 181801 (2017), [Addendum: Phys. Rev. Lett.119,19,199901(2017)], [arXiv:1704.08259].
- [337] ATLAS Collaboration, ATL-PHYS-PUB-2016-009 (2016).
- [338] ATLAS Collaboration, ATL-PHYS-PUB-2013-014 (2013).
- [339] ATLAS Collaboration, ATL-PHYS-PUB-2014-016 (2014).
- [340] G. Aad et al. (ATLAS), Rept. Prog. Phys. 88, 5, 057803 (2025), [arXiv:2412.01548].
- [341] A. Tumasyan et al. (CMS), Nature Phys. 18, 11, 1329 (2022), [arXiv:2202.06923].
- [342] G. Aad et al. (ATLAS) (2025), [arXiv:2504.07710].
- [343] G. Aad et al. (ATLAS), Phys. Lett. B 861, 139277 (2025), [arXiv:2407.10631].
- [344] M. Cepeda et al. (HL/HE-LHC WG2 group) (2019), [arXiv:1902.00134].
- [345] Y. Gao et al., Phys. Rev. D 81, 075022 (2010), [arXiv:1001.3396].
- [346] S. Bolognesi et al., Phys. Rev. **D86**, 095031 (2012), [arXiv:1208.4018].
- [347] J. F. Gunion et al., The Higgs Hunter's Guide, volume 80 (2000), ISBN 978-0-429-49644-8.
- [348] J. Brod, U. Haisch and J. Zupan, JHEP 11, 180 (2013), [arXiv:1310.1385].
- [349] S. Degenkolb *et al.* (2024), [arXiv:2403.02052].
- [350] G. Aad et al. (ATLAS) (2023), [arXiv:2304.09612].
- [351] CMS Collaboration, CMS-PAS-HIG-24-006 (2025), CMS-PAS-HIG-24-006, URL https://cds.cern.ch/record/2937958.
- [352] ATLAS Collaboration, ATL-PHYS-PUB-2025-031 (2025).

- [353] A. M. Sirunyan et al. (CMS), Phys. Rev. D **100**, 11, 112002 (2019), [arXiv:1903.06973].
- [354] G. Aad et al. (ATLAS), Phys. Rev. Lett. 125, 6, 061802 (2020), [arXiv:2004.04545].
- [355] (2023), [arXiv:2303.05974].
- [356] A. M. Sirunyan et al. (CMS), Phys. Rev. Lett. 125, 6, 061801 (2020), [arXiv:2003.10866].
- [357] A. M. Sirunyan et al. (CMS), Phys. Rev. D 104, 5, 052004 (2021), [arXiv:2104.12152].
- [358] A. Tumasyan et al. (CMS), JHEP 07, 092 (2023), [arXiv:2208.02686].
- [359] A. Tumasyan et al. (CMS), JHEP **06**, 012 (2022), [arXiv:2110.04836].
- [360] G. Aad et al. (ATLAS), Eur. Phys. J. C 83, 7, 563 (2023), [arXiv:2212.05833].
- [361] ATLAS Collaboration, ATL-PHYS-PUB-2019-008 (2019).
- [362] Y. Gershtein, and A. Pomarol, Extra Dimensions, in this volume.
- [363] L. E. Ibanez and G. G. Ross, Phys. Lett. 110B, 215 (1982); L. E. Ibanez, Phys. Lett. 118B,
 73 (1982); J. R. Ellis, D. V. Nanopoulos and K. Tamvakis, Phys. Lett. 121B, 123 (1983);
 L. Alvarez-Gaume, J. Polchinski and M. B. Wise, Nucl. Phys. B221, 495 (1983).
- [364] M. Carena et al., Phys. Rev. **D91**, 3, 035003 (2015), [arXiv:1410.4969].
- [365] M. Carena et al., Phys. Rev. **D93**, 3, 035013 (2016), [arXiv:1510.09137].
- [366] J. F. Gunion and H. E. Haber, Phys. Rev. **D67**, 075019 (2003), [hep-ph/0207010].
- [367] H. E. Haber and Y. Nir, Nucl. Phys. **B335**, 363 (1990).
- [368] S. Weinberg, Phys. Rev. **D13**, 974 (1976), [Addendum: Phys. Rev.D19,1277(1979)];
 L. Susskind, Phys. Rev. **D20**, 2619 (1979); For a review, see C. T. Hill and E. H. Simmons,
 Phys. Reports **381**, 235 (2003) [Erratum: 390, 553 (2004)], [arXiv:hep-ph/0203079].
- [369] Z. Chacko, R. Franceschini and R. K. Mishra, JHEP **04**, 015 (2013), [arXiv:1209.3259].
- [370] D. B. Kaplan, Nucl. Phys. **B365**, 259 (1991).
- [371] G. Panico et al., JHEP 03, 051 (2013), [arXiv:1210.7114].
- [372] A. Hebecker, J. Hisano, and N. Nagata, Grand Unified Theories, in this volume.
- [373] L.J. Rosenberg, G. Rybka, and B. Safdi, Axions and Other Similar Particles, in this volume.
- [374] M. D'Onofrio and F. Moortgat, Supersymmetry, Part II (Experiment), in this volume.
- [375] K. Hikasa, and M. Tanabashi, K. Terashi, N. Varelas Searches for Quark and Lepton Compositeness, in this volume.
- [376] H. E. Haber and G. L. Kane, Phys. Rept. 117, 75 (1985).
- [377] P. Slavich et al., Eur. Phys. J. C 81, 5, 450 (2021), [arXiv:2012.15629].
- [378] M. Carena and H. E. Haber, Prog. Part. Nucl. Phys. 50, 63 (2003), [hep-ph/0208209].
- [379] A. Djouadi, Phys. Rept. **459**, 1 (2008), [hep-ph/0503173].
- [380] E. L. Berger et al., Phys. Rev. **D66**, 095001 (2002), [hep-ph/0205342].
- [381] P. Bechtle et al., Eur. Phys. J. C77, 2, 67 (2017), [arXiv:1608.00638].
- [382] E. Bagnaschi et al., Eur. Phys. J. C79, 7, 617 (2019), [arXiv:1808.07542].
- [383] A. Djouadi, J. Kalinowski and P. M. Zerwas, Z. Phys. C57, 569 (1993).
- [384] G. Lee and C. E. M. Wagner, Phys. Rev. **D92**, 7, 075032 (2015), [arXiv:1508.00576].
- [385] D. Dicus et al., Phys. Rev. **D59**, 094016 (1999), [hep-ph/9811492].
- [386] M. Carena et al., JHEP 07, 091 (2012), [arXiv:1203.1041].
- [387] A. A. Barrientos Bendezu and B. A. Kniehl, Phys. Rev. **D64**, 035006 (2001), [hep-ph/0103018].

- [388] J. Alison et al., Rev. Phys. 5, 100045 (2020), [arXiv:1910.00012].
- [389] LHC Higgs Working Group, https://twiki.cern.ch/twiki/bin/view/LHCPhysics/LHCHWGMSSMCharged.
- [390] D. Dicus, A. Stange and S. Willenbrock, Phys. Lett. B 333, 126 (1994), [hep-ph/9404359];
 N. Craig et al., JHEP 06, 137 (2015), [arXiv:1504.04630];
 S. Gori et al., Phys. Rev. D 93, 7, 075038 (2016), [arXiv:1602.02782].
- [391] A. Djouadi, J. Ellis and J. Quevillon, JHEP **07**, 105 (2016), [arXiv:1605.00542]; M. Carena and Z. Liu, JHEP **11**, 159 (2016), [arXiv:1608.07282].
- [392] LHC Higgs Working Group for BSM Higgs, https://twiki.cern.ch/twiki/bin/view/LHCPhysics/LHCHWG3.
- [393] E. Bagnaschi et al., Eur. Phys. J. C 79, 7, 617 (2019), [arXiv:1808.07542].
- [394] A. Tumasyan et al. (CMS), JHEP 07, 073 (2023), [arXiv:2208.02717].
- [395] U. Ellwanger, C. Hugonie and A. M. Teixeira, Phys. Rept. 496, 1 (2010), [arXiv:0910.1785].
- [396] B. A. Dobrescu, G. L. Landsberg and K. T. Matchev, Phys. Rev. D63, 075003 (2001), [hep-ph/0005308]; R. Dermisek and J. F. Gunion, Phys. Rev. Lett. 95, 041801 (2005), [hep-ph/0502105].
- [397] J. Engel, M. J. Ramsey-Musolf and U. van Kolck, Prog. Part. Nucl. Phys. 71, 21 (2013), [arXiv:1303.2371].
- [398] H. Bahl et al., Eur. Phys. J. C 80, 10, 916 (2020), [arXiv:2005.14536].
- [399] R. S. Chivukula and H. Georgi, Phys. Lett. B188, 99 (1987); L. J. Hall and L. Randall, Phys. Rev. Lett. 65, 2939 (1990); A. J. Buras et al., Phys. Lett. B500, 161 (2001), [hep-ph/0007085]; G. D'Ambrosio et al., Nucl. Phys. B645, 155 (2002), [hep-ph/0207036].
- [400] M. Misiak and M. Steinhauser, Eur. Phys. J. C 77, 3, 201 (2017), [arXiv:1702.04571].
- [401] J. F. Gunion and H. E. Haber, Phys. Rev. D67, 075019 (2003), [hep-ph/0207010]; G. C. Branco et al., Phys. Rept. 516, 1 (2012), [arXiv:1106.0034].
- [402] N. G. Deshpande and E. Ma, Phys. Rev. **D18**, 2574 (1978).
- [403] A. Goudelis, B. Herrmann and S. O., JHEP **09**, 106 (2013), [arXiv:1303.3010].
- [404] M. Bauer, M. Carena and K. Gemmler, JHEP 11, 016 (2015), [arXiv:1506.01719]; M. Bauer,
 M. Carena and K. Gemmler, Phys. Rev. D94, 11, 115030 (2016), [arXiv:1512.03458].
- [405] C. D. Froggatt and H. B. Nielsen, Nucl. Phys. **B147**, 277 (1979).
- [406] K. S. Babu and S. Nandi, Phys. Rev. D62, 033002 (2000), [hep-ph/9907213]; G. F. Giudice and O. Lebedev, Phys. Lett. B665, 79 (2008), [arXiv:0804.1753].
- [407] E. Accomando et al., CERN Report **2006-009** (2006), [hep-ph/0608079].
- [408] T. Robens and T. Stefaniak, Eur. Phys. J. C75, 104 (2015), [arXiv:1501.02234].
- [409] S. L. Glashow and S. Weinberg, Phys. Rev. D15, 1958 (1977); E. A. Paschos, Phys. Rev. D15, 1966 (1977).
- [410] G. C. Branco, W. Grimus and L. Lavoura, Phys. Lett. B380, 119 (1996), [hep-ph/9601383]; F. J. Botella, G. C. Branco and M. N. Rebelo, Phys. Lett. B687, 194 (2010), [arXiv:0911.1753].
- [411] T. P. Cheng and M. Sher, Phys. Rev. D **35**, 3484 (1987).
- [412] D. Atwood, L. Reina and A. Soni, Phys. Rev. D 55, 3156 (1997), [hep-ph/9609279].
- [413] J. Schechter and J. W. F. Valle, Phys. Rev. D22, 2227 (1980); T. P. Cheng and L.-F. Li, Phys. Rev. D22, 2860 (1980).

- [414] H. Georgi and M. Machacek, Nucl. Phys. B262, 463 (1985); M. S. Chanowitz and M. Golden, Phys. Lett. 165B, 105 (1985); J. F. Gunion, R. Vega and J. Wudka, Phys. Rev. D42, 1673 (1990).
- [415] P. Nath et al., Nucl. Phys. Proc. Suppl. 200-202, 185 (2010), [arXiv:1001.2693].
- [416] J. Garayoa and T. Schwetz, JHEP **03**, 009 (2008), [arXiv:0712.1453].
- [417] H. E. Haber and H. E. Logan, Phys. Rev. D62, 015011 (2000), [hep-ph/9909335]; S. Kanemura and K. Yagyu, Phys. Rev. D85, 115009 (2012), [arXiv:1201.6287].
- [418] J. F. Gunion, R. Vega and J. Wudka, Phys. Rev. **D43**, 2322 (1991).
- [419] I. Low and J. Lykken, JHEP 10, 053 (2010), [arXiv:1005.0872]; I. Low, J. Lykken and G. Shaughnessy, Phys. Rev. D86, 093012 (2012), [arXiv:1207.1093].
- [420] H. E. Logan and M.-A. Roy, Phys. Rev. D82, 115011 (2010), [arXiv:1008.4869]; A. Falkowski,
 S. Rychkov and A. Urbano, JHEP 04, 073 (2012), [arXiv:1202.1532].
- [421] N. Arkani-Hamed et al., JHEP 07, 034 (2002), [hep-ph/0206021]; N. Arkani-Hamed, A. G. Cohen and H. Georgi, Phys. Lett. B513, 232 (2001), [hep-ph/0105239].
- [422] M. Perelstein, Prog. Part. Nucl. Phys. 58, 247 (2007), [hep-ph/0512128]; M. Schmaltz and D. Tucker-Smith, Ann. Rev. Nucl. Part. Sci. 55, 229 (2005), [hep-ph/0502182].
- [423] H. Georgi, A. E. Nelson and A. Manohar, Phys. Lett. 126B, 169 (1983); A. E. Nelson and M. J. Strassler, JHEP 09, 030 (2000), [hep-ph/0006251]; S. Davidson, G. Isidori and S. Uhlig, Phys. Lett. B663, 73 (2008), [arXiv:0711.3376].
- [424] R. Contino and G. Servant, JHEP 06, 026 (2008), [arXiv:0801.1679]; J. Mrazek and A. Wulzer, Phys. Rev. D81, 075006 (2010), [arXiv:0909.3977]; A. De Simone et al., JHEP 04, 004 (2013), [arXiv:1211.5663]; A. Azatov et al., Phys. Rev. D89, 7, 075001 (2014), [arXiv:1308.6601].
- [425] A. Banfi, A. Martin and V. Sanz, JHEP 08, 053 (2014), [arXiv:1308.4771]; A. Azatov and A. Paul, JHEP 01, 014 (2014), [arXiv:1309.5273]; C. Grojean et al., JHEP 05, 022 (2014), [arXiv:1312.3317].
- [426] A. Azatov et al., Phys. Rev. **D92**, 3, 035001 (2015), [arXiv:1502.00539].
- [427] K. Agashe, R. Contino and A. Pomarol, Nucl. Phys. B719, 165 (2005), [hep-ph/0412089];
 R. Contino, L. Da Rold and A. Pomarol, Phys. Rev. D75, 055014 (2007), [hep-ph/0612048];
 D. Pappadopulo, A. Thamm and R. Torre, JHEP 07, 058 (2013), [arXiv:1303.3062]; M. Montull et al., Phys. Rev. D88, 095006 (2013), [arXiv:1308.0559].
- [428] I. Low, R. Rattazzi and A. Vichi, JHEP 04, 126 (2010), [arXiv:0907.5413].
- [429] M. Ciuchini et al., JHEP 08, 106 (2013), [arXiv:1306.4644].
- [430] C. Grojean, O. Matsedonskyi and G. Panico, JHEP 10, 160 (2013), [arXiv:1306.4655].
- [431] P. Batra and Z. Chacko, Phys. Rev. D79, 095012 (2009), [arXiv:0811.0394]; R. Barbieri et al., JHEP 08, 161 (2015), [arXiv:1501.07803]; M. Low, A. Tesi and L.-T. Wang, Phys. Rev. D91, 095012 (2015), [arXiv:1501.07890].
- [432] D. Curtin et al., Phys. Rev. D 90, 7, 075004 (2014), [arXiv:1312.4992].
- [433] M. Cepeda *et al.*, Annual Review of Nuclear and Particle Science **72** (2022), [arXiv:2111.12751].
- [434] G. Arcadi, A. Djouadi and M. Raidal, Phys. Rept. 842, 1 (2020), [arXiv:1903.03616].
- [435] R. E. Shrock and M. Suzuki, Phys. Lett. B **110**, 250 (1982).
- [436] G. Aad et al. (ATLAS), Phys. Lett. B 842, 137963 (2023), [arXiv:2301.10731].

- [437] A. Tumasyan et al. (CMS), Eur. Phys. J. C 83, 10, 933 (2023), [arXiv:2303.01214].
- [438] B L. Baudis and S. Profumo, Dark Matter, in this volume.
- [439] G. Aad et al. (ATLAS), JHEP 07, 166 (2023), [arXiv:2302.05225].
- [440] A. M. Sirunyan et al. (CMS), Phys. Rev. D 104, 3, 032013 (2021), [arXiv:2105.03007].
- [441] A. Hayrapetyan et al. (CMS) (2023), [arXiv:2305.18106].
- [442] J. Adam et al. (MEG), Phys. Rev. Lett. 110, 201801 (2013), [arXiv:1303.0754].
- [443] R. Harnik, J. Kopp and J. Zupan, JHEP **03**, 026 (2013), [arXiv:1209.1397].
- [444] ATLAS Collaboration, JHEP 129, 010 (2017).
- [445] A. Tumasyan et al. (CMS), JHEP **02**, 169 (2022), [arXiv:2112.09734].
- [446] G. Aad et al. (ATLAS), Phys. Rept. 1116, 184 (2025), [arXiv:2405.04914].
- [447] D. Curtin et al., JHEP **02**, 157 (2015), [arXiv:1412.0018].
- [448] A. Hayrapetyan et al. (CMS), JHEP **05**, 047 (2024), [arXiv:2402.14491].
- [449] A. Tumasyan et al. (CMS), Eur. Phys. J. C 82, 4, 290 (2022), [arXiv:2111.01299].
- [450] G. Aad et al. (ATLAS), JHEP 03, 041 (2022), [arXiv:2110.13673].
- [451] G. Aad et al. (ATLAS), JHEP 08, 153 (2024), [arXiv:2406.01656].
- [452] A. M. Sirunyan et al. (CMS), JHEP 03, 011 (2021), [arXiv:2009.14009].
- [453] A. M. Sirunyan et al. (CMS), JHEP 10, 139 (2019), [arXiv:1908.02699].
- [454] A. Hayrapetyan et al. (CMS), Phys. Rept. 1115, 448 (2025), [arXiv:2405.13778].
- [455] A. Hayrapetyan et al. (CMS), Phys. Rept. 1115, 678 (2025), [arXiv:2403.16134].
- [456] G. Aad et al. (ATLAS), Phys. Rev. Lett. 132, 23, 231801 (2024), [arXiv:2311.15956].
- [457] A. Hayrapetyan et al. (CMS), Phys. Rept. 1115, 368 (2025), [arXiv:2403.16926].
- [458] ATLAS Collaboration, ATLAS-CONF-2023-035 (2023).
- [459] G. Aad et al. (ATLAS), JHEP 07, 155 (2023), [arXiv:2211.04172].
- [460] G. Aad et al. (ATLAS), JHEP **01**, 053 (2025), [arXiv:2407.07546].
- [461] CMS Collaboration, CMS-PAS-HIG-20-002 (2023).
- [462] CMS Collaboration, CMS-PAS-HIG-17-13 (2017).
- [463] M. Aaboud et al. (ATLAS), Phys. Lett. **B775**, 105 (2017), [arXiv:1707.04147].
- [464] A. M. Sirunyan et al. (CMS), Phys. Lett. B 793, 320 (2019), [arXiv:1811.08459].
- [465] CMS Collaboration, CMS-PAS-HIG-24-014 (2025).
- [466] A. Hayrapetyan et al. (CMS), Phys. Lett. B 860, 139067 (2025), [arXiv:2405.18149].
- [467] G. Aad et al. (ATLAS), Phys. Lett. B 848, 138394 (2024), [arXiv:2309.04364].
- [468] M. Aaboud et al. (ATLAS), JHEP 10, 112 (2017), [arXiv:1708.00212].
- [469] CMS Collaboration, CMS-PAS-HIG-16-014 (2016).
- [470] G. Aad et al. (ATLAS), Eur. Phys. J. C 81, 4, 332 (2021), [arXiv:2009.14791].
- [471] CMS Collaboration, CMS-PAS-HIG-16-033 (2016).
- [472] CMS Collaboration, CMS-PAS-HIG-24-002 (2024).
- [473] CMS Collaboration, CMS-PAS-HIG-16-023 (2016).
- [474] G. Aad et al. (ATLAS), Eur. Phys. J. C 83, 7, 633 (2023), [arXiv:2207.03925].
- [475] G. Aad et al. (ATLAS), Eur. Phys. J. C 80, 12, 1165 (2020), [arXiv:2004.14636].

- [476] CMS Collaboration, CMS-PAS-HIG-16-034 (2017).
- [477] A. M. Sirunyan et al. (CMS), Phys. Rev. D 102, 3, 032003 (2020), [arXiv:2006.06391].
- [478] ATLAS Collaboration, ATLAS-CONF-2016-082 (2016).
- [479] ATLAS Collaboration, ATLAS-CONF-2013-067 (2013).
- [480] ATLAS Collaboration, ATLAS-CONF-2022-066 (2022).
- [481] A. M. Sirunyan et al. (CMS), JHEP **03**, 034 (2020), [arXiv:1912.01594].
- [482] ATLAS Collaboration, ATLAS-CONF-2012-018 (2012).
- [483] M. Aaboud et al. (ATLAS), Phys. Lett. **B777**, 91 (2018), [arXiv:1708.04445].
- [484] G. Aad et al. (ATLAS), JHEP 09, 091 (2019), [arXiv:1906.08589].
- [485] CMS Collaboration, CMS-PAS-B2G-23-007 (2025).
- [486] M. Aaboud et al. (ATLAS), Phys. Rev. **D98**, 5, 052008 (2018), [arXiv:1808.02380].
- [487] G. Aad et al. (ATLAS), Phys. Rev. D 105, 9, 092002 (2022), [arXiv:2202.07288].
- [488] G. Aad et al. (ATLAS), Phys. Lett. B 858, 139007 (2024), [arXiv:2404.17193].
- [489] G. Aad et al. (ATLAS), Phys. Rev. D **106**, 5, 052001 (2022), [arXiv:2112.11876].
- [490] ATLAS Collaboration (2016); M. Aaboud et al. (ATLAS), JHEP 05, 124 (2019), [arXiv:1811.11028]; M. Aaboud et al. (ATLAS), Eur. Phys. J. C78, 12, 1007 (2018), [arXiv:1807.08567].
- [491] ATLAS Collaboration, ATLAS-CONF-2019-030 (2019); M. Aaboud et al. (ATLAS), Phys. Rev. Lett. 121, 19, 191801 (2018), [Erratum: Phys. Rev. Lett. 122, 089901 (2019)], [arXiv:1808.00336]; G. Aad et al. (ATLAS) (2019), [arXiv:1908.06765].
- [492] A. M. Sirunyan et al. (CMS), Phys. Lett. B 788, 7 (2019), [arXiv:1806.00408].
- [493] V. Khachatryan et al. (CMS), Phys. Lett. **B755**, 217 (2016), [arXiv:1510.01181].
- [494] A. Tumasyan et al. (CMS), JHEP 07, 095 (2023), [arXiv:2206.10268].
- [495] G. Aad et al. (ATLAS), Phys. Rev. Lett. 125, 5, 051801 (2020), [arXiv:2002.12223].
- [496] A. M. Sirunyan et al. (CMS), JHEP **09**, 007 (2018), [arXiv:1803.06553].
- [497] V. M. Abazov et al. (D0), Phys. Rev. Lett. 104, 151801 (2010), [arXiv:0912.0968].
- [498] D0 Collaboration, D0Note 5974-CONF (2011).
- [499] R. Aaij et al. (LHCb), JHEP 05, 132 (2013), [arXiv:1304.2591].
- [500] G. Aad et al. (ATLAS), JHEP 12, 126 (2024), [arXiv:2409.20381].
- [501] A. M. Sirunyan et al. (CMS), JHEP **05**, 210 (2019), [arXiv:1903.10228].
- [502] M. Aaboud et al. (ATLAS), JHEP 07, 117 (2019), [arXiv:1901.08144].
- [503] A. M. Sirunyan et al. (CMS) (2019), [arXiv:1907.03152].
- [504] A. M. Sirunyan et al. (CMS), JHEP **03**, 103 (2020), [arXiv:1911.10267].
- [505] G. Aad et al. (ATLAS), JHEP 08, 148 (2015), [arXiv:1505.07018].
- [506] G. Aad et al. (ATLAS), JHEP 08, 013 (2024), [arXiv:2404.18986].
- [507] G. Aad et al. (ATLAS), JHEP 07, 203 (2023), [arXiv:2211.01136].
- [508] A. M. Sirunyan et al. (CMS), JHEP **04**, 171 (2020), [arXiv:1908.01115].
- [509] A. Hayrapetyan et al. (CMS), CMS-HIG-22-013 (2025), [arXiv:2507.05119].
- [510] G. Aad et al. (ATLAS), Phys. Rev. D 102, 3, 032004 (2020), [arXiv:1907.02749].
- [511] V. Chekhovsky et al. (CMS), JHEP **06**, 144 (2025), [arXiv:2502.06568].

- [512] S. Chatrchyan et al. (CMS), Phys. Lett. B722, 207 (2013), [arXiv:1302.2892]; CMS Collaboration, CMS-PAS-HIG-16-025 (2016); A. M. Sirunyan et al. (CMS), JHEP 08, 113 (2018), [arXiv:1805.12191].
- [513] V. M. Abazov et al. (D0), Phys. Lett. **B698**, 97 (2011), [arXiv:1011.1931].
- [514] T. Aaltonen et al. (CDF), Phys. Rev. **D85**, 032005 (2012), [arXiv:1106.4782].
- [515] ATLAS Collaboration, ATLAS-CONF-2017-055 (2017).
- [516] G. Aad et al. (ATLAS), Phys. Rev. D 102, 11, 112008 (2020), [arXiv:2007.05293]; G. Aad et al. (ATLAS), Phys. Lett. B744, 163 (2015), [arXiv:1502.04478].
- [517] A. M. Sirunyan et al. (CMS), JHEP **03**, 065 (2020), [arXiv:1910.11634].
- [518] A. M. Sirunyan et al. (CMS), Eur. Phys. J. C79, 7, 564 (2019), [arXiv:1903.00941].
- [519] V. Chekhovsky et al. (CMS) (2025), [arXiv:2501.14825].
- [520] M. Aaboud et al. (ATLAS), Phys. Lett. B 783, 392 (2018), [arXiv:1804.01126].
- [521] G. Aad et al. (ATLAS), JHEP 10, 130 (2024), [arXiv:2401.04742].
- [522] G. Aad et al. (ATLAS), JHEP **02**, 197 (2024), [arXiv:2311.04033].
- [523] V. Khachatryan et al. (CMS), Phys. Lett. B **759**, 369 (2016), [arXiv:1603.02991].
- [524] A. Hayrapetyan et al. (CMS), Phys. Lett. B 866, 139568 (2025), [arXiv:2412.00570].
- [525] G. Aad et al. (ATLAS), Phys. Rev. Lett. 125, 22, 221802 (2020), [arXiv:2004.01678].
- [526] A. M. Sirunyan et al. (CMS), JHEP **03**, 055 (2020), [arXiv:1911.03781].
- [527] M. Aaboud et al. (ATLAS), Phys. Lett. **B759**, 555 (2016), [arXiv:1603.09203].
- [528] M. Aaboud et al. (ATLAS), JHEP **09**, 139 (2018), [arXiv:1807.07915].
- [529] G. Aad et al. (ATLAS), Phys. Rev. D 111, 7, 072006 (2025), [arXiv:2412.17584].
- [530] CMS Collaboration, CMS-PAS-HIG-16-031 (2016); A. M. Sirunyan *et al.* (CMS), JHEP **07**, 142 (2019), [arXiv:1903.04560].
- [531] ATLAS Collaboration, ATLAS-CONF-2012-010 (2012).
- [532] G. Aad et al. (ATLAS), Eur. Phys. J. C 85, 2, 153 (2025), [arXiv:2407.10096].
- [533] A. M. Sirunyan et al. (CMS), Phys. Rev. D 102, 7, 072001 (2020), [arXiv:2005.08900].
- [534] G. Aad et al. (ATLAS), JHEP **06**, 145 (2021), [arXiv:2102.10076].
- [535] A. M. Sirunyan et al. (CMS), JHEP 07, 126 (2020), [arXiv:2001.07763]; V. Khachatryan et al. (CMS), JHEP 11, 018 (2015), [arXiv:1508.07774]; A. M. Sirunyan et al. (CMS) (2019), [arXiv:1908.09206].
- [536] G. Aad et al. (ATLAS), Phys. Rev. Lett. 114, 23, 231801 (2015), [arXiv:1503.04233].
- [537] G. Aad et al. (ATLAS), Phys. Lett. B 860, 139137 (2025), [arXiv:2407.10798].
- [538] A. M. Sirunyan et al. (CMS), Phys. Rev. Lett. 119, 14, 141802 (2017), [arXiv:1705.02942].
- [539] A. M. Sirunyan et al. (CMS), Eur. Phys. J. C 81, 8, 723 (2021), [arXiv:2104.04762].
- [540] A. M. Sirunyan et al. (CMS), Phys. Rev. Lett. 123, 13, 131802 (2019), [arXiv:1905.07453].
- [541] G. Aad et al. (ATLAS), JHEP **02**, 143 (2025), [arXiv:2411.03969].
- [542] A. Tumasyan et al. (CMS), JHEP **09**, 032 (2023), [arXiv:2207.01046].
- [543] G. Aad et al. (ATLAS), JHEP **09**, 004 (2023), [arXiv:2302.11739].
- [544] A. M. Sirunyan et al. (CMS), JHEP 11, 115 (2018), [arXiv:1808.06575].
- [545] ATLAS Collaboration, ATLAS-CONF-2011-020 (2011).

- [546] G. Aad et al. (ATLAS), Phys. Rev. D 108, 9, 092007 (2023), [arXiv:2304.14247].
- [547] A. M. Sirunyan et al. (CMS), JHEP 11, 010 (2017), [arXiv:1707.07283].
- [548] G. Aad et al. (ATLAS), Phys. Rev. **D92**, 5, 052002 (2015), [arXiv:1505.01609].
- [549] ATLAS Collaboration, ATLAS-CONF-2012-079 (2012).
- [550] G. Aad et al. (ATLAS) (2025), [arXiv:2503.05463].
- [551] G. Aad et al. (ATLAS), JHEP 03, 190 (2025), [arXiv:2412.14046].
- [552] G. Aad et al. (ATLAS), Eur. Phys. J. C 84, 7, 742 (2024), [arXiv:2312.03306].
- [553] CMS Collaboration, CMS-PAS-EXO-24-025 (2025).
- [554] A. Tumasyan et al. (CMS), JHEP 07, 148 (2023), [arXiv:2208.01469].
- [555] A. Tumasyan et al. (CMS), Phys. Rev. Lett. 131, 101801 (2023), [arXiv:2209.06197].
- [556] A. M. Sirunyan et al. (CMS), JHEP 08, 139 (2020), [arXiv:2005.08694].
- [557] V. Khachatryan et al. (CMS), JHEP 10, 076 (2017), [arXiv:1701.02032].
- [558] A. M. Sirunyan et al. (CMS), Phys. Lett. **B795**, 398 (2019), [arXiv:1812.06359].
- [559] A. M. Sirunyan et al. (CMS), Phys. Lett. **B796**, 131 (2019), [arXiv:1812.00380].
- [560] A. M. Sirunyan et al. (CMS) (2019), [arXiv:1907.07235].
- [561] A. M. Sirunyan et al. (CMS), Phys. Lett. **B785**, 462 (2018), [arXiv:1805.10191].
- [562] A. M. Sirunyan et al. (CMS), JHEP 11, 018 (2018), [arXiv:1805.04865].
- [563] CMS Collaboration, CMS-PAS-HIG-18-015 (2019).
- [564] V. Chekhovsky et al. (CMS) (2025), [arXiv:2508.06947].
- [565] S. Schael *et al.* (ALEPH), JHEP **05**, 049 (2010), [arXiv:1003.0705].
- [566] V. M. Abazov et al. (D0), Phys. Rev. Lett. 103, 061801 (2009), [arXiv:0905.3381].
- [567] G. Aad et al. (ATLAS), Phys. Rev. D 105, 1, 012006 (2022), [arXiv:2110.00313].
- [568] M. Aaboud et al. (ATLAS), JHEP 10, 031 (2018), [arXiv:1806.07355].
- [569] G. Aad et al. (ATLAS) (2025), [arXiv:2507.01165].
- [570] G. Aad et al. (ATLAS), Phys. Rev. D 110, 5, 052013 (2024), [arXiv:2407.01335].
- [571] A. M. Sirunyan et al. (CMS), Phys. Lett. B **795**, 398 (2019), [arXiv:1812.06359].
- [572] A. M. Sirunyan et al. (CMS), Phys. Lett. B 785, 462 (2018), [arXiv:1805.10191].
- [573] CMS Collaboration, CMS-PAS-HIG-21-021 (2022).
- [574] A. Hayrapetyan et al. (CMS), JHEP 06, 097 (2024), [arXiv:2403.10341].
- [575] A. Hayrapetyan et al. (CMS), Eur. Phys. J. C 84, 5, 493 (2024), [arXiv:2402.13358].
- [576] G. Aad et al. (ATLAS), Phys. Lett. B 868, 139671 (2025), [arXiv:2411.16361].
- [577] G. Aad et al. (ATLAS), Phys. Lett. B 850, 138536 (2024), [arXiv:2312.01942].
- [578] A. Hayrapetyan et al. (CMS), Phys. Lett. B 852, 138582 (2024), [arXiv:2311.00130].
- [579] B. Aubert et al. (BaBar), Phys. Rev. Lett. 103, 081803 (2009), [arXiv:0905.4539].
- [580] B. Aubert et al. (BaBar), Phys. Rev. Lett. 103, 181801 (2009), [arXiv:0906.2219].
- [581] M. Aaboud et al. (ATLAS), JHEP 05, 124 (2019), [arXiv:1811.11028].
- [582] A. Tumasyan et al. (CMS), Phys. Lett. B 835, 137566 (2022), [arXiv:2203.00480].
- [583] G. Aad et al. (ATLAS), JHEP 10, 009 (2023), [arXiv:2307.11120].
- [584] G. Aad et al. (ATLAS), JHEP 11, 047 (2024), [arXiv:2404.12915].

- [585] G. Aad et al. (ATLAS), JHEP 10, 104 (2024), [arXiv:2405.20926].
- [586] G. Aad et al. (ATLAS) (2025), [arXiv:2510.02857].
- [587] CMS Collaboration, CMS-PAS-HIG-20-012 (2024).
- [588] A. Tumasyan et al. (CMS), Phys. Lett. B 842, 137392 (2023), [arXiv:2204.12413].
- [589] A. Tumasyan et al. (CMS), JHEP 11, 057 (2021), [arXiv:2106.10361].
- [590] A. Hayrapetyan et al. (CMS) (2025), [arXiv:2508.11494].
- [591] A. Hayrapetyan et al. (CMS) (2025), [arXiv:2506.23012].
- [592] CMS Collaboration, CMS-PAS-B2G-23-007 (2025).
- [593] ATLAS Collaboration, ATLAS-CONF-2016-051 (2016).
- [594] ATLAS Collaboration, ATLAS-CONF-2017-053 (2017).
- [595] M. Aaboud et al. (ATLAS), Eur. Phys. J. C79, 1, 58 (2019), [arXiv:1808.01899].
- [596] CMS Collaboration, CMS-PAS-HIG-16-036 (2017).
- [597] J. de Blas et al., in "Snowmass 2021," (2022), [arXiv:2206.08326].
- [598] J. de Blas et al., Briefing Book CERN-ESU-2025-001 (2025), URL https://cds.cern.ch/record/2944678.
- [599] J. Altmann et al., ECFA Higgs, electroweak, and top Factory Study, volume 5/2025 of CERN Yellow Reports: Monographs (2025), ISBN 978-92-9083-700-8, 978-92-9083-701-5, [arXiv:2506.15390].